INSOLATION UTILIZABILITY AND THE PREDICTION OF

INDUSTRIAL PROCESS HEATING SYSTEM PERFORMANCE


BY


DAVID SIGURD ODEGARD


A thesis submitted in partial fulfillment of the
requirements for the degree of


MASTER OF SCIENCE
(Mechanical Engineering)


at the


UNIVERSITY OF WISCONSIN-MADISON


1980

## ABSTRACT

This thesis examines the characteristics of solar industrial process heating (IPH) systems, the possible ways of predicting their performance, and hourly utilizability as a prediction means.

The simulated performance of closed load loop systems under different load patterns indicates that, for reasonable storage sizes, an existing design method adequately predicts system performance. A method of predicting the performance of systems without storage is presented. This method uses hourly utilizability to determine energy supplied to the load (and also dumped energy).

Hourly utilizability, based on the generalized Liu and Jordan clearness index distributions, is correlated with a different radiation parameter, and extended to a true hourly basis. An analytical expression for hourly utilizability is derived using a random insolation sequence, probability distribution.

Both the hourly generalized and analytical utilizability methods, can be used for non-south facing surfaces. These two methods predict the usable energy calculated from data, to within a few percent.

APPROVED: _S. A. Klein_
                  S.A. Klein, Associate Professor

DATE: _8/22/80_

## ACKNOWLEDGMENTS

TABLE OF CONTENTS

iv

# LIST OF FIGURES

# LIST OF TABLES

# NOMENCLATURE

This list contains the major parameters used in this study. Others are defined locally.

A               Collector area

$A_e$            Effective collector area

c               Specific heat

C               Probability distribution constant

$C_e$            Storage capacitance per unit of effective collector area

D               Number of days in the month

F               Annual fraction of the load met by solar energy

f               Cumulative frequency of occurrence

$F_R$            Collector heat removal factor

$G_{sc}$         Solar constant

H               Total daily insolation on a horizontal surface

$H_d$            Daily diffuse radiation on a horizontal surface

$H_T$            Total daily insolation on a tilted surface

$H_o$            Daily extraterrestrial insolation on a horizontal surface

I               Total hourly insolation on a horizontal surface

$I_c$            Critical insolation level

$I_d$            Hourly diffuse radiation on a horizontal surface

$I_{min}$        Minimum isolation level for collector operation

$I_{max}$        Maximum usable insolation level

| | |
|---|---|
| $I_T$ | Total hourly insolation on a tilted surface |
| $I_o$ | Hourly extraterrestrial insolation on a horizontal surface |
| $k_c$ | Critical clearness index |
| $k_{min}$ | Minimum observed hourly clearness index |
| $k_{max}$ | Maximum observed hourly clearness index |
| $k_T$ | Hourly clearness index |
| $K_T$ | Daily clearness index |
| $L$ | Latitude |
| $Ld$ | Process heating load |
| $n$ | Day of the year |
| $P\ (\ )$ | Probability of ( ) occurring |
| $Q_{dump}$ | Dumped energy |
| $Q_{sup}$ | Energy supplied to the load |
| $Q_u$ | Usable collected energy |
| $r_T$ | Ratio of total hourly to total daily insolation on a horizontal surface |
| $r_o$ | Ratio of extraterrestrial hourly to daily insolation on a horizontal surface |
| $R$ | Ratio of total hourly insolation on a tilted, to that on a horizontal surface |
| $R'$ | Ratio of total daily insolation on a tilted, to that on a horizontal surface |
| $\bar{R}$ | Ratio of monthly-average daily insolation on a tilted, to that on a horizontal surface |
| $R_b$ | Ratio of hourly beam radiation on a tilted, to that on a horizontal surface |

$R'_b$ — Ratio of daily beam radiation on a tilted, to that on a horizontal surface

$\bar{R}_b$ — Ratio of monthly-average daily beam radiation on a tilted, to that on a horizontal surface

$\bar{R}_{bh}$ — Ratio of monthly-average hourly beam radiation on a tilted surface, to that on a horizontal surface

$\bar{T}_a$ — Monthly-average daytime ambient temperature

$T_{min}$ — Minimum useable temperature

$U_{ij}$ — Useable energy over a time span

$U_L$ — Collector loss coefficient

$V$ — Storage volume

$V_{bd}$ — Hourly beam-diffuse view factor

$V'_{bd}$ — Daily beam-diffuse view factor

$X_c$ — Critical insolation ratio

$Y$ — Number of years in a summation

$\alpha$ — Collector absorbtance

$\beta$ — Collector slope

$\gamma$ — Exponential function constant

$\delta$ — Declination

$\rho$ — Ground reflectance

$\rho_s$ — Storage fluid density

$\tau$ — Collector cover transmittance

$\phi$ — Monthly-average hourly utilizability

$\phi'$ — Monthly-average hourly unutilizability

$\bar{\phi}$ — Monthly-average daily utilizability

$\overline{\phi}'$          Monthly-average daily unutilizability

$\psi$          Collector azimuth

$\omega$          Hour angle

$\omega_s$          Sunset hour angle

Subscripts

d          Day of the month

h          Hour of the day

m          Month of the year

y          Particular year

A " —" indicates monthly-average (except the special cases above).

A "+" means only positive values are to be considered.

A "." represents a time rate of occurrence.

# 1. INTRODUCTION

Industry is becoming interested in using solar energy due to the questioned availability, and increasing cost, of conventional energy sources. Industrial applications of solar energy differ from others in energy demand patterns, temperature requirements, and magnitude. For these reasons, existing methods of predicting a solar system's performance are not always applicable.

The nature of industrial process heating (IPH) is such that many applications can be done with conventional solar system configurations employing flat-plate collectors, with or without energy storage capabilities. Insolation utilizability concepts can be used as a basis for predicting the performance of these IPH systems.

Past studies of solar IPH systems can be broken into two general categories: general energy requirements (references 4, 7, 8, 11, 17, 18, 35) and system specific projects (21, 27, 31, 33, 37). The first group of studies is helpful in determining the characteristics of IPH load requirements, and the type of solar systems that should be examined for IPH use.

System specific IPH projects offer little insight to the general application of solar. They often spell out the hardware difficulties in retrofit operations, but do not quantify system-load interactions. There have been a few attempts to predict the performance of specific systems (27, 31), but not in a general way.

Currently available design methods based on insolation utiliza-
bility (2, 32) do not fully account for the particulars of IPH appli-
cations. This is due in part to the use of daily, rather than hourly,
utilizability. Past hourly utilizability studies (30, 42) have not
developed it to a usable form.

The goals of this thesis are to: 1) determine when current de-
sign methods can be used for solar IPH systems, 2) present a method
of predicting the performance of systems without storage based on
hourly utilizability, and 3) examine hourly utilizability in detail
to obtain a usable form.

To achieve the above ends, first the general characteristics of
IPH will be presented and possible solar system configurations ex-
amined. Next, the effects of different load patterns on system per-
formance will be examined to determine the applicability of existing
design methods. A procedure for predicting the performance of sys-
tems without storage based on hourly utilizability will be presented.
A review and improvement of generalized hourly utilizability, along
with an analytically derived expression for hourly utilizability, are
the topics of Chapter 4. It is determined that both the generalized
and analytical methods do a good job of predicting usable energy.
Finally, an example of using these two methods to predict the per-
formance of a solar IPH system without storage will be presented.

## 2. INDUSTRIAL APPLICATION CHARACTERISTICS

Industrial process heat (IPH) is thermal energy used specifically in the preparation and/or treatment of manufactured goods. It has been determined (8, 17, 18) that about 25% of the total U.S.A. energy use is for IPH applications. The characteristics of IPH requirements, and possible solar system configurations, are the subject of this chapter.

### 2.1 Industrial Process Heat Characteristics

Industrial process heating applications have three unique characteristics: 1) the temperature at which energy becomes useful, 2) the magnitude and type of load, and 3) the time distribution of the load.

To characterize the temperature of IPH systems, the minimum usable temperature is defined as; the temperature that must be reached by the energy source before it will meet part (or all) of the process energy demand (e.g., the temperature of water entering a boiler). The approximate minimum usable temperature distribution for all U.S. IPH energy requirements (17) is shown in Figure 2.1-1. Inspection of this plot shows that about 25% of this energy could be delivered using flat-plate collectors (assuming a maximum operating temperature of 100°C).

Industrial process heating loads can be divided into two main categories; direct and indirect. Direct-heat applications have a
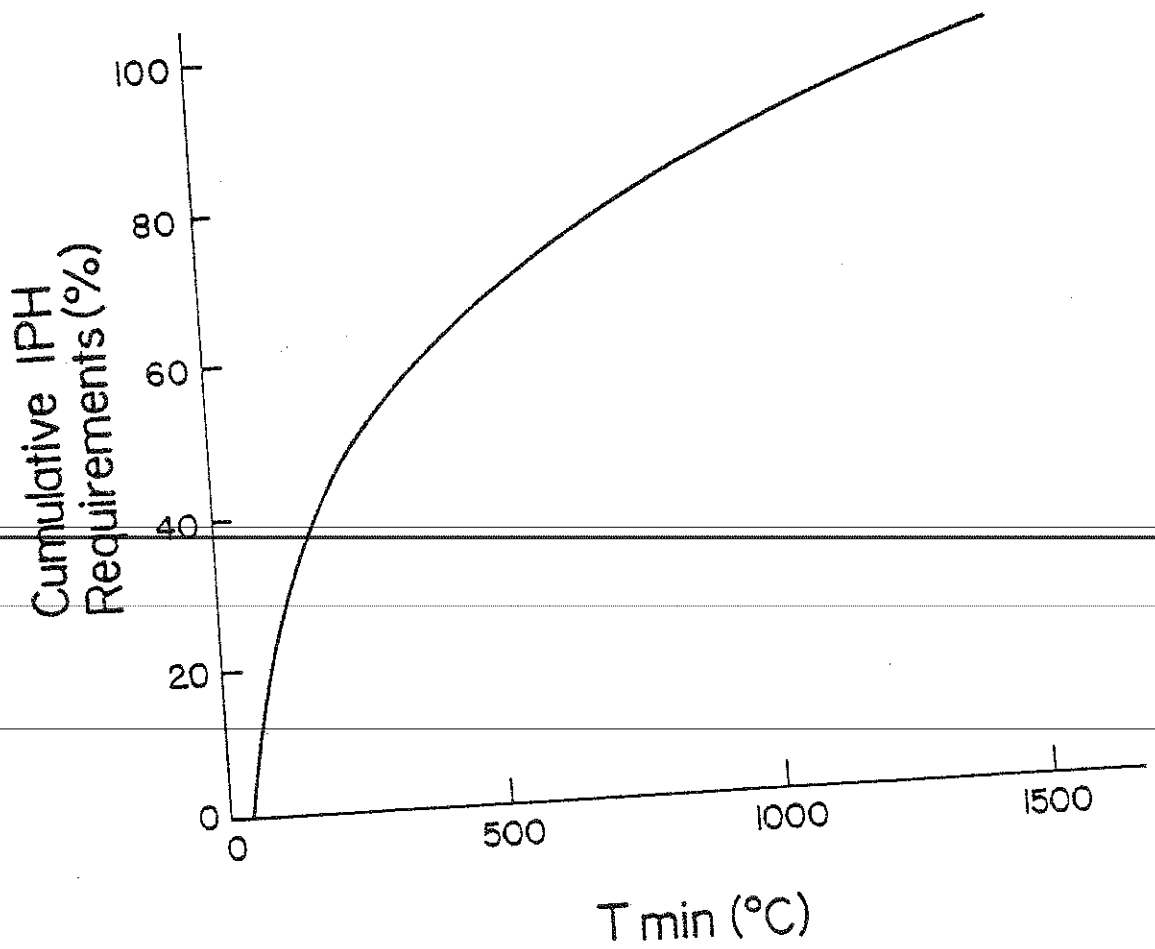
Figure 2.1-1:  Temperature distribution of IPH energy requirements
(from Fraser 1977)

mass as well as an energy requirement. An example of a direct-heat application would be the use of hot water for washing (27, 37), or air for painting operations (16). Indirect-heat applications have only an energy requirement. Such applications as the curing of cement blocks (37), and supplying energy to an absorption air conditioner fall into this category.

The final characteristic of IPH is the load demand schedule. Industrial loads usually have a fixed pattern over a period of time (a day, week, and/or month). These patterns vary from a continuous 24 hour per day, 365 days per year load, to a batch operation that occurs once a week.

## 2.2 Solar System Configurations

In light of the IPH characteristics described in the previous section, the configuration of two different generic solar systems, and a limiting case common to both, will be considered.

The solar system shown schematically in Figure 2.2-1 is applicable to direct heating situations. Here, the minimum usable temperature could be the incoming water mains temperature for water based systems, or the ambient air temperature for air based systems. The auxiliary energy supply is in series, to assure the required delivery temperature. This is commonly called an open load loop system.
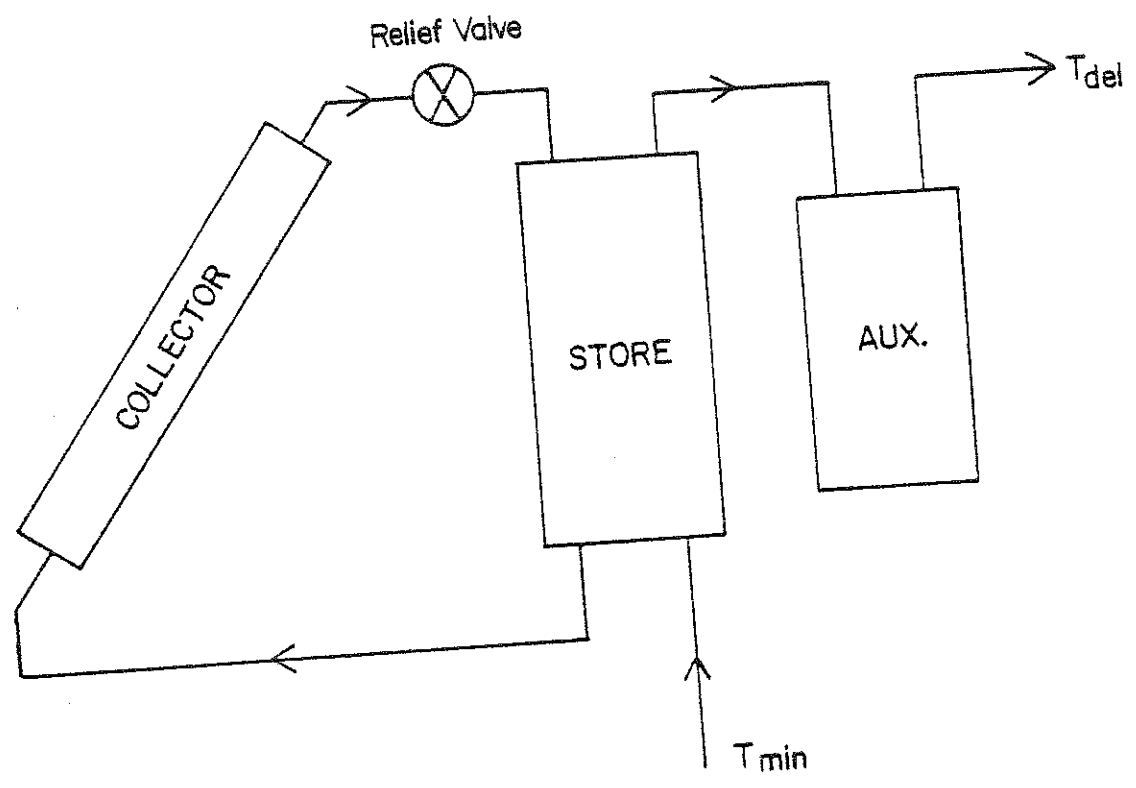
Figure 2.2-1:   Solar System for direct heating
                (open load loop)

For indirect heating applications (i.e., an energy demand only), the system shown in Figure 2.2-2 can be used. Here, the entire load can be met with energy at (or above) $T_{min}$. This is a closed load loop system.

The difference between the open and closed load loop systems is that, the open system energy delivery is determined by the load mass flow rate, and the closed one's by the load heat exchanger parameters. This difference will (usually) result in a different tank (and thus collector inlet) temperature for the two systems operating with the same $T_{min}$. If, however, all the available solar energy is delivered to the load immediately upon collection, both systems would have tank temperatures (almost) equal to $T_{min}$.

The above limiting situation is a common one in IPH applications where the loads are usually far greater than a solar system, covering all the available area, can supply. Since provisions for storing solar energy would not be used to any great extent in this situation, it has been suggested (37, 16) that system costs could be reduced, with little or no loss in performance, by excluding storage. A system without storage is shown in Figure 2.2-3. As the above discussion affirms, this system is representative of both open and closed load loop applications (for the open loop case the heat exchanger would be considered perfect). For direct heating, the auxiliary energy supply would be in series, and for indirect in parallel, with the solar system.
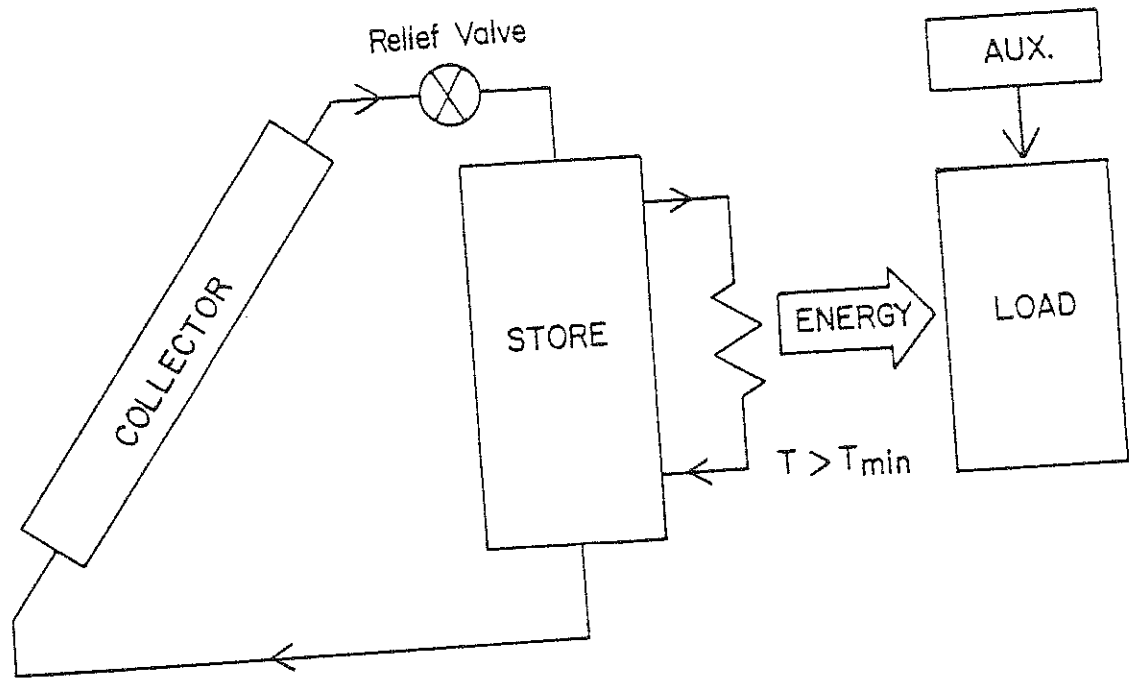
Figure 2.2-2:  Solar system for indirect heating
               (closed load loop)
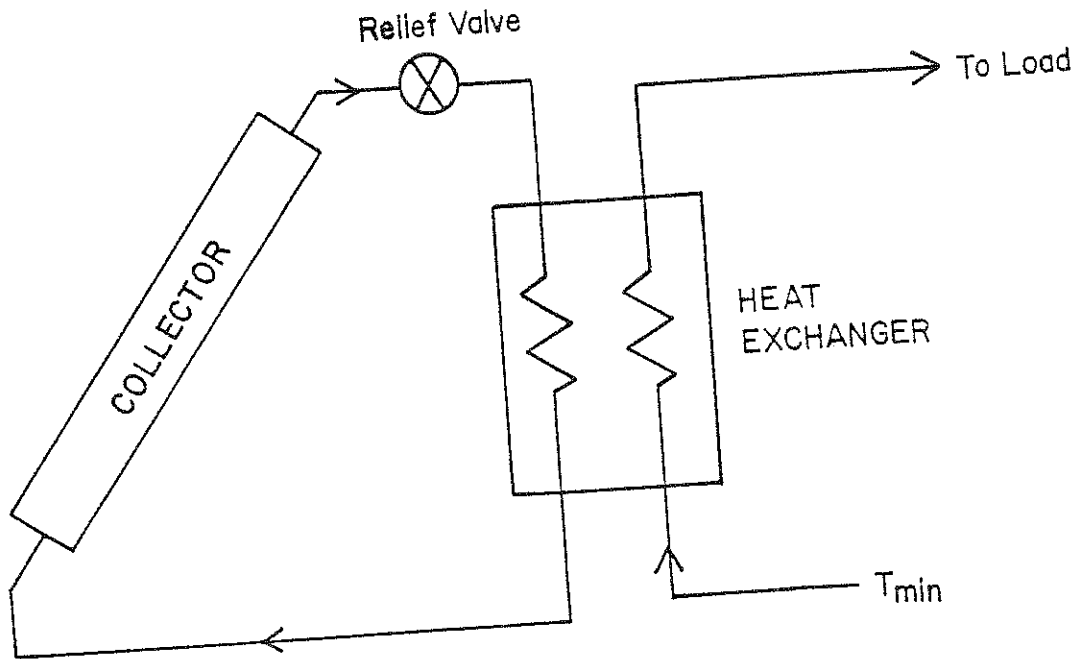
Figure 2.2-3:  No storage solar system

The remainder of this study will be devoted to determining and predicting, the performance of the closed load loop system of Figure 2.2-2, and the no storage system of Figure 2.2-3.

# 3. PREDICTING SYSTEM PERFORMANCE

## 3.1 Introduction

This chapter begins with a description of the system simulation models used in this study. The simulated performance of these systems for many "common" and some "not-so-common" load profiles is presented and examined. Finally, simplified methods of predicting system performance are presented and discussed. It is determined that utilizability is a useful tool for predicting system performance.

## 3.2 System Description

Using the simulation program TRNSYS (26), the closed load loop system of Figure 2.2-2 was examined. In modeling this system, the following assumptions were made.

1. The load is a demand for energy at or above $T_{min}$.

2. The collector fluid has a high boiling point so that no energy dumping occurs (only for systems with storage).

3. No energy losses from pipes.

4. Collector loop heat exchanger effectiveness of unity (not applicable to systems without storage).

5. Load heat exchanger of infinite capacity.

6. No energy losses from storage.

The first assumption is a restriction on the type of system.

It indicates that the simulation results are not applicable to open loop systems of Figure 2.2-1, which have a mass demand, not just an energy demand. The "no boil-off" assumption is quite plausible for the industrial application considered in this study. To prevent boil-off, the solar system fluid could be pressurized water or one of many available fluids with a higher boiling point. The remaining assumptions were made for initial simplicity, they will be removed later. For systems with reasonable storage, these assumptions will have a fairly equal impact on system performance for all load patterns. If desired, pipe losses and the existence of a non-perfect collector loop heat exchanger could be accounted for by modifying the collector parameters as suggested by Beckman (1), and de Winter (15) respectively.

Aside from the basic system assumptions mentioned above, some comments about specific components are in order.

The flat-plate collector was modeled according to the Hottel-Whillier equation (42). The transmittance-absorptance product was assumed to be a constant, independent of insolation incident angle. The overall collector loss coefficient was taken to be constant, independent of wind velocity and ambient temperature. The above two restrictions correspond to a TRNSYS type 1, mode 1 collector.

The storage tank was modeled with a single mode. This represents a fully mixed, unstratified tank.

The load heat exchanger was modeled to be sufficiently large to deliver the load energy rate whenever the storage temperature was greater than $T_{min}$.

Using the above assumptions and modeling techniques, two TRNSYS decks were assembled corresponding to Figures 2.2-2 and 2.2-3. A complete set of system parameters will be found with these programs in Appendix C.

## 3.3 Simulated System Performance

Using the system models described in the previous section, simulations were performed for various load patterns and locations. For any one location and set of load patterns, the collector area and the total yearly energy requirement were held constant. The results are based on loads symmetric about solar noon.

The graphical presentations to follow are plots of the annual fraction of the load met by solar, $F$, as a function of the storage capacitance per effective square meter of collector area, $C_e$. These parameters are defined as:

$$F = \frac{Q_{sup}}{Ld} \tag{3.3-1}$$

where Ld is the annual process heating load and $Q_{sup}$ the annual solar energy supplied to the load.

And,

$$C_e = \frac{V \cdot \rho_s \cdot c}{A_e} \tag{3.3-2}$$

where:  V = Storage Volume

$\rho_s$ = Storage fluid density

c = Storage fluid specific heat

$A_e$ = Effective collector area

The effective collector area was defined by Klein and Beckman (25)

as:

$$A_e = A\ F_R \tag{3.3-3}$$

where A and $F_R$* are the collector area and heat removal factor re-

spectively. The effective area removes the effect of different

$F_R$ s on the $\bar{F}$ vs. $C_e$ curves. This makes results plotted in such a

fashion more general. For reference, a standard $C_e$ for domestic

water heating applications is about 350 KJ/°C-m$^2$.

If a given load pattern results in a flat $\bar{F}$ vs. $C_e$ curve, it

indicates that the energy flows into and out of storage ($C_e > 0$)

are fairly synchronous (i.e., the energy collection and demand are

in phase with each other). If $\bar{F}$ varies significantly with $C_e$,

it indicates that the energy collector and demand are not

synchronized.

Using a year of typical meteorological data (19, 39) for

Albuquerque, TRNSYS simulations were performed to examine the

---

*A collector heat removal factor modified to account for a
non-perfect collector-loop heat exchanger, as suggested by de Winter
(15), can be used in place of $F_R$ throughout this study.

effects of various load patterns on system performance.

The effect that the number of hours per day the load is distributed over has on F is shown in Figure 3.3-1 for 7 day per week loads centered at solar noon. The two sets of curves indicate that for a reasonable range of collector areas, the number of load hours per day makes a maximum difference of 3% F at the standard storage size. At twice the standard storage size these differences are almost zero.

The small difference between the above curves can be understood by realizing that for the load profiles presented, the load is demanding energy for almost all hours of collector operation. As indicated before, this balancing of energy supply and demand reduces the need for a large storage capacitance.

All the loads of Figure 3.3-1 were symmetric about solar noon. If these same loads were out of phase, the hierarchy of performance results would be reversed. Indeed, if they were symmetrical about midnight, the 24 hour per day load would perform the same, but the 8 hour per day load would suffer drastically.

The effect of the number of days per week the load is distributed over is shown in Figure 3.3-2. These results are for the same system and location as Figure 3.3-1, with a constant 8 hour per day load. This plot indicates that the number of days per week the load is distributed over is of larger significance than the hours per day (Figure 3.3-1). Also, comparison of the on-a-day,
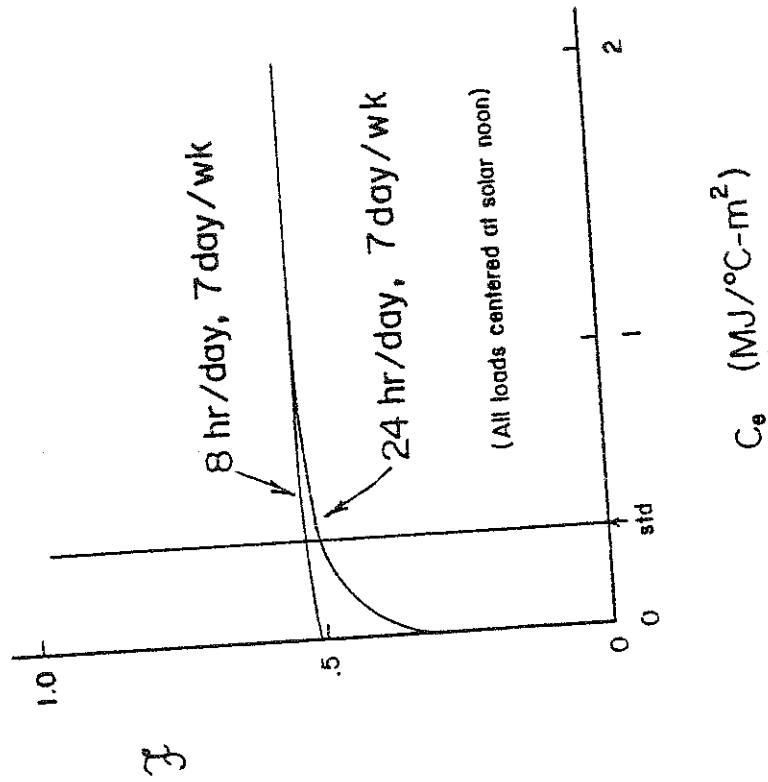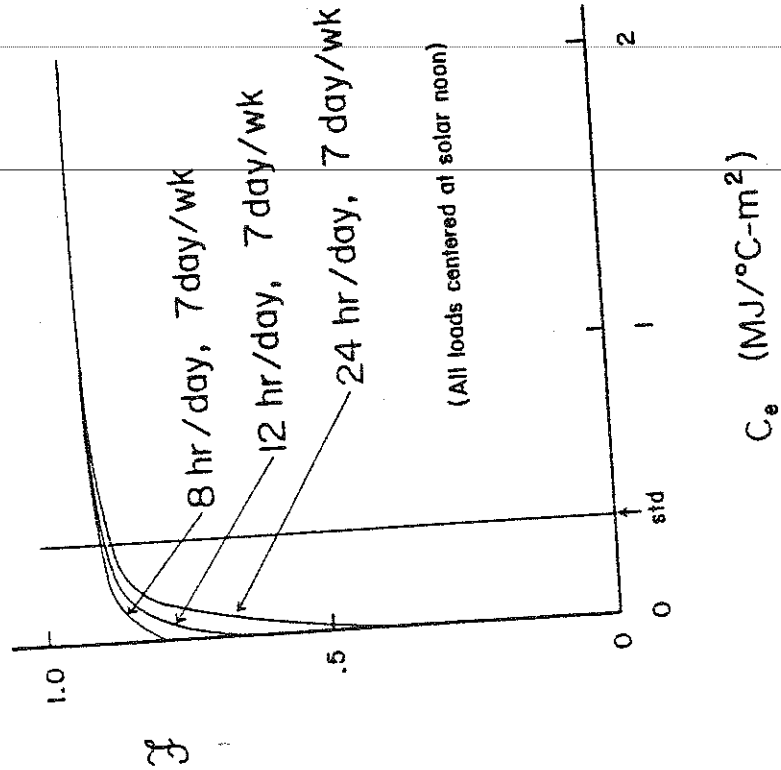
Figure 3.3-1: Load hours per day effect on system performance
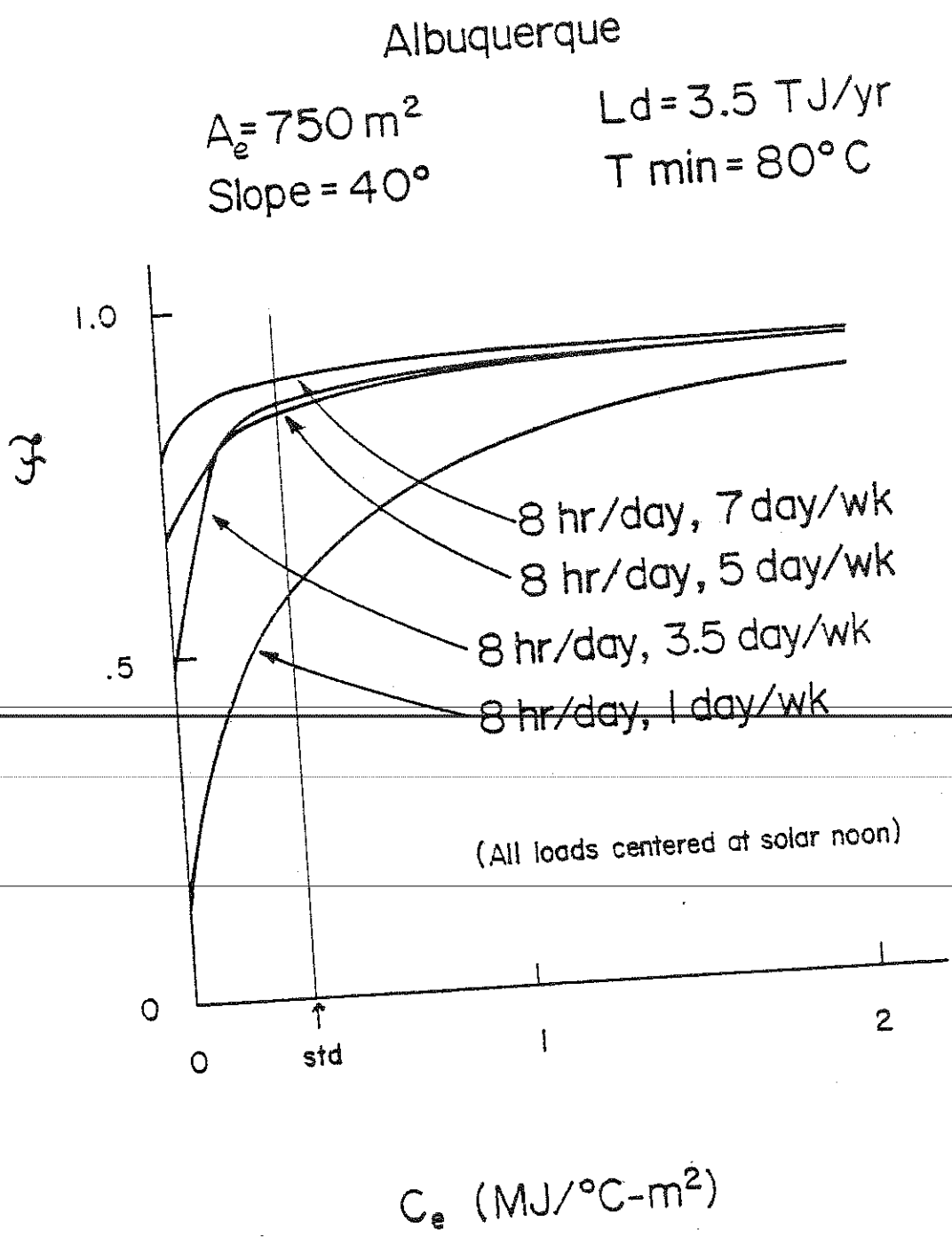
Figure 3.3-2:  Load days per week effect on system performance
(Albuquerque)

off-a-day (3.5 days/week) and the 5 continuous days a week loads indicates that load continuity can be of significance, especially at low values of $C_e$.

Applying the same day-to-day variation in load profiles as above to Madison data produces the results of Figure 3.3-3. Comparing these results to those of Figure 3.3-2 indicates that the same set of load profiles have about the same difference in system performance between them, independent of location. This is not to say that the general shape of all load profiles is independent of location. Further comparison of Figures 3.3-2 and 3.3-3 shows that generally, the system responses in Madison improve by a larger amount with increasing $C_e$ than their counterparts in Albuquerque. This is due to the fact that (as will be shown in Section 4.3) Albuquerque insolation is more consistent than Madison's. More consistent insolation will balance the storage tank energy flows better. Thus, increasing $C_e$ has a smaller effect in Albuquerque than in Madison.

A $2^2$ factorial design experiment was performed on the load patterns described above for Albuquerque with a standard storage. It was determined that the hours per day and days per week effects are fairly independent of each other. That is, the results in Figure 3.3-1 are indicative of the load hours per day effect, independent of how many days per week the load is distributed over. The reverse is true for the days per week effect of Figures 3.3-2 and 3.3-3.
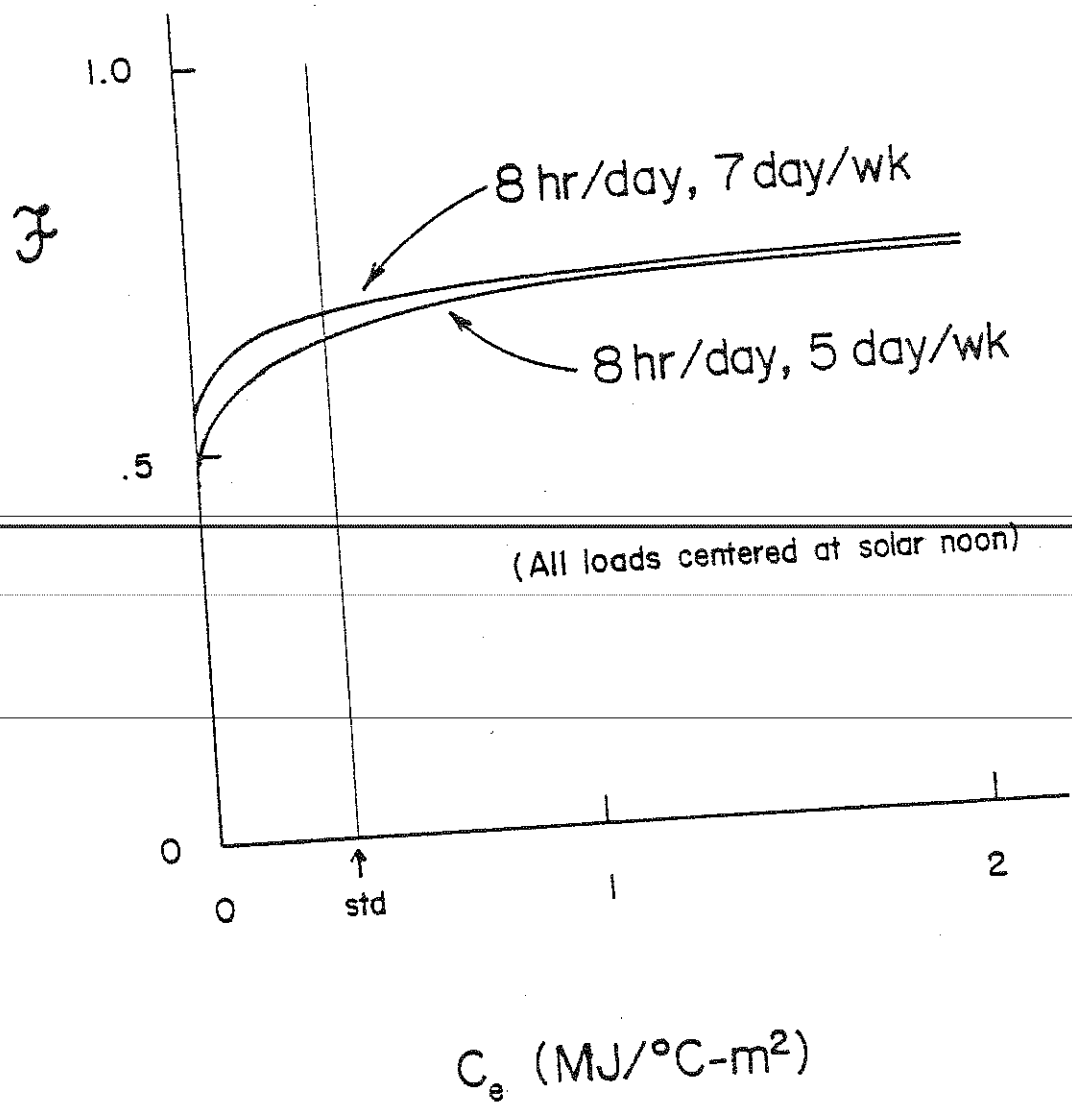
Figure 3.3-3:  Load days per week effect on system performance
(Madison)

The no storage cases, $C_e = 0$ in Figures 3.3-1 through 3.3-3, indicate that the load pattern makes a very sizable difference when there is no storage available. This indicates that systems without storage should be examined separately.

The simulated performance for a no storage system with a fixed total yearly load, and specific load pattern, is displayed in Figure 3.3-4 as a function of collector area. For the situation depicted in Figure 3.3-4, F is linear with collector area until approximately 600 m$^2$. At this point there begins to be certain peak insolation times (e.g., June at noon) that the collected energy exceeds the load demand on an instantaneous basis. Without storage, this excess energy is dumped resulting in the departure from linearity in Figure 3.3-4. As the collector area is increased still further, solar energy gradually meets and exceeds the instantaneous load demand more often. To meet the entire 8 hour per day, 5 days per week load of Figure 3.3-4, the collector area would have to be large enough to meet the load during periods of minimal insolation (e.g., a cloudy January morning).

All the previous results were arrived at through simulation. A less involved method of predicting system performance is the subject of the next section.

## 3.4 Predicting System Performance

The performance of closed load loop solar systems can be pre-

# NO STORAGE

## Albuquerque

$$T \min = 80° C \qquad Ld = 3.5 \text{ TJ/yr}$$



8 hr/day, 5 day/wk

$A \ (m^2)$
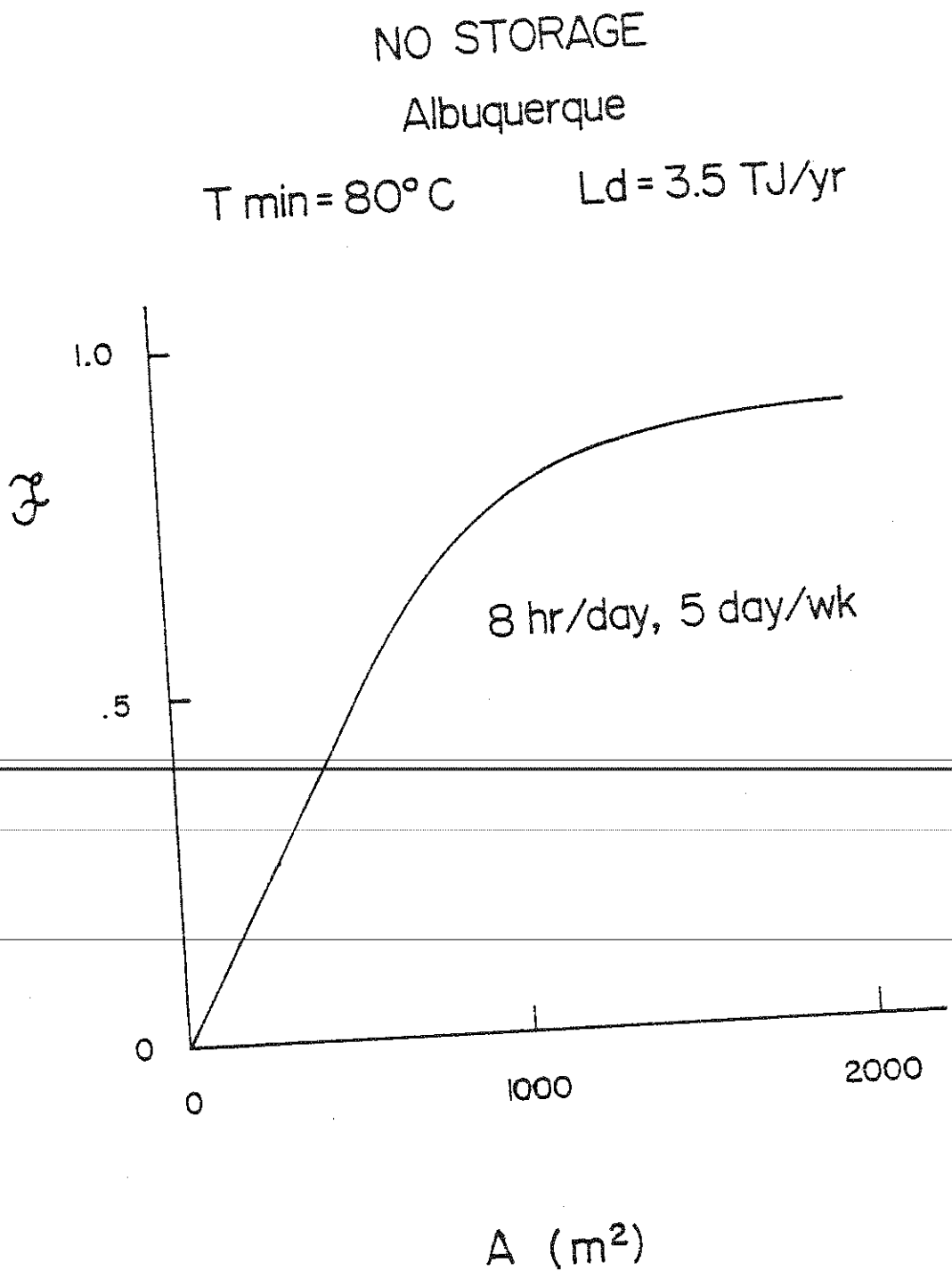
Figure 3.3-4: No storage system performance as a function of collector area

dicted through a detailed simulation or, the use of a statistical radiation relation known as utilizability. Computer simulations offer the most accurate available means of predicting systems performance. Unfortunately, simulations are difficult and time consuming to set up, and expensive to perform.

This section will first present the concepts of hourly and daily utilizability, for predicting long-term average, flat-plate collector performance. Then, the ability of an existing design method, based on daily utilizability, to predict closed load loop IPH system performance will be examined. Finally, a method of predicting the long-term average performance of no storage IPH systems employing flat-plate collector will be developed.

### 3.4.1 Definition of Utilizability

Utilizability was first presented by Whillier (42) as a method of predicting the long-term average performance of flat-plate collectors.

Starting with the Hottel-Whillier flat-plate collector equation,

$$Q_{u-hm} = A\, F_R \left[ I_{T-hm}(\tau\alpha) - U_L \left( T_{in} - T_a \right) \right] \qquad (3.4\text{-}1)$$

where:
- $h$ = hour of the day
- $m$ = month of the year
- $Q_{u-hm}$ = Useful collector output for hour h in month m
- $I_{T-hm}$ = Total hourly insolation on a tilted surface for hour h in month m
- $(\tau\alpha)$ = Collector transmittance absorptance product

$U_L$ = Overall collector loss coefficient

$T_{in}$ = Collector fluid inlet temperature

$T_a$ = Ambient temperature.

Setting $Q_{u-hm}$ in Equation 3.4-1 equal to zero, and solving for $I_{T-mh}$, a minimum isolation level for collector operation is defined.

$$I_{min} = \frac{F_R U_L \left(T_{in} - T_a\right)}{F_R (\tau\alpha)} \tag{3.4-2}$$

When $I_{T-mh}$ equals $I_{min}$, the collector's solar gains just balance its losses to ambient.

Monthly-average hourly utilizability is now defined as the long-term average fraction of the $m^{th}$ month's, $h^{th}$ hour's, total insolation that is above $I_{min}$.

$$\phi_{mh} = \frac{\sum_{y=1}^{Y} \sum_{d=1}^{D_m} \left(I_{T-mhyd} - I_{min-m}\right)^+}{\sum_{y=1}^{Y} \sum_{d=1}^{D_m} I_{T-mhyd}} \tag{3.4-3}$$

Where:  y = A particular year

Y = Number of years included

d = A particular day in month m

D = Number of days in month m

+ = Only positive values are to be summed.

To obtain a true long-term average, Y should be (40) at least ten years.  Since $I_{min}$ is assumed to be constant in Equation 3.4-3,

the long-term, monthly-average, day-time ambient temperature should

be used in Equation 3.4-2.

$$\overline{T}_{a-m} = \frac{\sum\limits_{y=1}^{Y} \sum\limits_{d=1}^{D_m} \sum\limits_{h=1}^{24} T_{a-mhdy}^{*}}{24 \quad YD_m \sum\limits_{h=1} 1^{*}} \qquad (3.4-4)$$

where the * indicates that only hours between sunrise and sunset are

to be considered. A graphical presentation of Equation 3.4-3 is

shown in Figure 3.4-1. For the sequence of days shown, is the

sum of the shaded areas divided by the sum of the total areas

for hour h.

The utilizability concept was extended by Klein (22) to in-

clude all hours of the day. Klein (22) defines monthly-average

daily utilizability as the long-term average fraction of the $m^{th}$

month's total insolation that is above $I_{min}$,

$$\overline{\phi}_m = \frac{\sum\limits_{y=1}^{Y} \sum\limits_{d=1}^{D_m} \sum\limits_{h=1}^{24} \left( I_{T-mydh} - I_{min-m} \right)^{+}}{\sum\limits_{y=1}^{Y} \sum\limits_{d=1}^{D_m} \sum\limits_{h=1}^{24} I_{T-mydh}} \qquad (3.4-5)$$

A graphical representation of this relation is shown in Figure

3.4-2. Here, $\overline{\phi}$ is the sum of the shaded areas divided by the sum

of the total areas under the curve. This relation for $\overline{\phi}$ has been

correlated, first by Klein (22) and later by Theilacker (40).
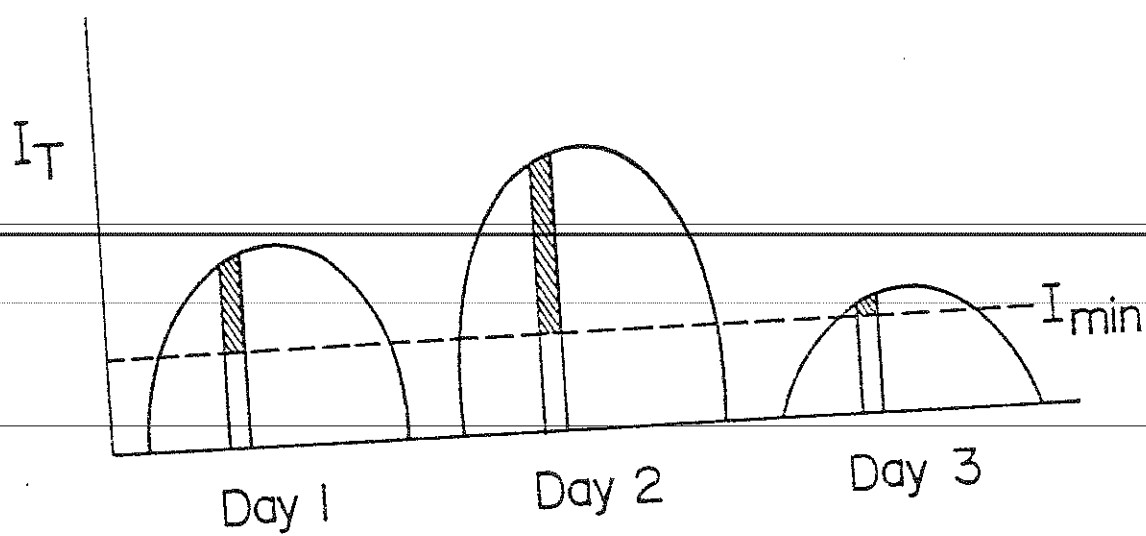
Figure 3.4-1:  Conceptual graphic representation of $\phi$.
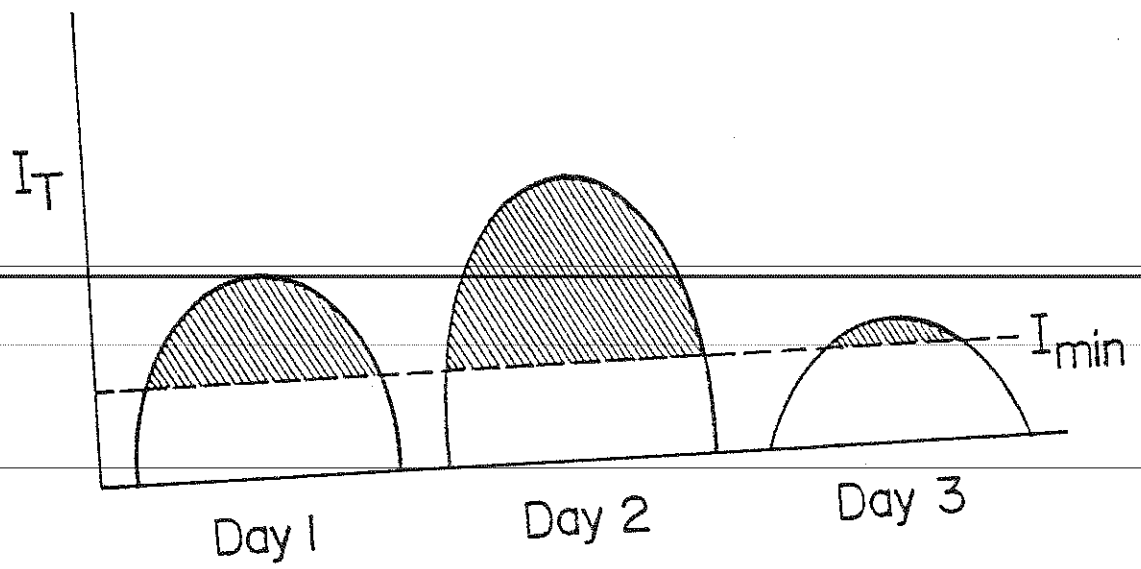
Figure 3.4-2: Conceptual Graphic representation of $\overline{\phi}$.

### 3.4.2  Using Utilizability

Monthly average daily utilizability was used by Klein and Beckman (25) to develop a generalized design procedure for closed load loop systems with storage. As will be shown, both monthly-average daily, and monthly-average hourly utilizability can be used to predict the performance of systems without storage. However, the hourly version is more general.

### 3.4.2a  Systems with storage

The generalized design method (25) for closed load loop systems like Figure 2.2-2, starts with the same assumptions that were used in the simulation given in Section 3.3. In addition to these, the load is taken to be 12 hours per day, 7 days per week for energy collection and storage calculations. The design method then accounts for storage tank heat losses, finite storage capacity, and finite load heat exchangers.

Since different load patterns with the same yearly total load have different load rates, different patterns can be accounted for in finite load heat exchanger calculations. This is the extent of the design procedure's ability to predict load pattern effects, because of the assumed load pattern in the energy collection and storage calculations. Recalling Figures 3.3-1 through 3.3-3 it can be seen that the load pattern is of minor effect so this treatment should not be too far off.

A comparison of the design method ($\bar{\phi}$-FCHART (25)) and simulation results is shown in Figure 3.4-3. Since the load heat exchanger was assumed infinite and the tank heat losses zero for both cases, the difference shown here is due to the treatment of collected and stored energy. For a system with an infinite load heat exchanger, the FCHART curve of Figure 3.4-3 is the only one attainable. This is because FCHART does not account for the load distribution in energy collection and storage calculations.

### 3.4.2b  Systems with no storage

For systems without storage, the collector inlet temperature will always be $T_{min}$. Thus, $I_{min}$ will not be a function of a fluctuating tank temperature, and utilizability methods can be used directly. Finite load heat exchangers can be accounted for by modifying $F_R$ in the same way (15) as for collector loop heat exchangers, in systems with storage. This allows the direct use of utilizability for all no storage systems.

Rewriting Equation 3.4-1 in terms of $\phi$, the long-term average minimum useful energy for month m is:

$$\bar{Q}_{u-m} = A_e D_m (\tau\alpha) \sum_{h=1}^{24} \bar{I}_{T-mh} \phi_{mh} \qquad (3.4-6)$$

where $\bar{I}_{T-mh}$ is the long-term average hourly insolation on a tilted surface, for hour h in month m. The corresponding equation based on $\bar{\phi}$ is:

Albuquerque

$A = 750 \, m^2$      $Ld = 3.5 \, TJ/yr$

$Slope = 35°$      $T \, min = 80° \, C$

$\mathcal{F}$

1.0

Simulation (TRNSYS)

Design Method (FCHART)

Heat Exchangers:
Collector - Perfect
Load - Infinite

.5

(Both loads 12 hr/day, 7 day/wk
centered at solar noon)

0

0      1      2

$C \quad (MJ/°C\text{-}m^2)$
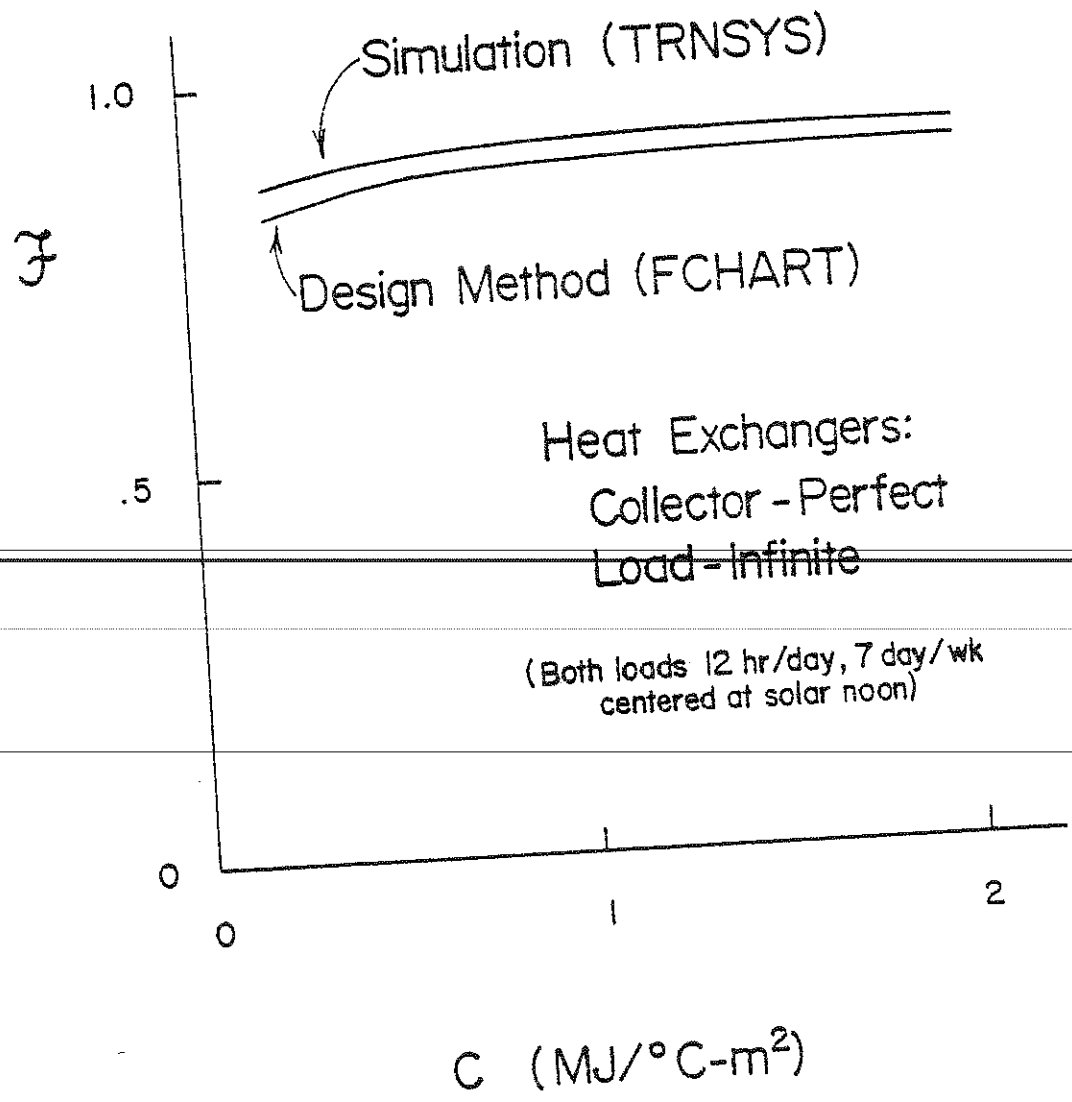
Figure 3.4-3:  Comparison of simulation and closed load loop
design method.

$$\overline{Q}_{u-m} = A_e D_m \ (\overline{\tau\alpha}) \ \overline{H}_{Tm} \ \overline{\phi}_m$$ 

(3.4-7)

where $\overline{H}_{Tm}$ is the long-term average total daily insolation on a tilted surface for month m. (This relation is only valid for no-storage systems when the load spans the entire day's insolation.)

Equations 3.4-6 and 3.4-7 are linear with collector area. This is reminiscent of the $\overline{F}$ vs. A plot of Figure 3.3-4. If the collector area were such that the load were always greater than $Q_u$ on an instantaneous basis, and the load duration spanned the days insolation, then all the collected energy could be used by the load. For applications that the load is not always greater than $Q_u$ and/or does not span the days insolation, energy dumping will occur. This must be estimated before system performance can be deter-mined.

Setting the instantaneous collector output equal to the in-stantaneous load, a maximum usable insolation level can be defined for no storage systems:

$$\dot{Q}_u = \dot{L}d = A_e \left[ I_{max}(\tau\alpha) - U_L \left( T_{in} - \overline{T}_a \right) \right]$$ 

(3.4-8)

Solving for $I_{max}$ we have:

$$I_{max} = I_{min} + \frac{\dot{L}d}{A_e \ (\tau\alpha)}$$ 

(3.4-9)

Monthly-average hourly and daily unutilizabilities can now be defined by replacing $I_{min}$ with $I_{max}$ in Equations 3.4-3 and 3.4-5.

$$\phi'_{mh} = \frac{\sum\limits_{y=1}^{Y} \sum\limits_{d=1}^{D_m} \left( I_{T\text{-mhyd}} - I_{max\text{-}m} \right)^{+}}{\sum\limits_{y=1}^{Y} \sum\limits_{d=1}^{D_m} I_{T\text{-mhyd}}} \qquad (3.4\text{-}10)$$

and

$$\overline{\phi}'_{m} = \frac{\sum\limits_{y=1}^{Y} \sum\limits_{d=1}^{D_m} \sum\limits_{h=1}^{24} \left( I_{T\text{-mydh}} - I_{max\text{-}m} \right)^{+}}{\sum\limits_{y=1}^{Y} \sum\limits_{d=1}^{D_m} \sum\limits_{h=1}^{24} I_{T\text{-mydh}}} \qquad (3.4\text{-}11)$$

A graphical representation of $\overline{\phi}'$ is shown in Figure 3.4-4. Here, $\overline{\phi}'$ is the shaded area in day 2 divided by the total area for all 3 days.

The long-term average amount of energy that would be dumped by a no storage system is

$$\overline{Q}_{dump\text{-}m} = A_e D_m (\tau\alpha) \sum\limits_{h=1}^{24} \overline{I}_{T\text{-mh}} \; \phi'_{mh} \qquad (3.4\text{-}12)$$

or

$$\overline{Q}_{dump\text{-}m} = A_e D_m (\tau\alpha) \; \overline{H}_{T\text{-}m} \; \overline{\phi}'_{m} \qquad (3.4\text{-}13)$$

(Equation 3.4-13 is restricted as Equation 3.4-7 was.)

The long-term average energy supplied to the load for month m can now be written as:

$$\overline{Q}_{sup\text{-}m} = \overline{Q}_{u\text{-}m} - \overline{Q}_{dump\text{-}m} \qquad (3.4\text{-}14)$$
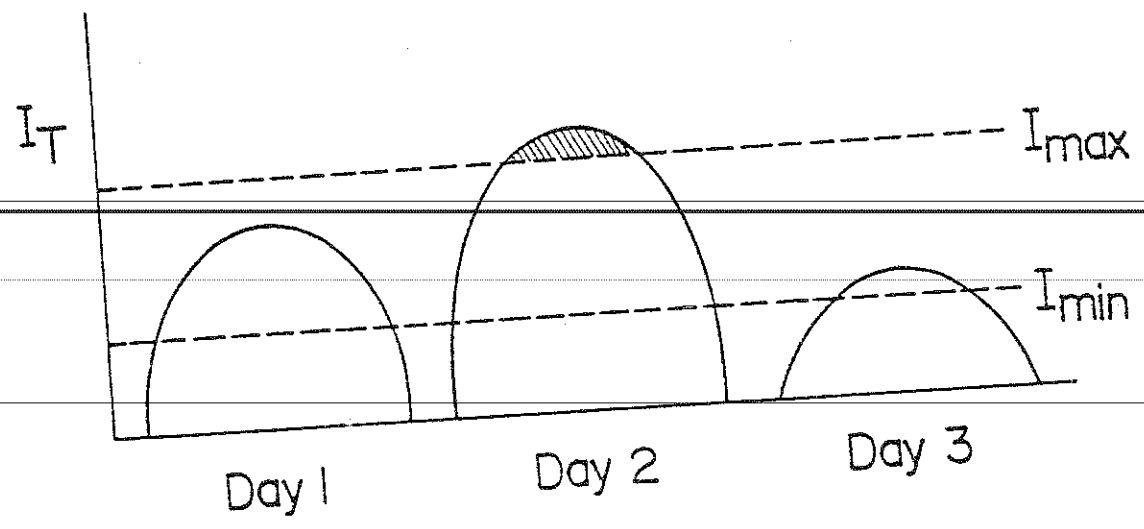
Figure 3.4-4:   Conceptual graphic representation of $\overline{\phi}'$

If the load is of sufficient duration to span the entire day's insolation, $\overline{Q}_{sup}$ (corresponding to the 3 day sequence we have been following) is the shaded area of Figure 3.4-5 times $A_e (\tau\alpha)$. This can be expressed as

$$\overline{Q}_{sup-m} = A_e D_m (\tau\alpha) \sum_{h=1}^{24} \overline{I}_{T-mh} \left( \phi_{mh} - \phi'_{mh} \right) \qquad (3.4\text{-}15)$$

or

$$\overline{Q}_{sup-m} = A_e D_m (\tau\alpha) \overline{H}_{T-m} \left( \overline{\phi}_m - \overline{\phi}'_m \right) \qquad (3.4\text{-}16)$$

Rewriting Equation 3.3-1 in monthly form, the long-term average annual fraction of the load net by solar is:

$$F = \frac{\sum\limits_{m=1}^{12} \overline{Q}_{sup-m}}{\sum\limits_{m=1}^{12} Ld_m} \qquad (3.4\text{-}17)$$

where either Equation 3.4-15 or 3.4-16 (if appropriate) can be used for $\overline{Q}_{sup-m}$.

To account for different load distributions for no storage systems is a relatively simple matter. If the load spans the days insolation, either $\phi$ or $\overline{\phi}$ can be used. If the load is off during some of the daylight hours, $\phi$ must be used ($\phi$ for no-load hours is zero). Accounting for the number of hours per day the load is on, $\overline{Q}_{sup}$ can be calculated for a 7 day per week load. For loads other
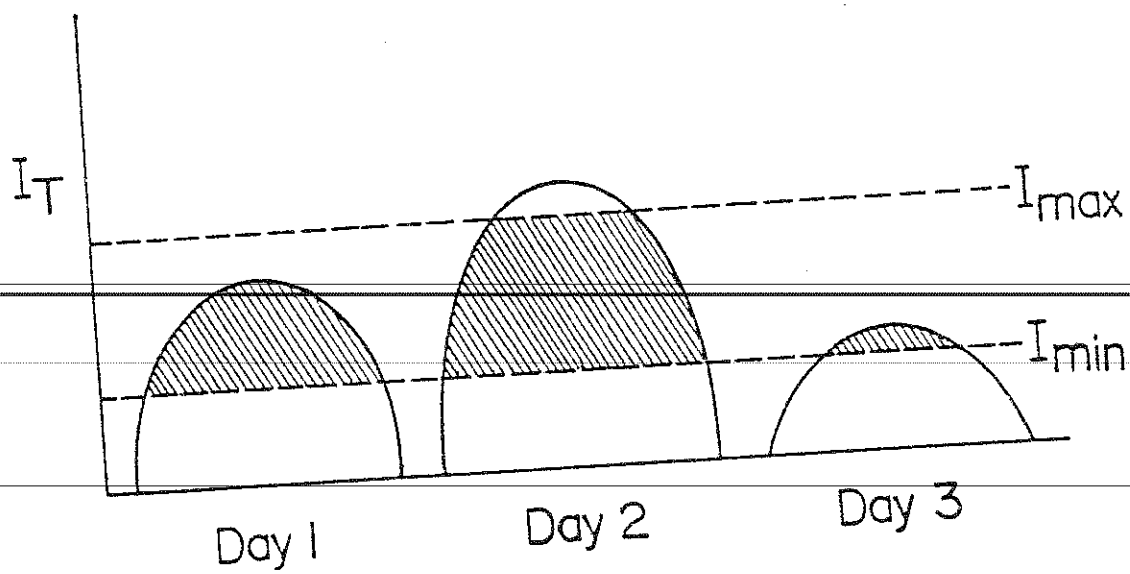
Figure 3.4-5:  Conceptual graphic representation for
$\overline{Q}_{sup}/A_e \ (\tau\alpha)$

than 7 days per week, multiply the value arrived at above by the weeks fraction (e.g., 5/7 for a 5 day a week load, 3.5/7 for an alternate day load).

There may be instances when $\phi$ is better suited for Q supply calculations than $\bar{\phi}$. Since $\bar{\phi}$ is across the whole day, the critical insolation levels $I_{min}$ and $I_{max}$ are taken to be constant. In reality, the load requirements may change $T_{min}$ (and thus $I_{min}$ and $I_{max}$ for no storage systems) throughout the day. Also, the load rate may change throughout the day changing $I_{max}$. In both of these cases, $\phi$ is much better suited to predict $\bar{Q}$ supply. One other advantage of $\phi$ over $\bar{\phi}$ is that using $\phi$ will give more information about the distribution of required auxiliary energy. This may be important in designing a complete working energy system. Daily utilizability has one distinct advantage, it has a factor of about 8 fewer calculations than hourly utilizability. An example of using $\phi$ is presented in the next section.

3.5  Conclusions

The simulated system performance of closed load loop systems indicates that for the same total yearly energy load, the number of days per week the load is distributed over has more of an effect than does the number of hours per day. For large storage sizes, the load pattern has a minimal effect and the performance can be predicted by the $\bar{\phi}$-FCHART design method. For systems with no

storage, the system performance can be determined from utilizability concepts. Hourly utilizability is more versatile but the calculations are more laborious than for daily utilizability.

Daily utilizability has been well treated by Klein (22), Theilacker (40), and Collares-Pereira and Rabl (14). At this point, hourly utilizability is not as well refined. It will be examined in detail in the next chapter.

# 4. MONTHLY-AVERAGE HOURLY UTILIZABILITY

## 4.1 Introduction

This chapter first presents the concept of monthly-average hourly utilizability, as originally formulated by Whillier (42). The results of analyzing 23 years of insolation data by this method are presented for 2 locations. Next, generalized hourly utiliza- bility as presented by Liu and Jordan (30) is re-examined. It is shown that this method has a number of shortcomings in predicting $\phi$. This method is consequently improved and extended. An analytical expression for $\phi$ is then derived from a random insolation sequence probability distribution. The two methods of estimating $\phi$ s are compared with $\phi$ s calculated from data. The comparison indicates that both methods adequately predict usable energy, but the analyti- cal method can give a better prediction of dumped energy for a no storage system. Finally, an example of the use of both methods for predicting no storage system performance is presented.

## 4.2 Interpretation of monthly-average hourly utilizability

Recalling the definition of $\phi$ from Chapter 3, it can be ex- pressed as

$$\phi_{mh} = \frac{\sum\limits_{y=1}^{Y} \sum\limits_{d=1}^{D_m} \left( I_{T-mhyd} - I_{c-m} \right)^+}{Y \, D_m \overline{I}_{T-mh}} \qquad (4.2-1)$$

38

where $I_c$ is the critical insolation level of interest, and $\overline{I}_T$ is the long-term average hourly insolation on a tilted surface.

Monthly-average hourly utilizability is a statistical parameter that indicates the long-term average fraction of the incident insolation occurring in hour h and month m, that is above $I_c$. The basis of this concept is that insolation levels for hour h change from day-to-day in a rather random fashion.

The effect of insolation variation from day-to-day on $\phi$ is displayed in Figure 4.2-1. Here, both sequences of days have the same average and total insolation for the indicated hour. The first sequence, with its large insolation variation, has more insolation above $I_c$ than does the second sequence, which has 3 identical days. Thus, sequence A has a larger hourly $\phi$ than B.

Another graphical representation of Equation 4.2-1 is presented in Figure 4.2.2. Here, observed insolation values, for a particular hour and month, are plotted in ascending order as a function of f, the cumulative frequency of occurrence. An f of zero coincides with the minimum, and an f of 1 the maximum, observed $I_T$. The total area under this curve equals $\overline{I}_T$. The $\phi$ for the situation depicted in Figure 4.2-2 is the shaded area divided by the total area.

Graphically integrating Figure 4.2-2 for various values of $I_c$ results in the $\phi$-curve plotted in Figure 4.2-3. The critical ratio used for the independent variable is:
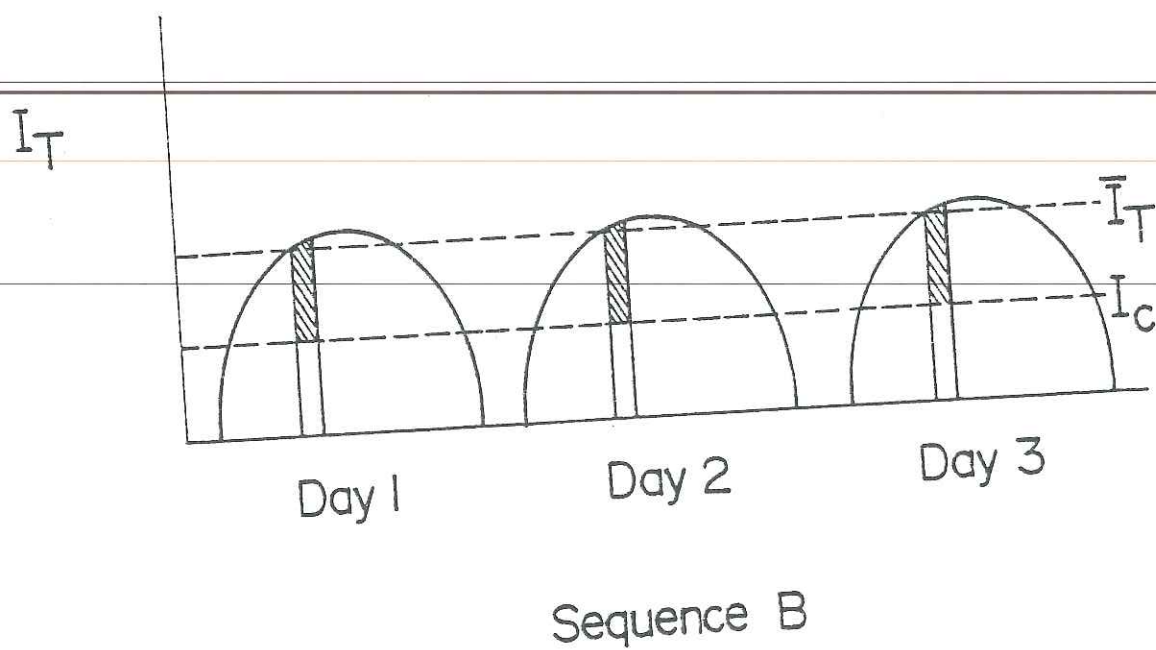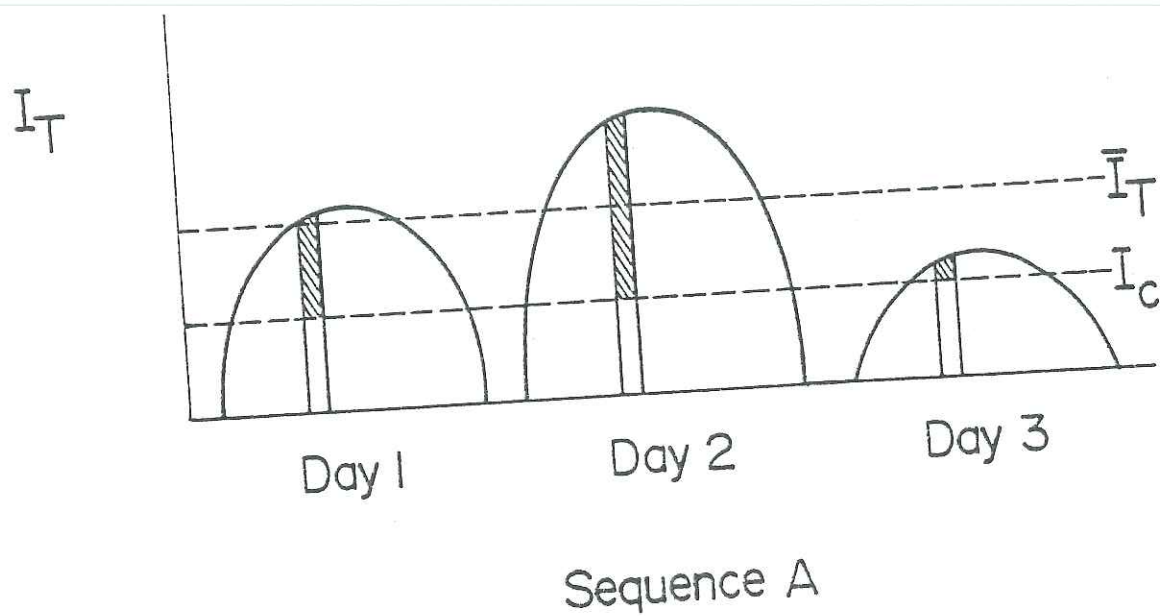
Figure 4.2-1:  Effect of insolation variation on φ.
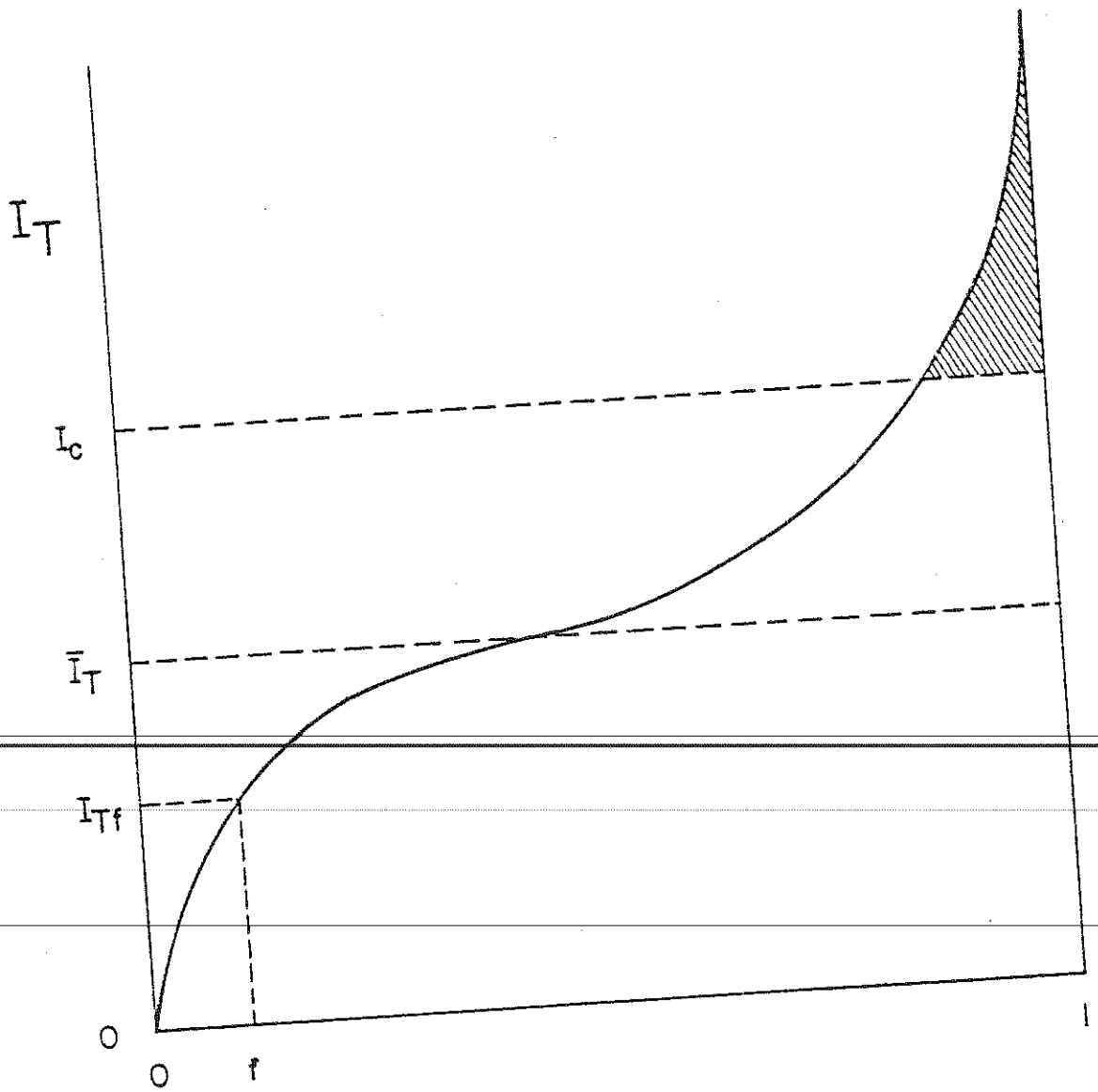
Figure 4.2-2:  Cumulative frequency of $I_T$ for determining $\phi$.
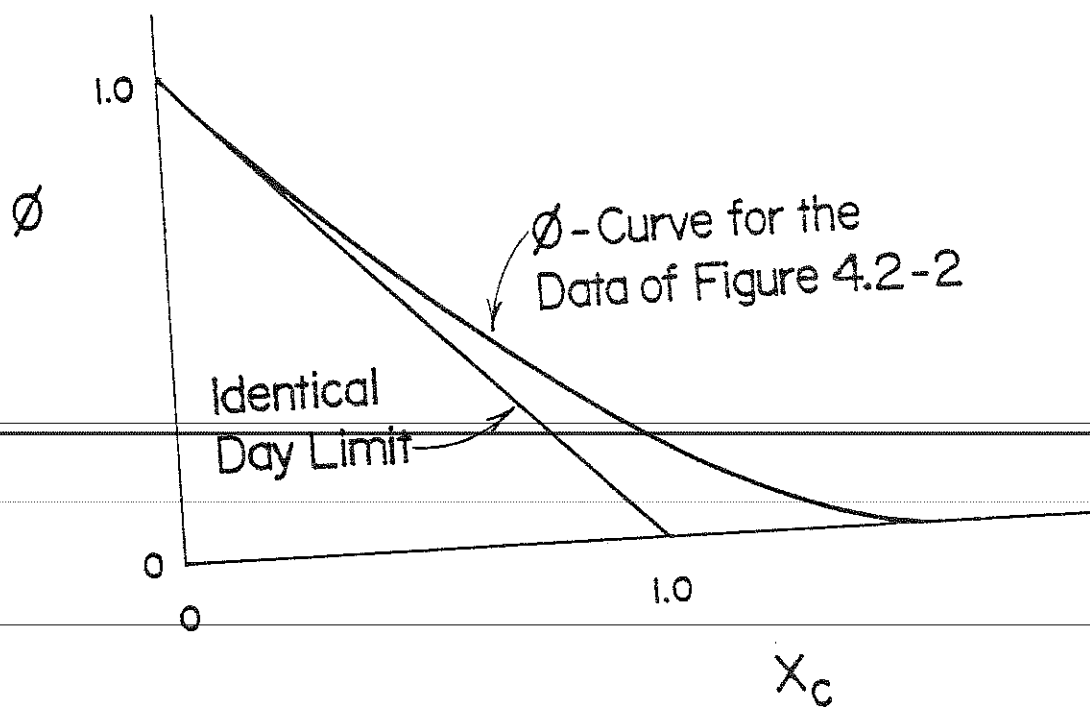
Figure 4.2-3:  Hourly utilizability by integration of
Figure 4.2-2.

$$X_c = \frac{I_c}{\overline{I}_T} \qquad\qquad (4.2-2)$$

This dimensionless form of the critical level has been found (42, 30) to be a useful independent variable for plotting $\phi$.

A few points about the shape of the $\phi$-curve of Figure 4.2-3 are of particular interest. If all the i-hours of month j had the same value for $I_T$ (as in Figure 4.2-1b) the resulting frequency distribution corresponding to Figure 4.2-2 would consist of a straight horizontal line at $\overline{I}_T$. Integration of a curve of this form would result in the straight line $\phi$-curve labeled "identical day limit" in Figure 4.2-3. For this situation, there would be no isolation above a critical ratio of unity. This is indicated by a $\phi$ of zero for the identical day limit, when $X_c \geq 1$.

Any real data, however, has a distribution much the same in shape as the data plotted in Figure 4.2-2. The tail near $f = 1$ results in an elongated $\phi$-curve at higher critical ratios, as shown in Figure 4.2-3.

The next section presents calculated $\phi$ s using the method depicted in Figure 4.2-2 for data covering a 23 year period. The results of this calculation are actual long-term average hourly utilizability curves.

4.3 Calculation of Hourly Utilizability for Hourly Insolation Data

The calculation of hourly utilizability for a particular loca-

tion can be performed quite easily with the aid of a computer.

Starting with hourly total insolation on a horizontal surface (assumed constant over the hour), $I_T$ can be obtained from:

$$I_T = I \ R \qquad (4.3-1)$$

where I is the total hourly insolation on a horizontal surface and R is the ratio of total hourly insolation on a tilted surface, to that on a horizontal surface. The hourly insolation ratio (16) is given as:

$$R = \left(1 - I_d/I\right) \ R_b + I_d/I \left(\frac{1 + \cos\beta}{2}\right) \qquad (4.3-2)$$
$$+ \ \rho \left(\frac{1 - \cos\beta}{2}\right)$$

where:

$I_d$ = Hourly diffuse ratiation on a horizontal surface

$R_b$ = Ratio of beam radiation on a tilted surface, to that on a horizontal surface

$\beta$ = Collector slope

$\rho$ = Ground reflectance

The three components of Equation 4.3-2 can be interpreted as: 1) the fraction of the total radiation that is beam, times the ratio of hourly beam radiation on a tilted surface to that on a horizontal surface, 2) the fraction of the total radiation that is diffuse, times the collector-sky view factor, and 3) the total radiation re-

flected off the ground, times the collector-ground view factor.

The two diffuse terms in Equation 4.3-2 assume that the diffuse radiation is isotropic over the sky and ground. This results in a conservative estimate of $I_T$. If the diffuse radiation were not assumed isotropic, it would be centered more about the sun (or posibly the horizon). The collector, being tilted to receive radiation from the suns position in the sky (also sees the horizon better), would see more diffuse radiation if it is anisotropic than if it had been isotropic. Thus, the isotropic assumption is conservative. Throughout this study $\rho$ will be taken as 0.2. This also gives a conservative estimation of $I_T$, because often, in the winter when there may be snow on the ground, the ground reflectance is as high as .7.

The hourly beam radiation geometry factor, $R_b$ in Equation 4.3-2, is determined solely on the earth-sun-collector geometry, (16) and is given as:

$$R_b = \frac{\sin\delta\sin L\cos\beta - \sin\delta\cos L\sin\beta\cos\psi + \cos\delta\cos L\cos\beta\cos\omega + \cos\delta\sin L\sin\beta\cos\psi\cos\omega + \cos\delta\sin\beta\sin\psi\sin\omega}{\sin\delta\sin L + \cos\delta\cos L\cos\omega}$$

(4.3-3)

which can be expressed equivalently as

(4.3-4)

$$R_b = \cos\theta_T/\cos\theta_z$$

where;

$\delta$ = Declination angle

$L$ = Latitude (north positive)

$\psi$ = Collector azimuth angle (west positive)

$\omega$ = Hour angle

$\theta_T$ = Angle of incident beam radiation on a titled surface

$\theta_z$ = Solar zenith angle

The declination angle is a simple matter of geometry, and is related to the day of the year, n, by:

$$\delta = 23.45 \sin\left(\frac{360}{365}(284 + n)\right) \tag{4.3-5}$$

The hourly beam radiation geometry factor is plotted in Figure 4.3-1, as a function of hour angle, for a collector slope equal to the latitude of 45°. The two extreme months are shown.

Relations for the hourly diffuse fraction, $I_d/I$, have been developed using the hourly clearness index, defined as:

$$k_T = I/I_o \tag{4.3-6}$$

where $I_o$ is the hourly extraterrestrial radiation on a horizontal surface. It has been found by experiment and geometry (16) to be:

$$I_o = G_{sc} \cos\theta_z \left\{1 + 0.033 \cos\left(\frac{360\,n}{365}\right)\right\} \tag{4.3-7}$$

where $G_{sc}$ is the solar constant (1353 W/m$^2$).

$\beta = \mathcal{L} = 45°$
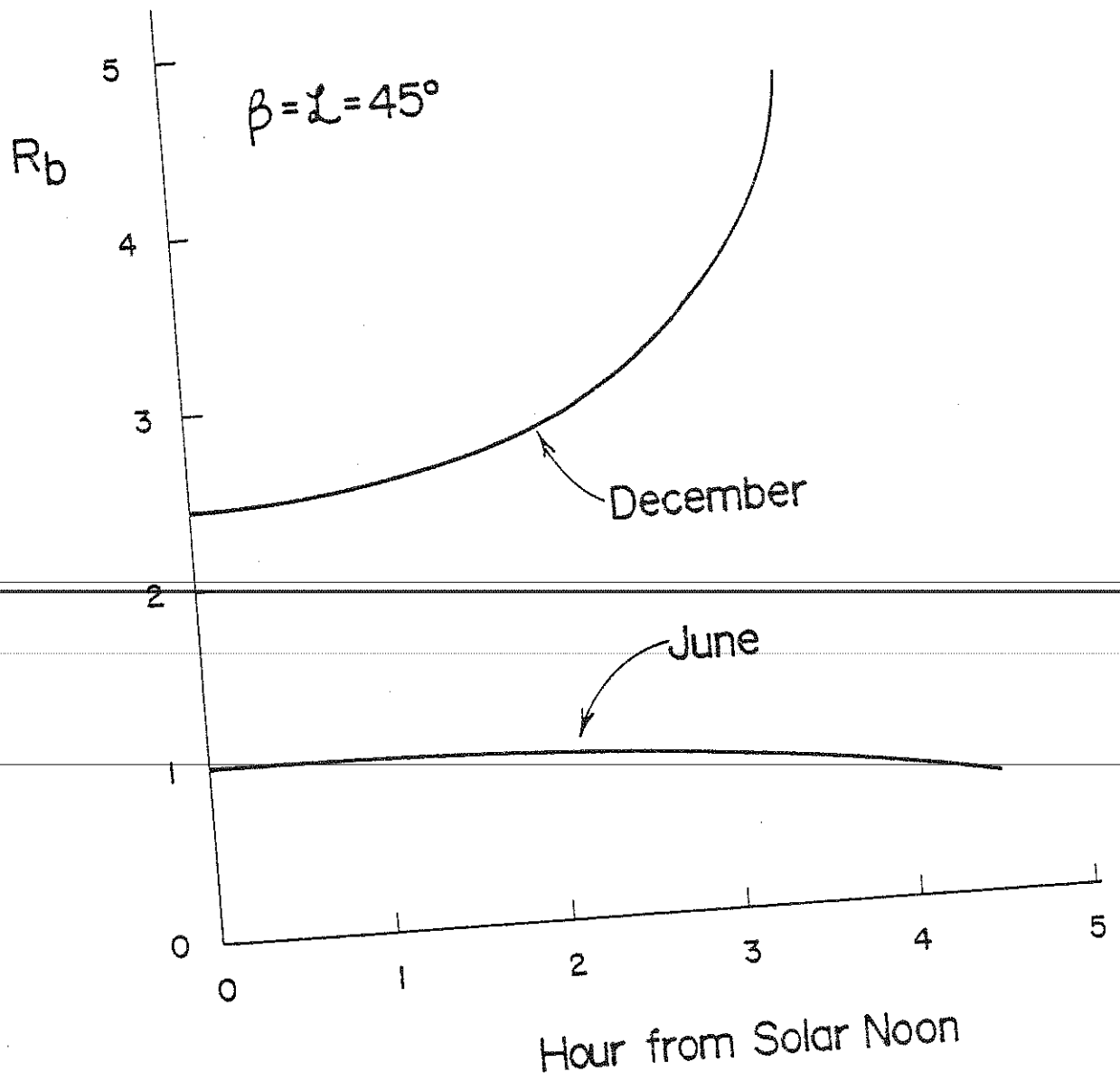
Figure 4.3-1: $R_b$ as a function of season and time from solar noon.

There have been many diffuse fraction correlations presented for daily data (6, 9, 10, 13, 29, 34, 36, 41). The data indicate (34, 13) that a daily diffuse fraction correlation is representative of hourly values as well. At this date, the correct correlation is not known with real certainty. Since the Liu and Jordan (29) correlation is in common use (TRNSYS), and it seems to give acceptable results, it will be used throughout this study. Using their correlations will also make comparisons with past studies more direct. A curve fit (24) to the Liu and Jordan daily diffuse fraction curve resulted in the following diffuse fraction correlation (to be used on a hourly basis).

$$I_d/I = 1.0045 + 0.04349\, k_T - 3.5227\, k_T^2 + 2.6313\, k_T^3 \quad (4.3\text{-}8)$$

This relation is shown in Figure 4.3-2. As expected, the clearer the sky, the smaller the diffuse fraction and vice versa. A detailed discussion of diffuse correlations in Section 4.4.3 indicates that using a different correlation has little effect on $\phi$.

Using the above relations, R is plotted in Figure 4.3-3 as a function of $k_T$ for various values of $R_b$. As indicated, R is a stronger function of $k_T$ for larger values of $R_b$.

Three computer programs were developed to calculate $\phi$ s from data. PREPHI uses Equations 4.3-1 through 4.3-8 to convert I s to $I_T$ s, RADAVE calculates $\overline{I}_T$ s, and HRPHIXC calculates $\phi$ s and $X_c$ s
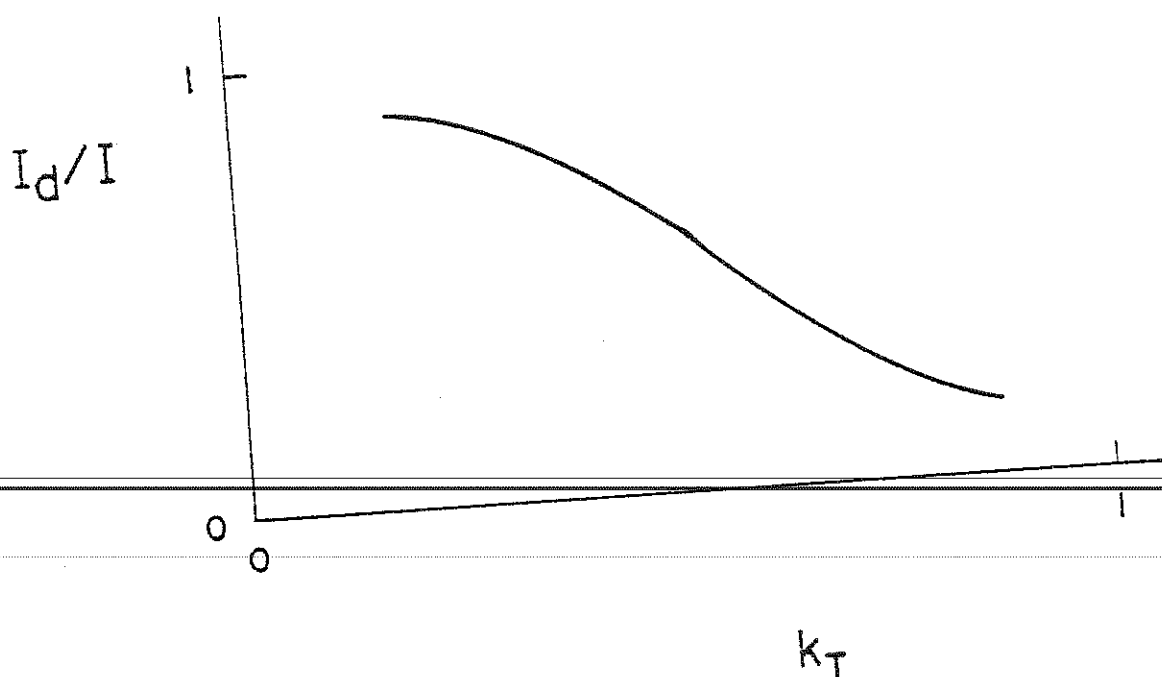
Figure 4.3-2:  Liu and Jordan daily (assumed hourly) diffuse fraction correlation
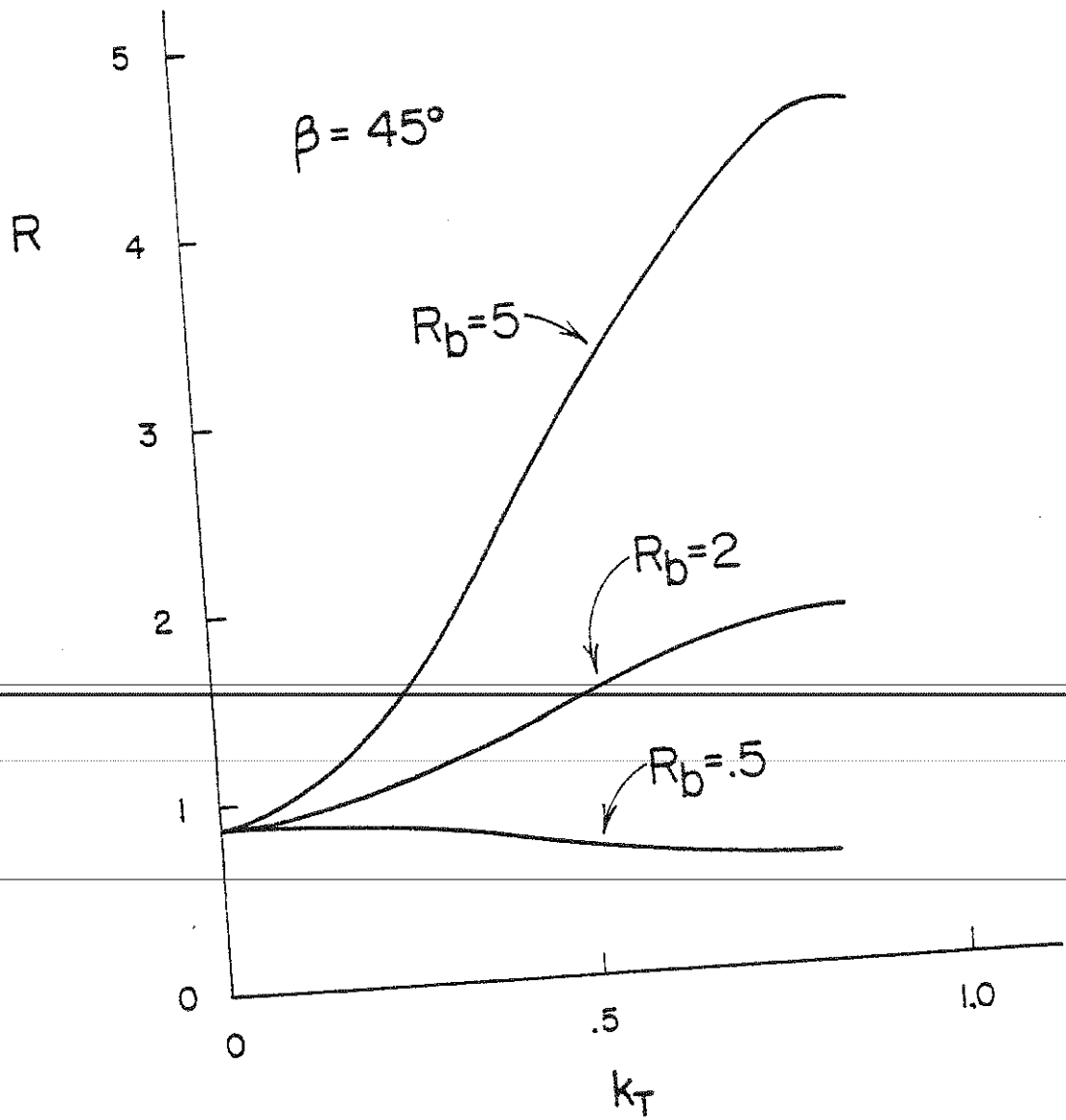
Figure 4.3-3:   R as a function of $R_b$ and $k_T$

according to Equations 4.2-1 and 4.2-2. These programs are listed in Appendix C.

The above 3 programs were used with 23 years of hourly insolation data (38) for Madison and Albuquerque, with south facing collectors and $\beta=L$. Some of the resulting long-term, monthly-average hourly utilizability curves, for Madison are in Figure 4.3-4, and for Albuquerque in Figure 4.3-5.

The curve identified as 1/2 hour from noon represents the pair of hours centered 1/2 hour from solar noon (hours 11 to 12 and 12 to 13). Over the 23 year period, the occurrence of morning and afternoon insolation was such that the same $\phi$-curve was obtained for each hour pair from noon. This means that for $\phi$-curve purposes, the $I_T$ distributions of Figure 4.2-2 can be considered equivalent for hours symmetric about noon. This same phenomena was observed by Theilacker (40) for Miami, Fort Worth, and Seattle.

In general, the Albuquerque $\phi$-curves are much closer to the identical day limit than are the Madison curves. This is because Albuquerque has less insolation variation from day-to-day.

Examination of the $\phi$-curves of Figures 4.3-4 and 4.3-5 reveals that, in the winter, $I_T$ has more variation about its mean for hours further from noon. Recalling Figures 4.3-1 and 4.3-3, one reason for this trend becomes apparent. Since $R_b$ is larger for hours further from noon, observed values of I get multiplied by a wider range of R values than would hours closer to noon with
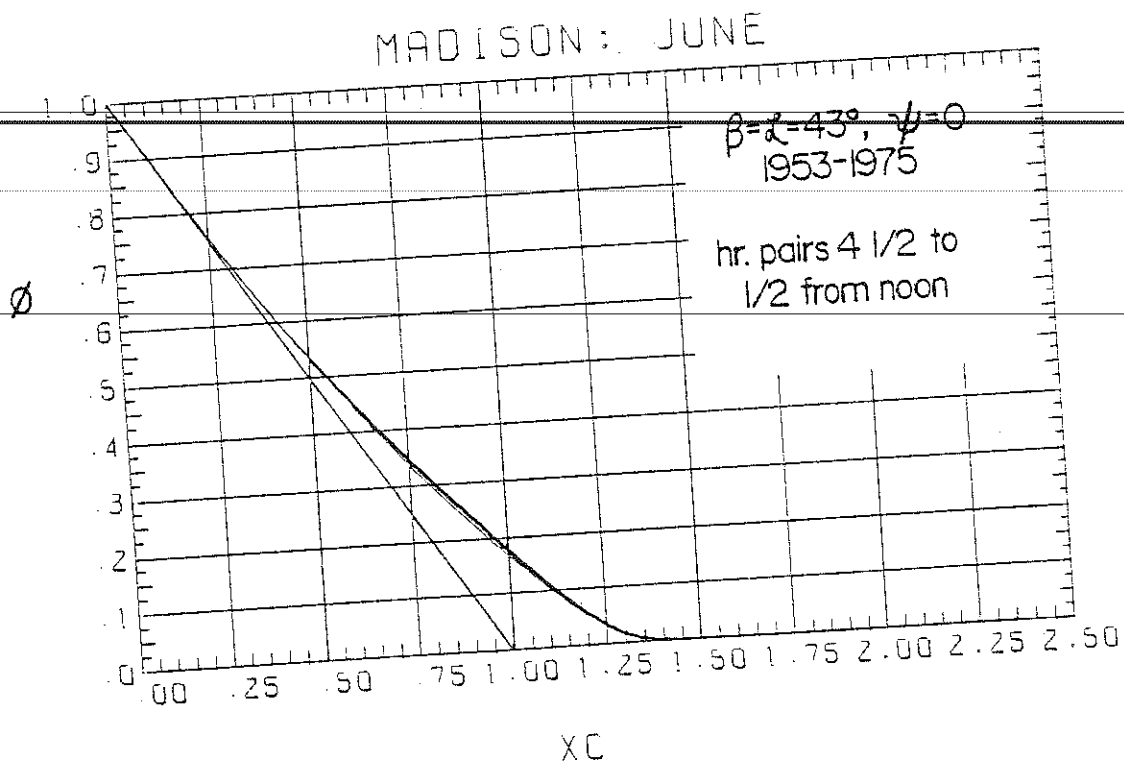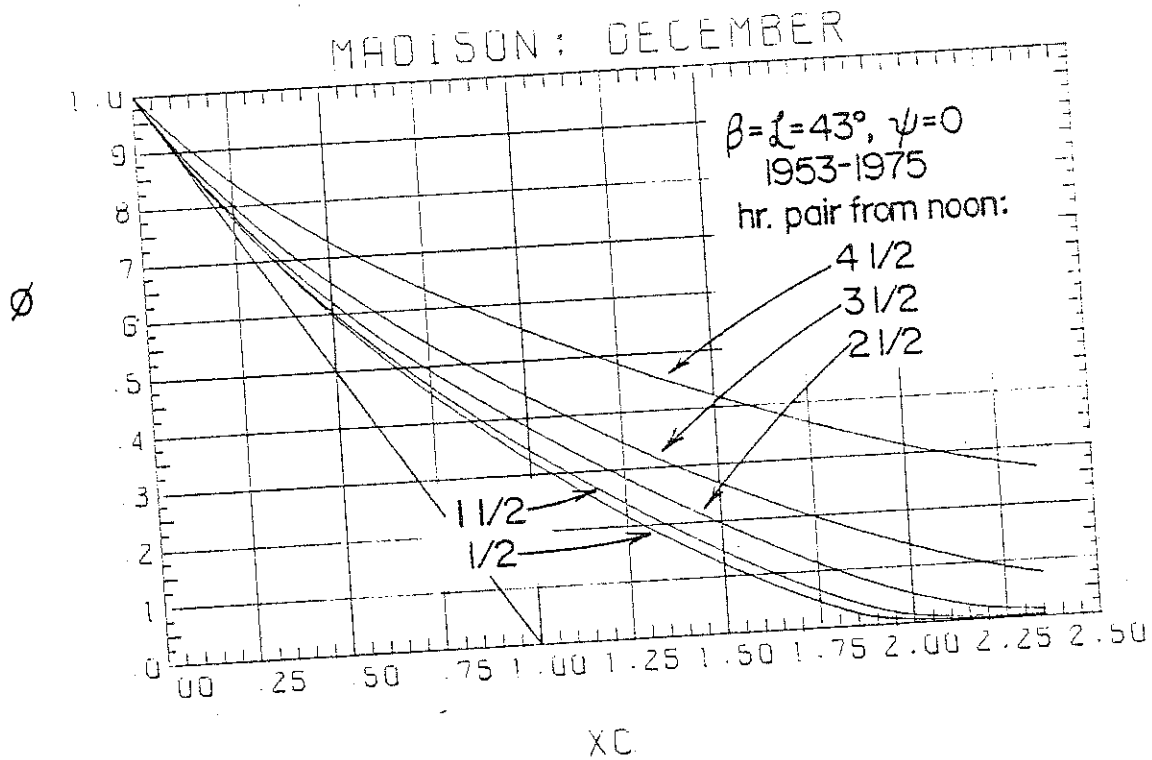
Figure 4.3-4: φ-curves based on 23 years of Madison data (β=L)
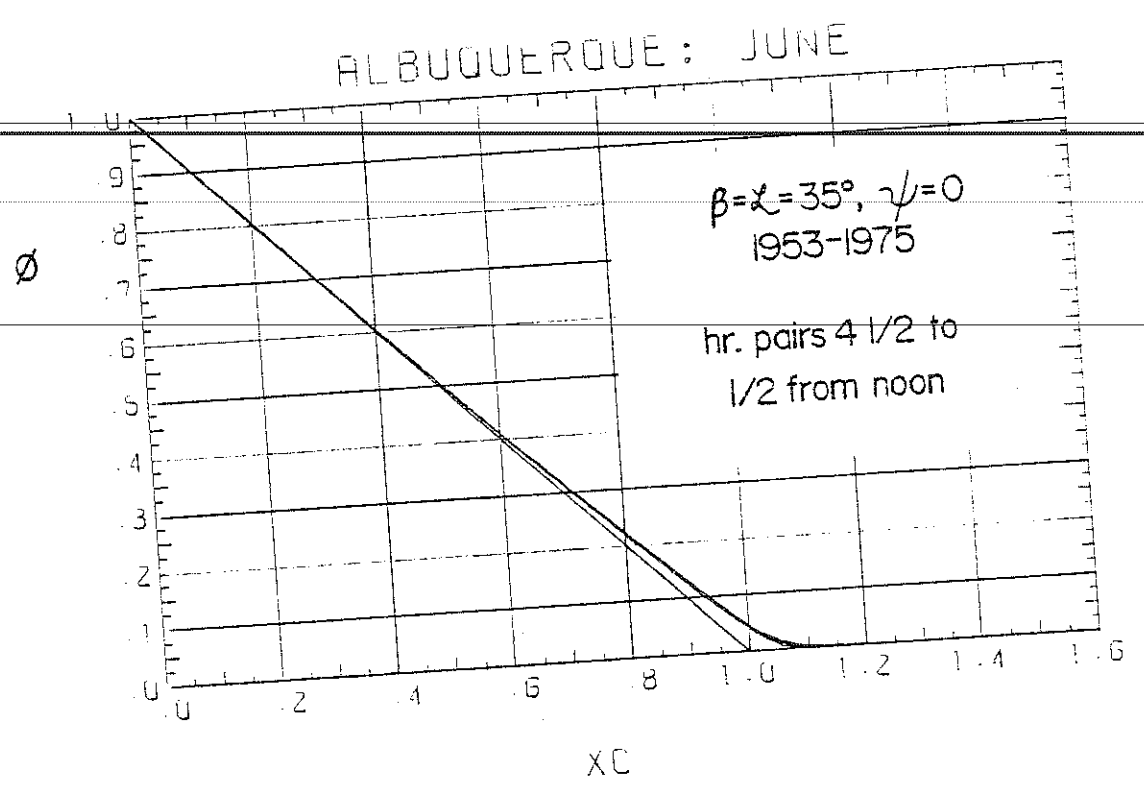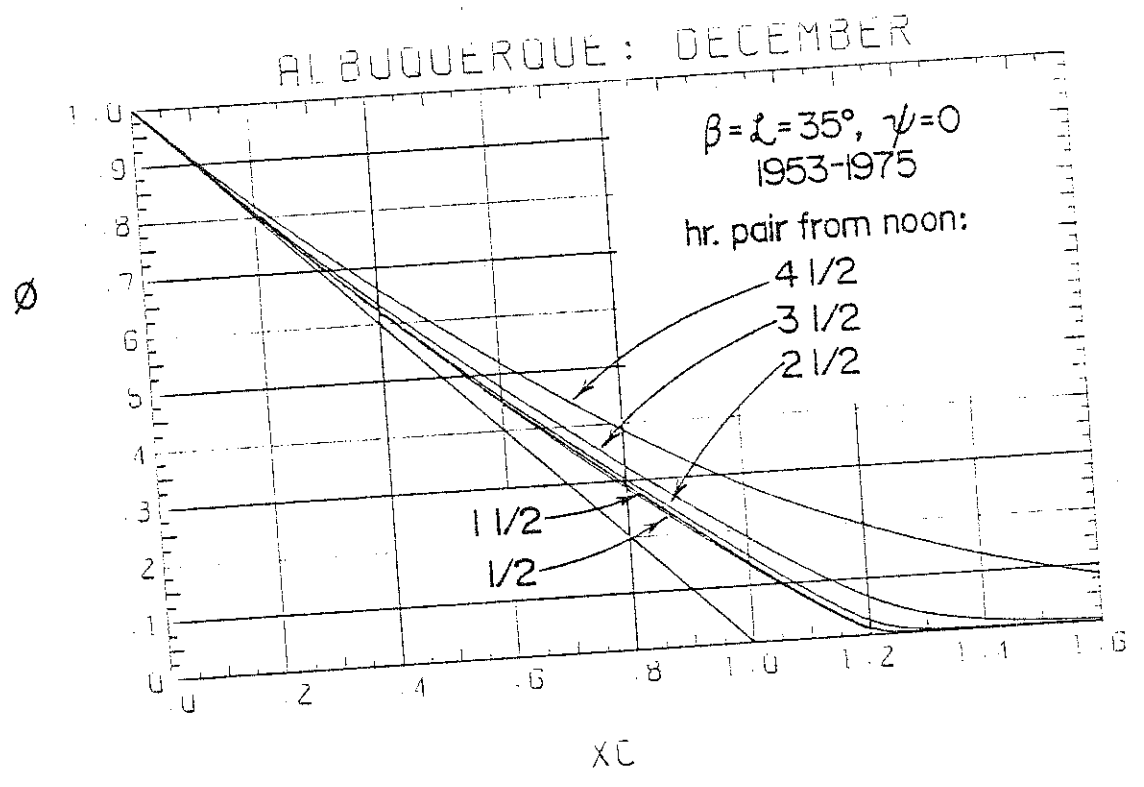
Figure 4.3-5: φ-curves based on 23 years of Albuquerque data (β=L)

the same variation in $k_T$. This results in a larger variation in $I_T$ and a corresponding $\phi$-curve elongation for hours further from noon. The magnitude of this effect can be seen by examining the Madison December $\phi$-curves calculated for a horizontal surface in Figure 4.3-6. These curves both fall closer to the identical day limit, and have less spread between them, than the tilted surface $\phi$-curves that were affected by R. The other reason for the spread between both tilted surface and horizontal $\phi$-curves will become apparent in the next section.

Figures 4.3-4 through 4.3-6 indicate that a different $\phi$-curve is obtained for every different hour, month, location, and collector orientation. This variability, along with the large amount of computing required, makes calculating $\phi$ an unattractive method of predicting long-term average collector performance. The next section deals with generalizing the $\phi$ calculation from long-term average insolation statistics.

## 4.4 Generalized Hourly Utilizability

The method of calculating the long-term average hourly utilizability presented in the previous section does not readily adapt itself to a general situation. For every new location and/or collector slope, extensive data must be manipulated to obtain the appropriate set of $\phi$-curves. To eliminate the need for such massive computing, a generalized hourly utilizability method was proposed
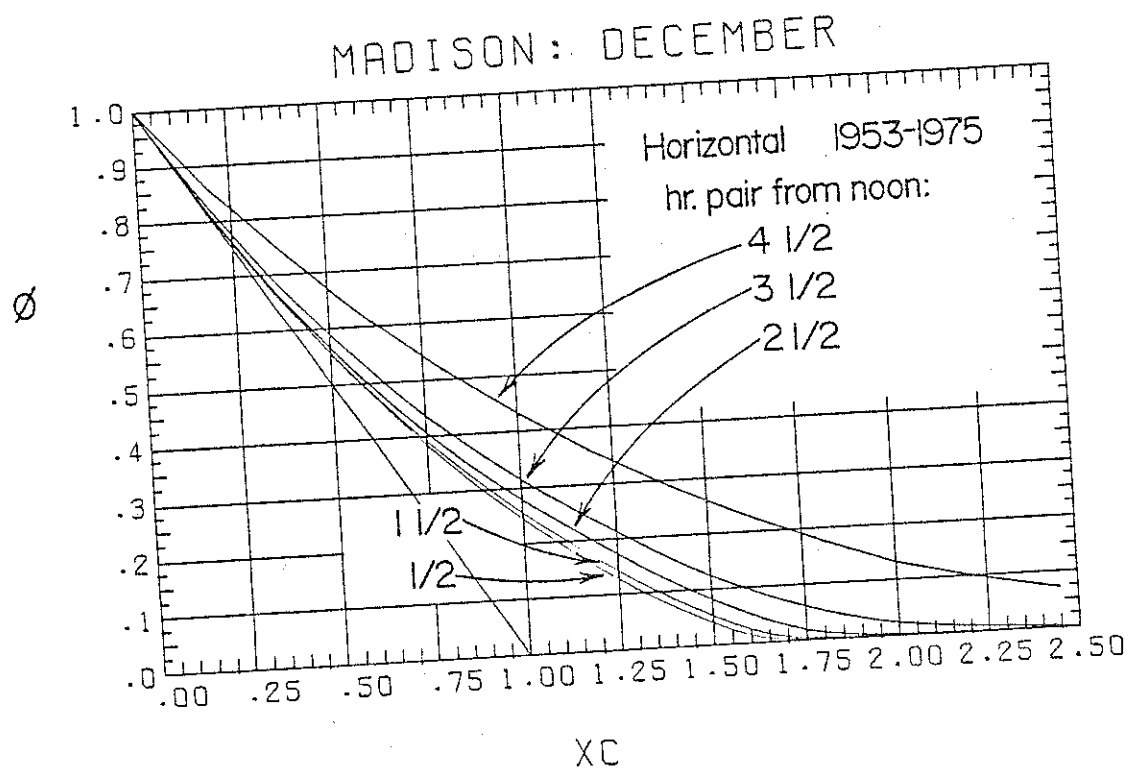
Figure 4.3-6:  φ-curves based on 23 years of
Madison data (β=0)

by Whillier (42), and later pursued by Liu and Jordan (30).

4.4.1 Review of Generalized Utilizability

To determine $\phi$ for a horizontal surface, Whillier wrote Equation 4.2-1 equivalently as:

$$\phi = \int_{f_c}^{1} \left( \frac{I}{\bar{I}} - \frac{I_c}{\bar{I}} \right) df \qquad (4.4-1)$$

where $f_c$ is the cumulative frequency of occurrence corresponding to $I_c$. This integral is shown graphically in Figure 4.4-1. Here, $\phi$ is the shaded area above $X_c$ divided by the total area under the curve. (Plotted in this dimensionless form, the total area under the curve is unity.) The plot of Figure 4.4-1 is a better representation of $\phi$ than Figure 4.2-2. Whillier (42) found that for a given location and month, the cumulative frequency distributions of all hours were roughly the same shape, independent of $\bar{I}$.

Whillier (42) examined 3 years of horizontal surface data for only three hours either side of solar noon. He found that $\phi$-curves based on a single year of data were significantly different from those obtained from all 3 years combined, indicating that 3 years is probably not enough data to accurately predict true long-term average results. Since the horizontal surface $\phi$-curves Whillier ob-
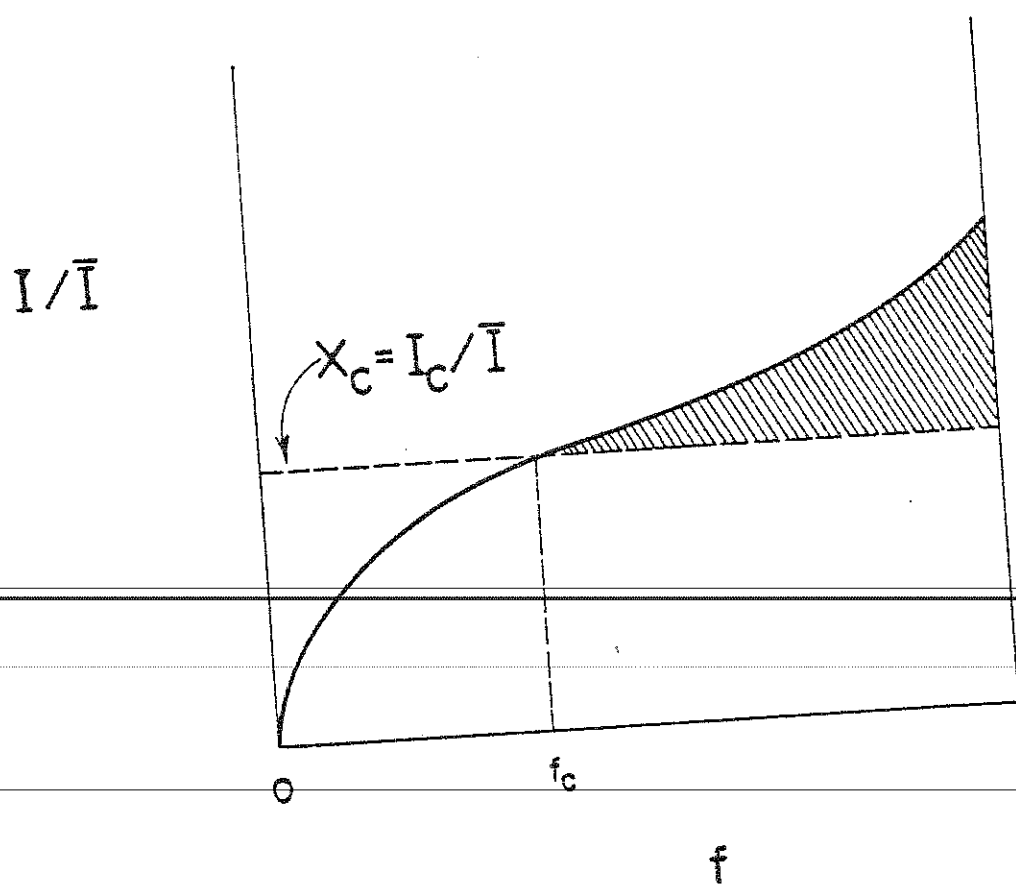
Figure 4.4-1: Cumulative frequency of $I/\overline{I}$ for determining $\phi$

tained from his limited data varied only marginally from hour-to-hour, he suggested that the curve for the hour pair 10-11/13-14 be used to represent all hours of the day.

To use this single horizontal surface $\phi$-curve to predict the performance of a tilted collector, Whillier (42) suggested using R as follows:

$$\overline{Q}_{u\text{-}mh} = A_e D_m \ (\tau\alpha) \ R_h \phi_m \ \overline{I}_{mh} \tag{4.4-2}$$

where $\phi_m$ is the hourly utilizability for the hour pair 10-11/13-14 to be used for all the hour calculations of month m. The long-term, monthly-average total hourly insolation on a horizontal surface can be obtained from:

$$\overline{I}_{mh} = r_{T\text{-}mh} \ \overline{H}_m \tag{4.4-3}$$

where $r_{T\text{-}mh}$ is the long-term average hourly to daily total insolation ratio.

A least-squares curve fit to extensive data (13) has resulted in the following relation:

$$r_T = \frac{\pi}{24} \ (a + b \ \cos\omega) \left( \frac{\cos\omega - \cos\omega_s}{\sin\omega_s - \omega_s \ \cos\omega_s} \right) \tag{4.4-4}$$

where:

$$a = 0.409 + 0.5016 \ \sin \ (\omega_s - 1.047)$$

$$b = 0.6609 - 0.4767 \sin (\omega_s - 1.047)$$

$\omega_s$ = Sunset hour angle  (in radians)

The sunset hour angle is determined from geometry to be:

$$\omega_s = \arccos (-\tan L \tan \delta) \qquad\qquad (4.4\text{-}5)$$

Equation 4.4-4 is plotted in Figure 4.4-2 as a function of $\omega_s$ and the midpoint of the hour from noon.

Using Equation 4.4-2 will give erroneous results. Since R was not used to obtain the $\phi$-curve, the insolation distribution used for the $\phi$-curve was not spread (as discussed in the previous section) as much as the true tilted surface would experience. Because of this, the horizontal $\phi$ used in Equation 3.4-2 will be closer to the identical day limit, thus underpredicting the utilizable energy.

The lack of hourly data (and availability of daily data) prompted Whillier (42) to suggest that daily insolation values could be used to represent hourly statistical patterns. Liu and Jordan (30) pursued this concept. They plotted daily and hourly cumulative tilted surface insolation ratios, as shown in Figure 4.4-3, discovering that they had very similar shapes.

If the daily distribution is used for shape only, a $\phi$-curve can be obtained by integrating it for various values of $X_c$. The $\phi$-curve obtained from this method is shown in Figure 4.4-4 along with the hourly curves for the same situation. As shown, the $\phi$-curve based on daily data agrees rather well with the hourly based curves.
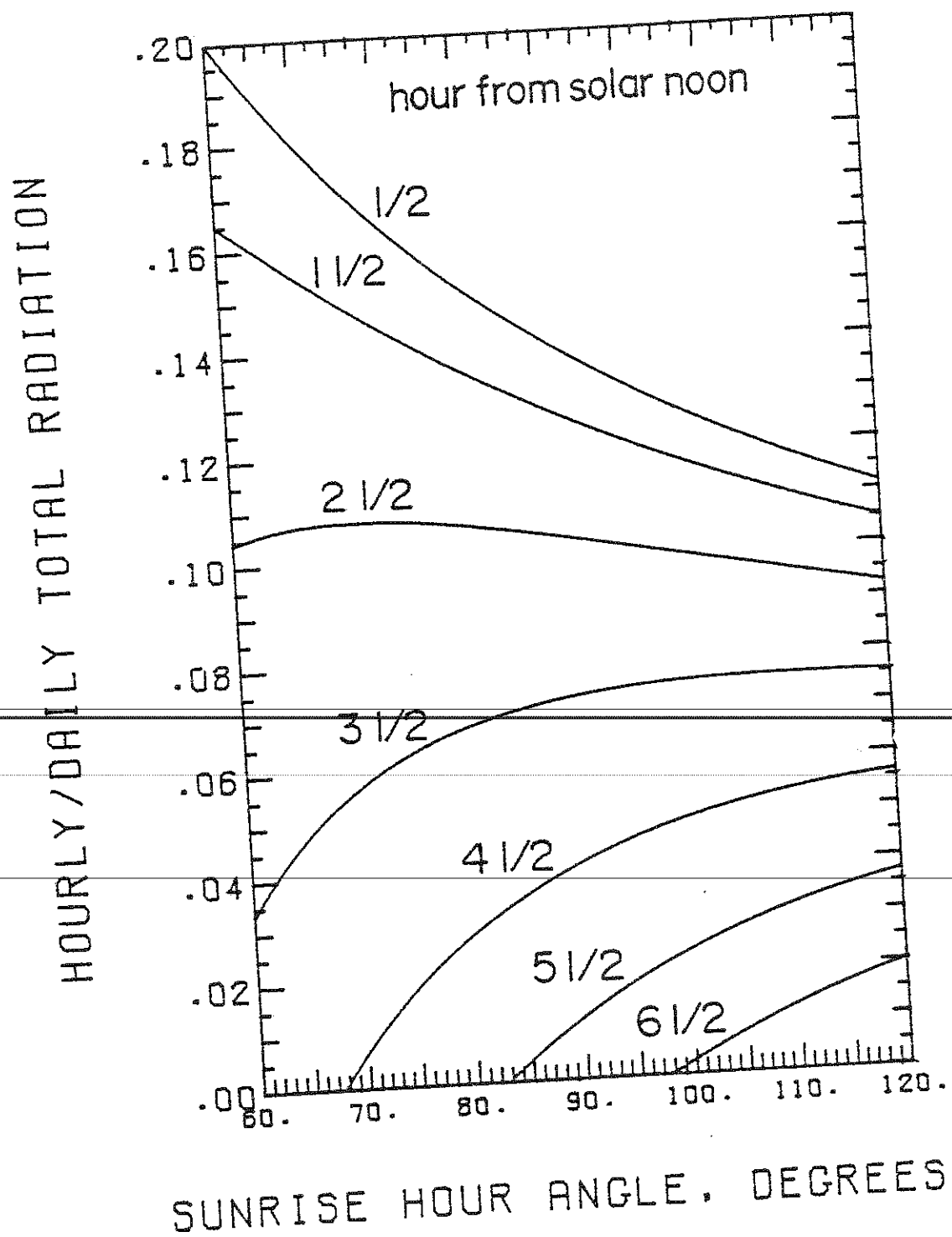
Figure 4.4-2: $r_T$ a function of time of day and $\omega_s$
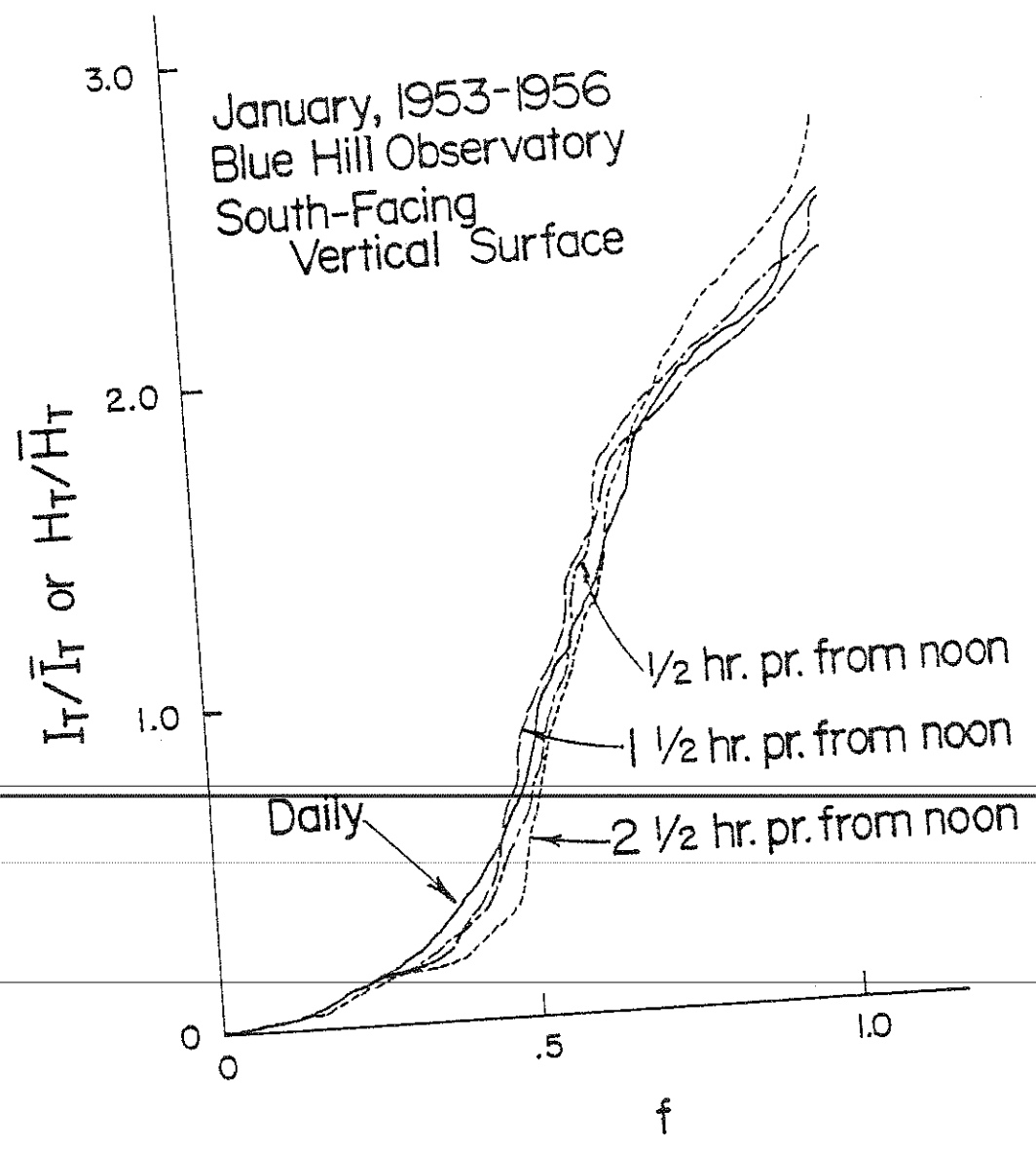
Figure 4.4-3:   Comparison of $I_T/\overline{I}_T$ and $H_T/\overline{H}_T$ cumulative frequency distributions (from Liu and Jordan (30)).
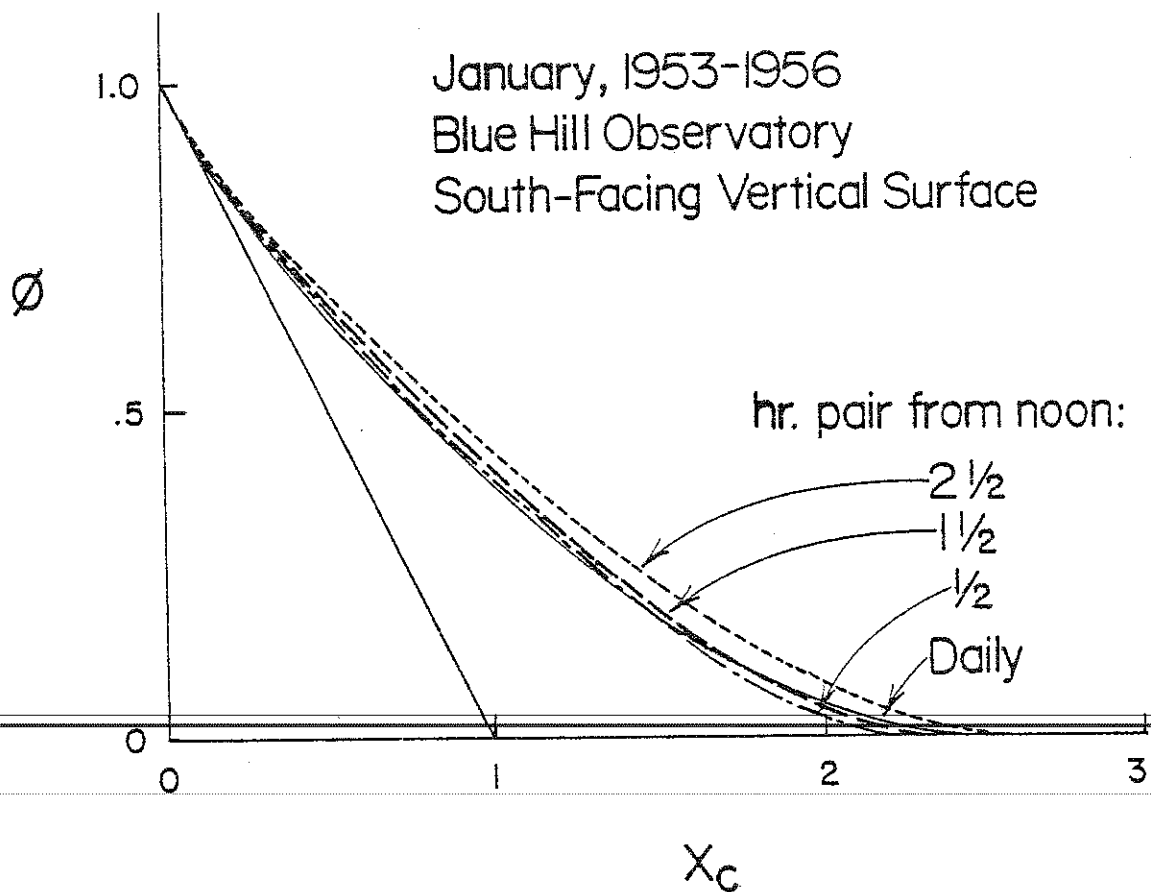
Figure 4.4-4: Comparison of $I_T/\overline{I}_T$ and $H_T/\overline{H}_T$ based $\phi$-curves
(from Liu and Jordan (30)).

Because of this, Liu and Jordan (30) recommended that daily derived
$\phi$-curves be used to describe all the hour's $\phi$-curves.

Liu and Jordan (29) devised a generalized method of correlating a daily insolation frequency distribution. They found that if the observed daily clearness indices,

$$K_T = H/H_o \qquad (4.4-6)$$

where:

H = Daily horizontal surface insolation

$H_o$ = Daily extraterrestrial insolation on a horizontal surface

were plotted in a cumulative frequency of occurrence, nearly the same curve was obtained for all locations with the same monthly-average daily clearness index,

$$\overline{K}_T = \overline{H}/\overline{H}_o \qquad (4.4-7)$$

where:

$\overline{H}$ = Monthly-average daily horizontal surface insolation

$\overline{H}_o$ = Monthly-average daily extraterrestrial insolation on a horizontal surface

The daily extraterrestrial insolation is found (16) by the integration of Equation 4.3-6 to be:

$$H_o = \frac{24}{\pi} G_{sc} \left[1+0.033\cos\left(\frac{360\ n}{365}\right)\right] \times \left[\cos L \cos\delta \sin\omega_s \right.$$
$$\left. + \frac{2\pi\omega_s}{360} \sin L \sin\delta \right] \qquad (4.4-8)$$

Equation 4.4-8 can also be used to determine $\overline{H}_o$ by using the values of n (24) listed in Table 4.4-1. These are the days that will give the most accurate value of $\overline{H}_o$ for each month.

The results of the Liu and Jordan investigation are shown in Figure 4.4-5 through the use of a curve fit by Cole (12). These curves, being the result of many months of data, represent long-term average daily clearness index distributions.

The shapes of these generalized distributions indicate that as $\overline{K}_T$ increases, the days making up the distribution get more like each other. In the limit, if $\overline{K}_T$ were unity, all the days would have to have $H = H_o$. This would be represented by a horizontal line at $K_T = 1$ in Figure 4.4-5. The total area under any particular distribution equals the $\overline{K}_T$ for that distribution.

Representative comparisons (40) between the Liu and Jordan $K_T$ distributions and 23 years of Madison data are shown in Figure 4.4-6. While the $K_T$ frequency distributions for January, February, and June agree rather well with the generalized ones, April is significantly different. This can be attributed to the occurrence of successive weather fronts (April showers) that bring with them a series of clear and overcast days with few partly cloudy ones in between. The agreement here is generally quite good considering that the Liu and Jordan $K_T$ distributions are representative of many locations and months, thus smoothing out any seasonal and/or location effect. Theilacker (40) found that the distribution

Table 4.4-1: Days to use in Equation 4.4-8 to obtain $\overline{H}_o$.

| Month | Day to obtain $\overline{H}_o$ |
|---|---|
| January | 17 |
| February | 47 |
| March | 75 |
| April | 105 |
| May | 135 |
| June | 162 |
| July | 198 |
| August | 228 |
| September | 258 |
| October | 288 |
| November | 318 |
| December | 344 |
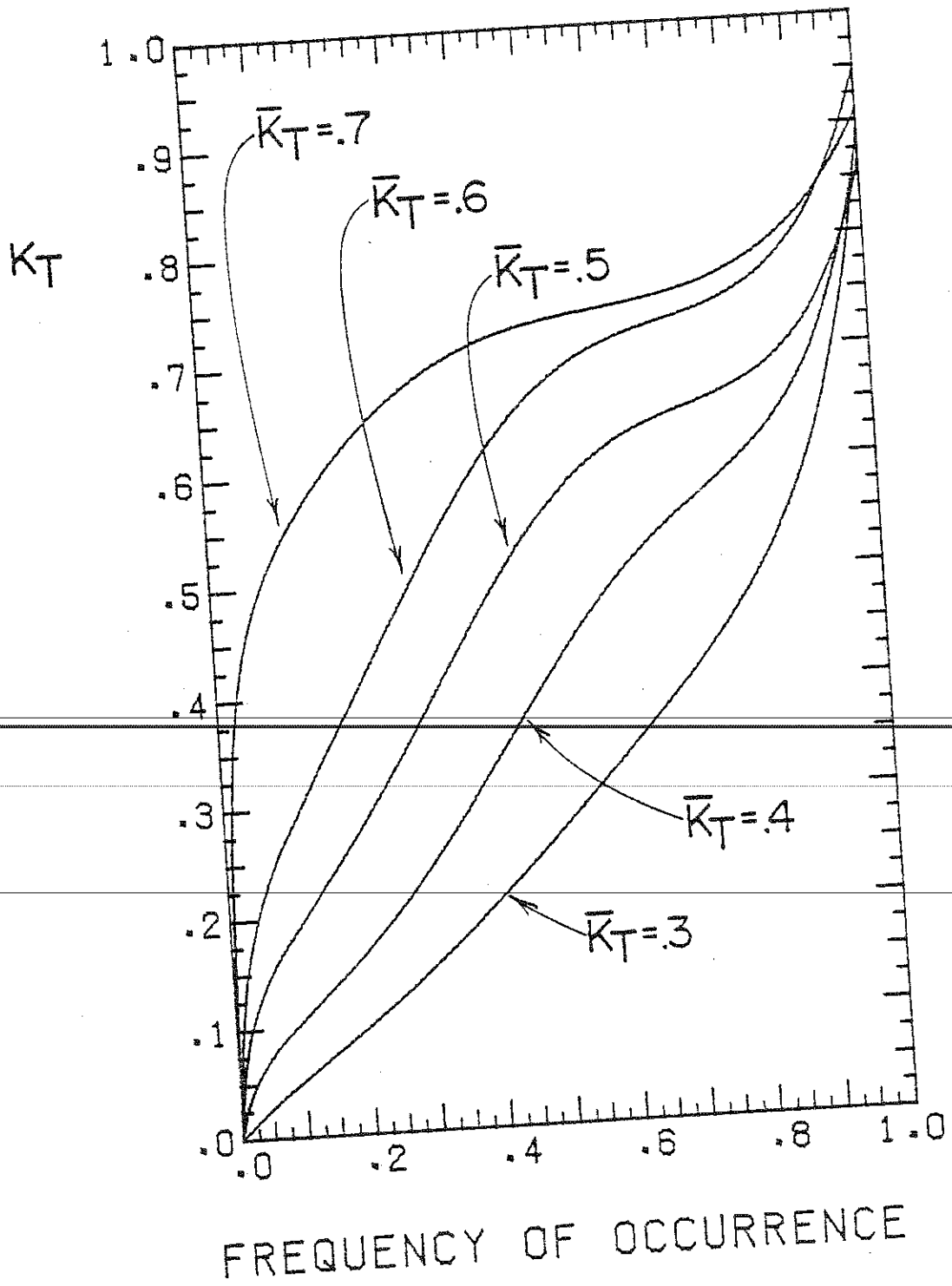
Figure 4.4-5:   Generalized $K_T$ distributions
(from Liu and Jordan (30)).
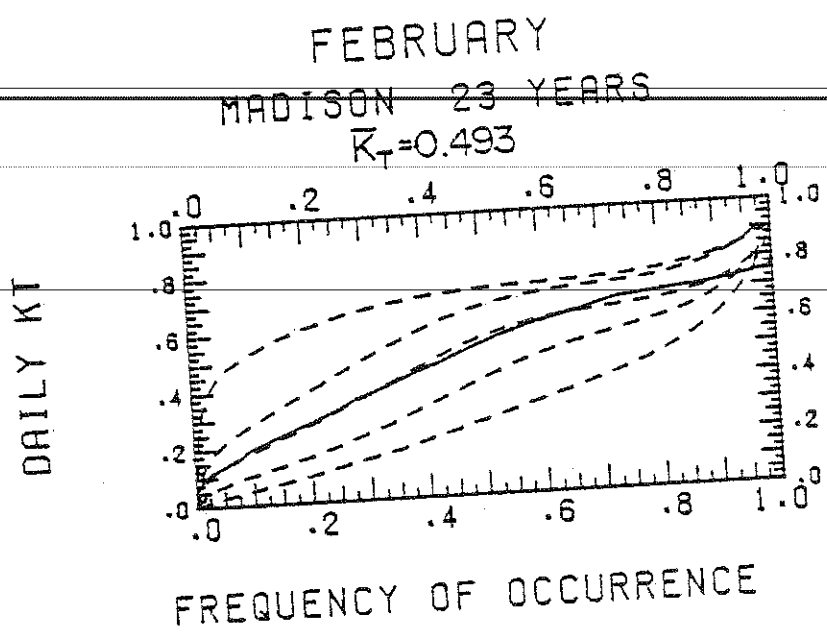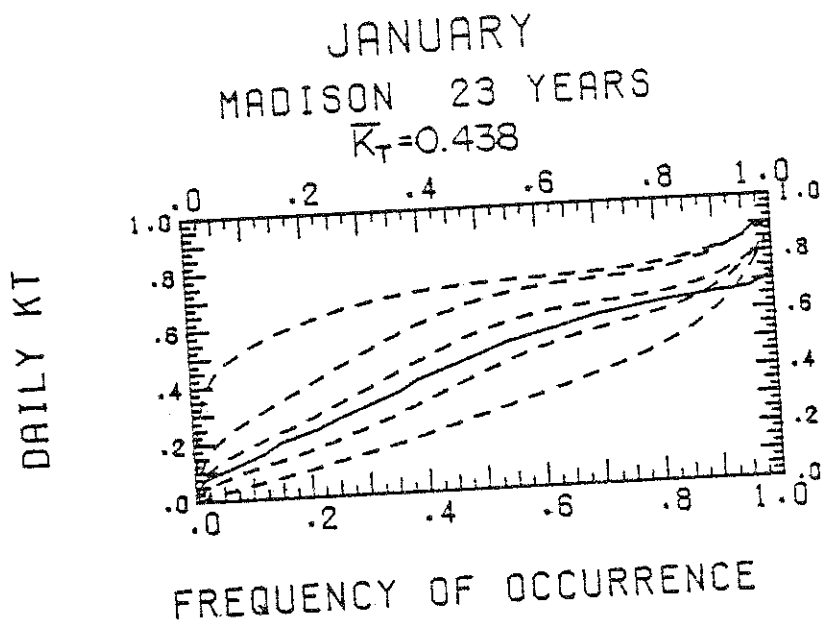
Figure 4.4-6: Comparison of generalized and 23 year $K_T$ distributions (from Theilacker)

APRIL
MADISON 23 YEARS
$\overline{K}_T$=0.474

DAILY KT

FREQUENCY OF OCCURRENCE

JUNE
MADISON 23 YEARS
$\overline{K}_T$=0.534

DAILY KT

FREQUENCY OF OCCURRENCE
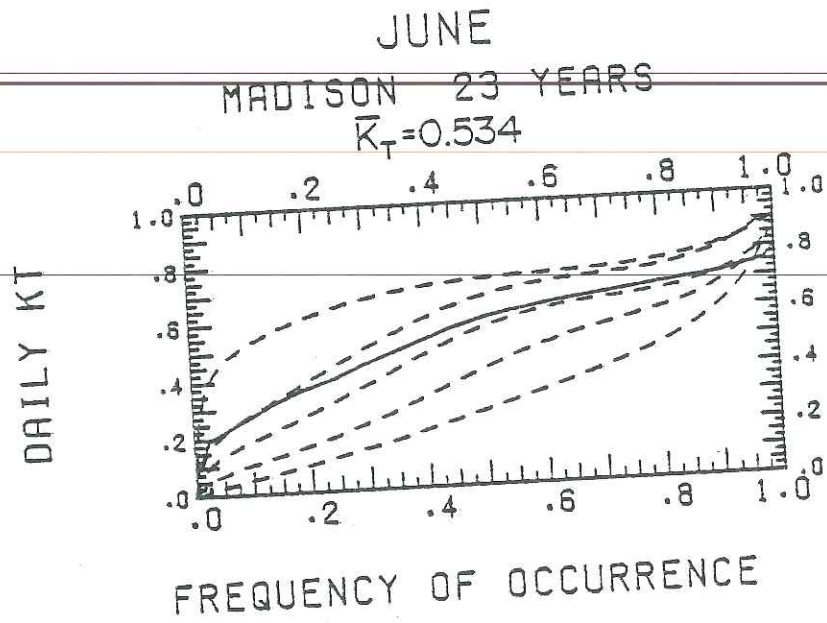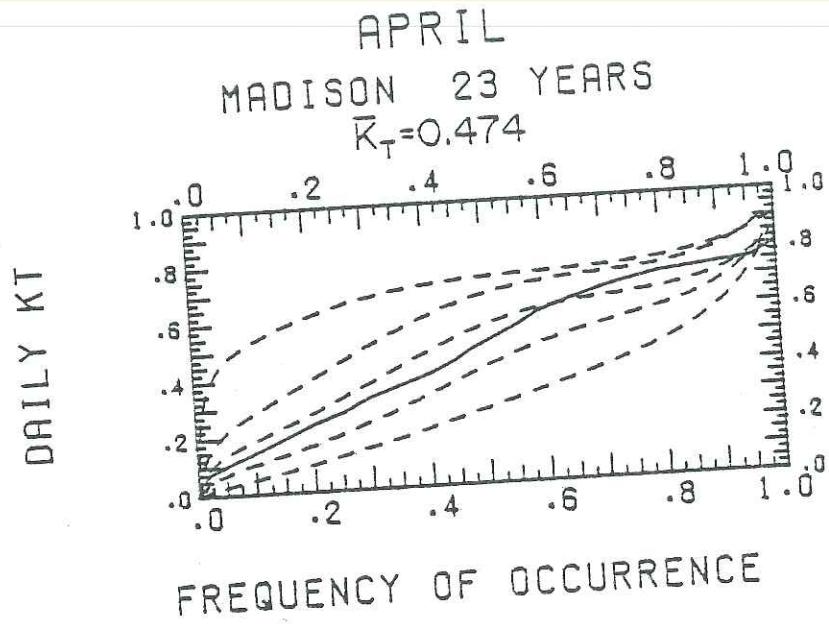
Figure 4.4-6 (continued)

agreements presented here for Madison are comparable to those for Fort Worth, better than Miami and Seattle, and worse than Albuquerque.

Almost all the above-mentioned calculated $K_T$ frequency distributions do not have the tail for $f > 0.9$ exhibited by the generalized curves. It has been suggested (3, 40) that the tails are the result of using $\overline{H}_o$ rather than daily $H_o$ s to calculate $K_T$ s. Doing this results in a skew in the distributions away from their mean, because $\overline{H}_o$ under predicts $H_o$ for half of the month, and over predicts for the other half.

Using Figure 4.4-5, generalized $H/\overline{H}$ frequency distributions corresponding to Figures 4.4-3 can be generated. From these distributions, generalized $\phi$-curves for a horizontal surface can be obtained by graphical integration.

As indicated earlier, the horizontal $\phi$-curves obtained would not be applicable to tilted surfaces. To remove this restriction, Liu and Jordan transformed $H$ and $\overline{H}$ to their tilted surface counterparts ($H_T$ and $\overline{H}_T$), generated an insolation ratio frequency distribution corresponding to Figure 4.4-3, and graphically integrated to obtain $\phi$-curves for tilted surfaces.

The daily insolation on a tilted surface is:

$$H_T = H_o \, K_T \, R'$$

<div align="right">(4.4-9)</div>

The ratio of daily total insolation on a tilted surface to that

on a horizontal surface is:

$$R' = (1 - H_d/H) \, R'_b + H_d/H \left(\frac{1 + \cos\beta}{2}\right) \qquad (4.4\text{-}10)$$

$$+ \, \rho \left(\frac{1 - \cos\beta}{2}\right)$$

where $R'_b$ is the ratio of daily beam radiation on a tilted surface to that on a horizontal surface. The daily diffuse fraction was presented in the previous section (where it was used as an hourly correlation).

When using the generalized $K_T$ frequency distributions to generate a $\phi$-curve, the day of the month that each generalized $K_T$ occurred on is unknown. For this reason, it becomes necessary to use $\overline{H}_o$ and $\overline{R}_b$ in Equations 4.4-9 and 4.4-10. The ratio of monthly-average daily beam radiation on a tilted surface to that on a horizontal surface for south-facing surfaces is (28):

$$\overline{R}_b = \frac{\cos(L-\beta)\cos\delta\cos\omega'_s + \pi/180 \; \omega'_s \sin(L-\beta)\sin\delta}{\cos L \cos\delta \sin\omega_s + \pi/180\omega_s \; \sin L \; \sin\delta} \qquad (4.4\text{-}11)$$

where $\omega'_s$, the sunset hour angle on a tilted surface is:

$$\omega'_s = \text{minimum} \left( \begin{array}{l} \omega_s \\[6pt] \arccos(-\tan(L-\beta)\tan\delta) \end{array} \right) \qquad (4.4\text{-}12)$$

The ratio $\overline{R}_b$ of Equation 4.4-11 is really $R'_b$ as originally derived by Liu and Jordan (28). Since $R'_b$ is actually a function of atmospheric transmittance, it was recommended that the derived relation be used on a long-term average basis (thus the nomenclature $\overline{R}_b$).

In this manner, the effect of a day with very low transmittance being multiplied by a value that was derived assuming a clear sky would be greatly reduced. In calculating $\overline{R}_b$, the average day from Table 4.4-1 should be used.

The monthly-average daily insolation on a tilted surface is:

$$\overline{H}_T = \overline{H}_o \, \overline{K}_T \, \overline{R} \qquad\qquad (4.4\text{-}13)$$

where $\overline{R}$, the ratio of monthly-average daily total indication on a tilted surface to that on a horizontal surface is:

$$\overline{R} = (1 - \overline{H}_d/\overline{H}) \, \overline{R}_b + \overline{H}_d/\overline{H} \left( \frac{1 + \cos\beta}{2} \right) + \rho \left( \frac{1 - \cos\beta}{2} \right) \ (4.4\text{-}14)$$

Many correlations (6, 10, 13, 29, 34) have been suggested for the monthly-average daily diffuse correlation, $\overline{H}_d/\overline{H}$. To be consistent with the daily diffuse correlation, the monthly-average daily correlation presented by Liu and Jordan (29) will be used. A curve fit (24) to this correlation yields:

$$\overline{H}_d/\overline{H} = 1.390 - 4.027 \, \overline{K}_T + 5.531 \, \overline{K}_T^{\,2} - 3.108 \, \overline{K}_T^{\,3} \qquad (4.4\text{-}15)$$

Using Equations 4.4-6 through 4.4-14 and plots for $H_d/H$, $\overline{H}_d/\overline{H}$ and the generalized $K_T$ distributions, Liu and Jordan (63) generated generalized frequency distributions of $H_T/\overline{H}_T$ and graphically integrated them to obtain the generalized $\phi$-curves of Figure 4.4-7. As expected, the general trend is toward the identical day limit with increasing $\overline{K}_T$. As shown, $\overline{R}_b$ was used for a tilted surface
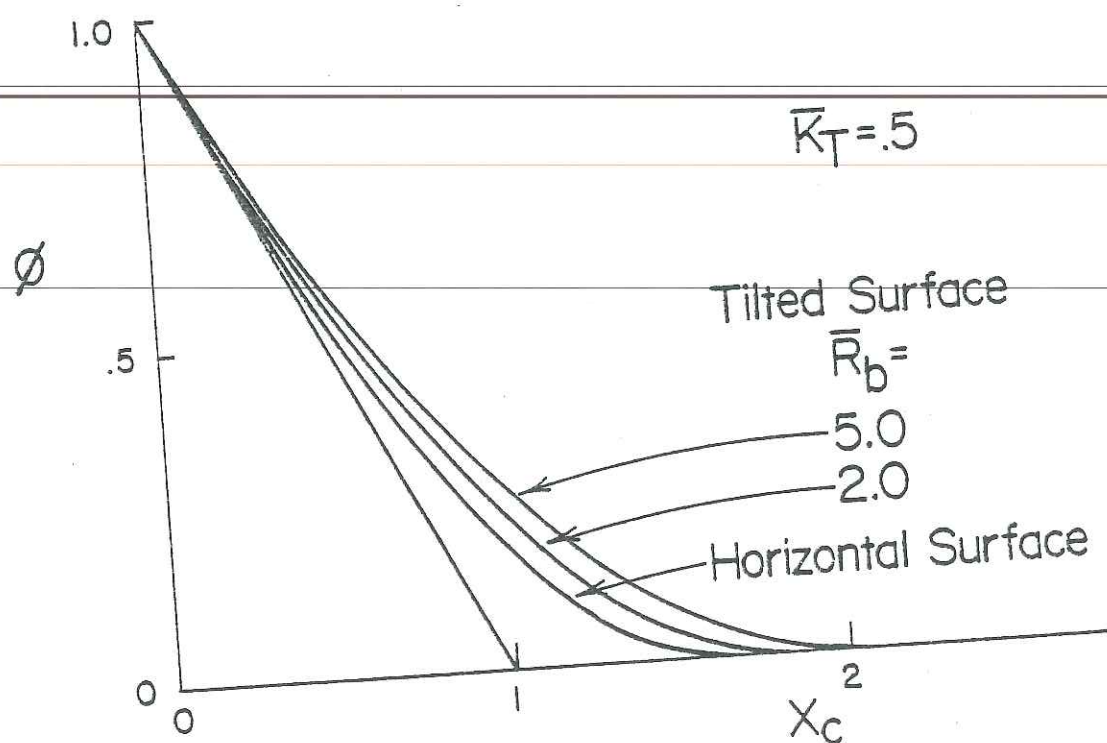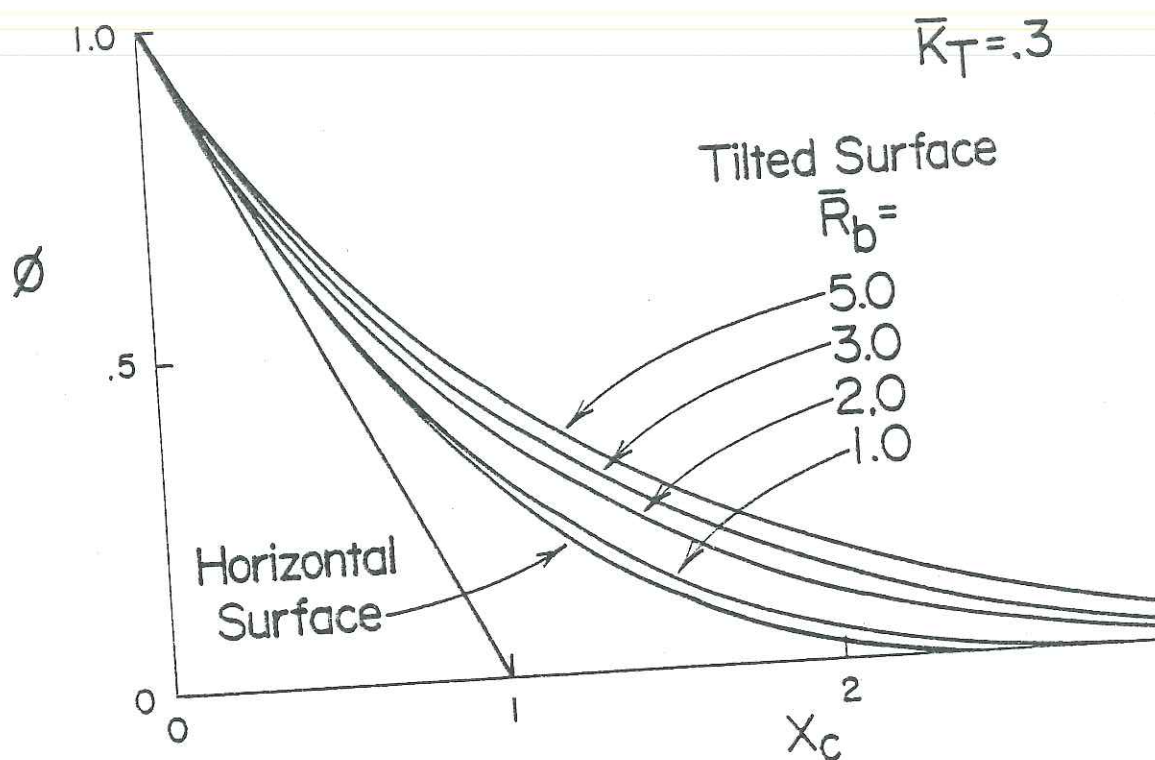
Figure 4.4-7: Liu and Generalized $\phi$-curves

correlating parameter, which restricts the $\phi$-curves to south facing

surfaces (30).

Performing the graphical integration described above is

equivalent to:

$$\phi = \frac{\displaystyle\int_{H_c}^{H_{max}} (H\ R' - H_c)\ P(H)\ dH}{\displaystyle\int_{H_{min}}^{H_{max}} H\ R'\ P(H)\ dH} \qquad (4.4-16)$$

where:

$P(H)$ = Long-term average probability of H occurring

$H_{max}$ = Maximum daily insolation

$H_{min}$ = Minimum daily insolation

$H_c$ = Critical daily insolation

The critical daily insolation is defined as:

$$H_c = X_c\ \overline{H}_T \qquad (4.4-17)$$

and has no significance of its own, since the $H_T/\overline{H}_T$ distribution

is being used for shape only.

A comparison of the 23 year calculated $\phi$-curves for February

in Madison and the corresponding generalized Liu and Jordan $\phi$-curve

is shown in Figure 4.4-8. Using the generalized $\phi$-curve for

February would result in a substantial error in the estimation of $\phi$
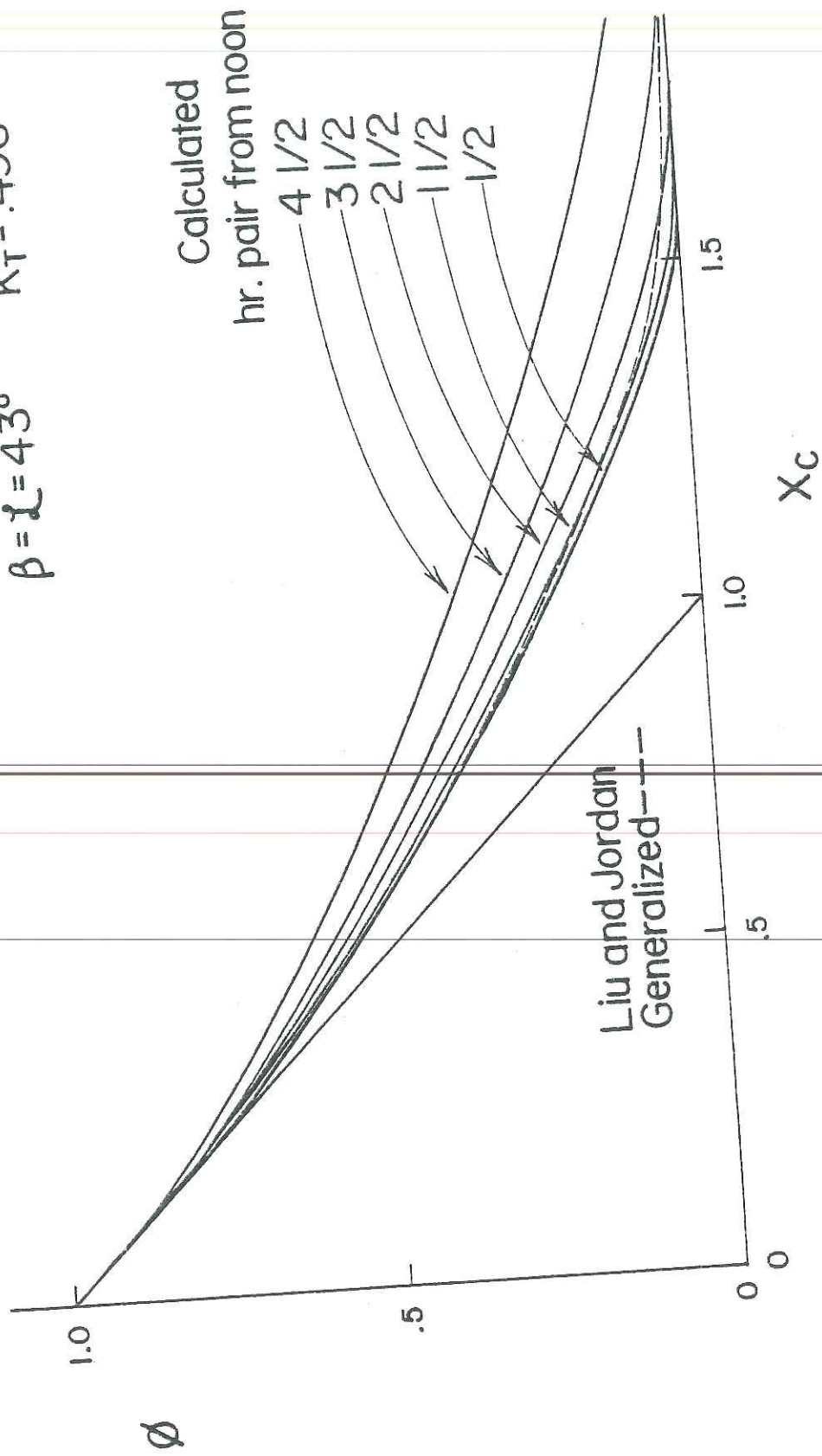
Figure 4.4-8: Comparison of 23 year calculated, and Liu and Jordan generalized φ-curves.

for hours other than the 1/2 and 1 1/2 hours from noon. Since the actual February $K_T$ frequency distribution agrees quite well with the corresponding generalized distribution (Figure 4.4-6), the generalized $\phi$-curve in Figure 4.4-8 is about as close an approximation as can be obtained for the winter months.

The Liu and Jordan generalized $\phi$-curve will agree much better for summer months when the $\phi$-curves for all hours are closer to the mid-day curve (see Figure 4.3-4). The reason for the better agreement in summer months will become apparent in the next section.

## 4.4.2  Improving Generalized Utilizability

The $\phi$-curves of Figure 4.4-7 are not complete, because no value of $\overline{R}_b < 1$ is considered. This situation is not uncommon for fixed collectors in summer months. As the previous section's discussion of $\overline{R}_b$ indicates, it is the strongest single parameter operating in the integral of Equation 4.4-16. However, the existence of a separate curve for $\overline{R}_b = 1$ and a horizontal surface (where $\overline{R}_b = 1$ by definition) indicates that $\overline{R}_b$ is not the only parameter of importance for tilted surface utilizability.

To examine the properties of generalized $\phi$-curves, the computer program PHIGEN was developed. PHIGEN generates $\phi$-curves using Equations 4.3-7, 4.4-6 through 4.4-16, and curve fits (12) to the generalized $K_T$ distributions of Figure 4.4-5. The only difference between this method and Liu and Jordan's is that here the generation and

integration of a $H_T/\overline{H}_T$ curve is done numerically rather than graph-ically. A listing of PHIGEN can be found in Appendix C.

As the separate curves for a horizontal surface and $\overline{R}_b = 1$ of Figure 4.4-7 indicate, the collector slope is of major significance in determining the shape of the $\phi$-curve. Using PHIGEN, the inter-action of $\overline{R}_b$ and $\beta$ was examined. Limiting cases of $\overline{R}_b$ and $\beta$ com-binations are shown in Figure 4.4-9. The effect of $\beta$ is seen to be quite marked, especially at lower values of $\overline{R}_b$. The identical curves for $\overline{R}_b = 0.5$, $\beta = 90°$ and $\overline{R}_b = 1$, $\beta = 0°$ expose an interaction between these two parameters.

Rewriting Equation 4.4-10,

$$R' = \overline{R}_b + H_d/H \left( \frac{1 + \cos\beta}{2} - \overline{R}_b \right) + \rho \left( \frac{1 - \cos\beta}{2} \right) \qquad (4.4-18)$$

we see that when the collector-sky view factor equals the beam radiation ratio, R' is constant for all H. A constant R' will can-cel in Equation 4.4-16, resulting in identical $\phi$-curves for any $\overline{R}_b$ and $\beta$ combination such that $\overline{R}_b = (1 + \cos\beta)/2$. We thus define the daily beam-diffuse view factor as:

$$V'_{bd} = \overline{R}_b - \frac{1 + \cos\beta}{2} \qquad (4.4-19)$$

Using PHIGEN, $\phi$-curves were generated for the limiting cases of $V'_{bd}$ as shown in Figure 4.4-10. These results indicate that the difference between limiting cases of a constant $V'_{bd}$ (the bottom two curves) is less than limiting cases of $\overline{R}_b$ (the second and third curves from the bottom). Generally, the uncertainty in $\phi$ has been reduced by about a factor of 2 by correlating with the collector-sky
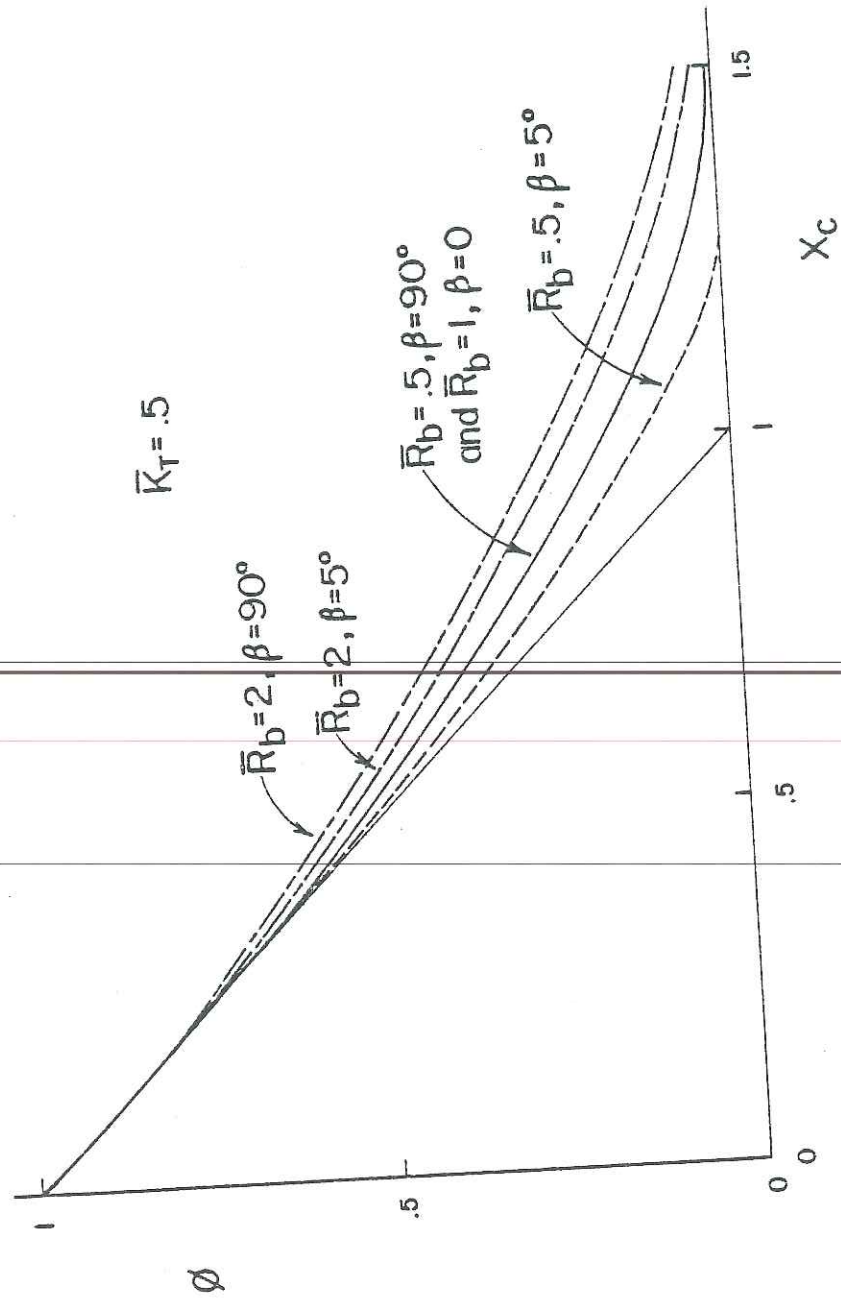
Figure 4.4-9: Slope and $\bar{R}_b$ effect on $\phi$-curves

$\overline{K}_T = .5$

$V'_{bd} = 1.5$; $\overline{R}_b = 2.0$; $\beta = 90$

$V'_{bd} = 1.5$; $\overline{R}_b = 2.5$; $\beta = 0$

$V'_{bd} = 0$; $\overline{R}_b = 1$; $\beta = 0$
and $\overline{R}_b = .5$; $\beta = 90$

$V'_{bd} = -.5$; $\overline{R}_b = .5$; $\beta = 0$

$V'_{bd} = -.5$; $\overline{R}_b = 0$; $\beta = 90$

$X_c$

$\phi$
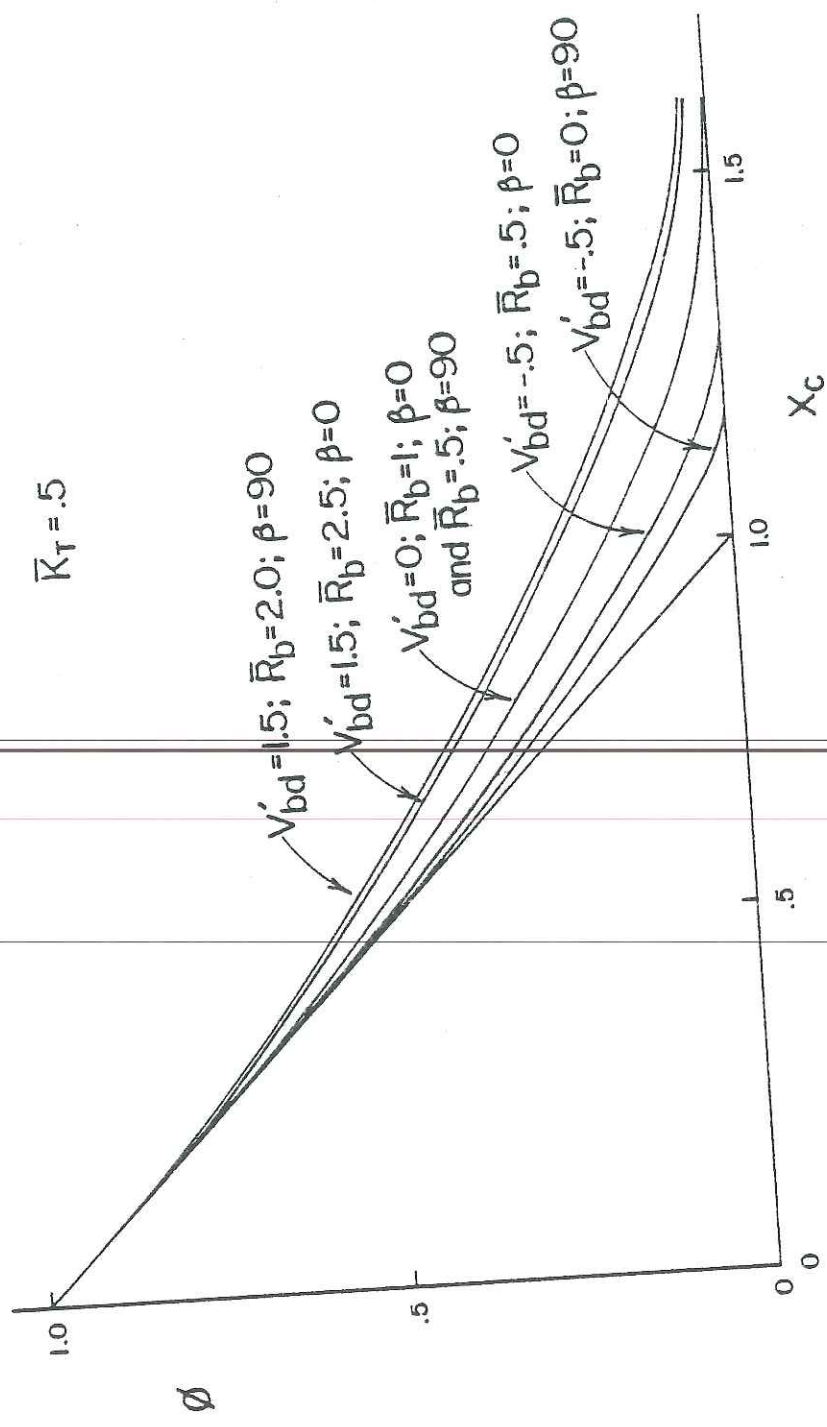
Figure 4.4-10:   Limiting $\phi$-curves for constant $V'_{bd}$

view factor in conjunction with $\overline{R}_b$ (i.e., $V'_{bd}$).

As indicated in Figure 4.4-10, $V'_{bd} = 0$ represents a horizontal surface (among others), $V'_{bd} > 0$ indicates that the surface in question will have a $\phi$ larger than that for a horizontal surface, and $V'_{bd} < 0$ indicates a $\phi$ less than that for a horizontal surface. A general range for $V'_{bd}$ to be expected is $-0.5 \leq V'_{bd} \leq 3$.

The next step in developing a good generalized method of determining $\phi$ is to account for the variation that has been exhibited for the different hours of the day in different seasons. This will be done by generating $\phi$-curves on an hourly basis. To do this requires a knowledge of the hourly clearness index, $k_T$, frequency distributions corresponding to the $K_T$ distribution of Figure 4.4-5, and the long-term average ratio of total hourly radiation on a tilted surface to that on a horizontal surface.

Some $k_T$ distributions based on 23 years of Madison data (40) are compared to the generalized $K_T$ distributions in Figure 4.4-11. The agreement here can be considered generally quite good, with April showing the largest difference (as did the April $K_T$ distribution). If more data were included, these distributions would smooth somewhat, removing the jagged edges. It will be assumed that the generalized $K_T$ distributions adequately describe the actual $k_T$ distributions and can thus be used as such.

The long-term average ratio of total hourly insolation on a tilted surface to that on a horizontal surface is:

JANUARY

MADISON 9-10AM 23 YEARS

$\bar{k}_T = 0.411$



HOURLY KT

FREQUENCY OF OCCURRENCE

JANUARY

MADISON 11-12AM 23 YEARS

$\bar{k}_T = 0.478$



HOURLY KT

FREQUENCY OF OCCURRENCE
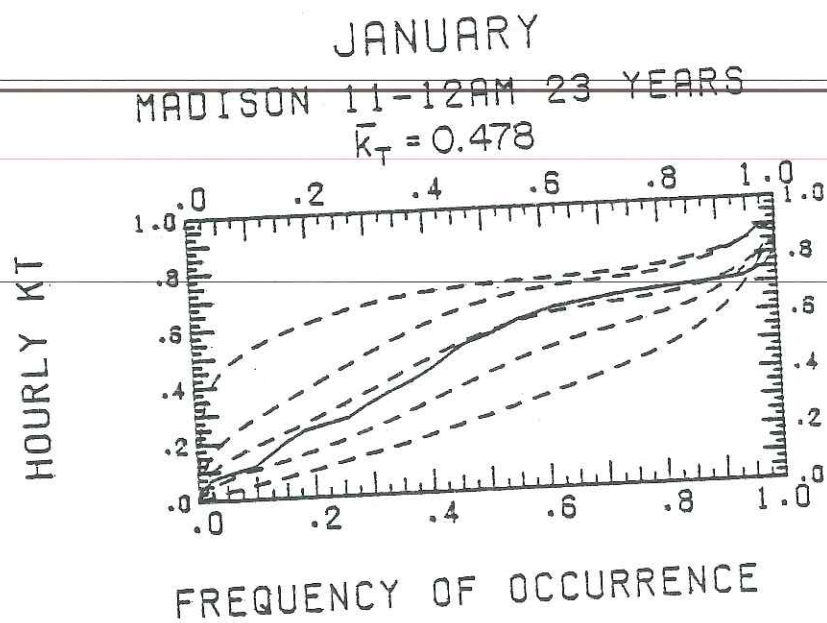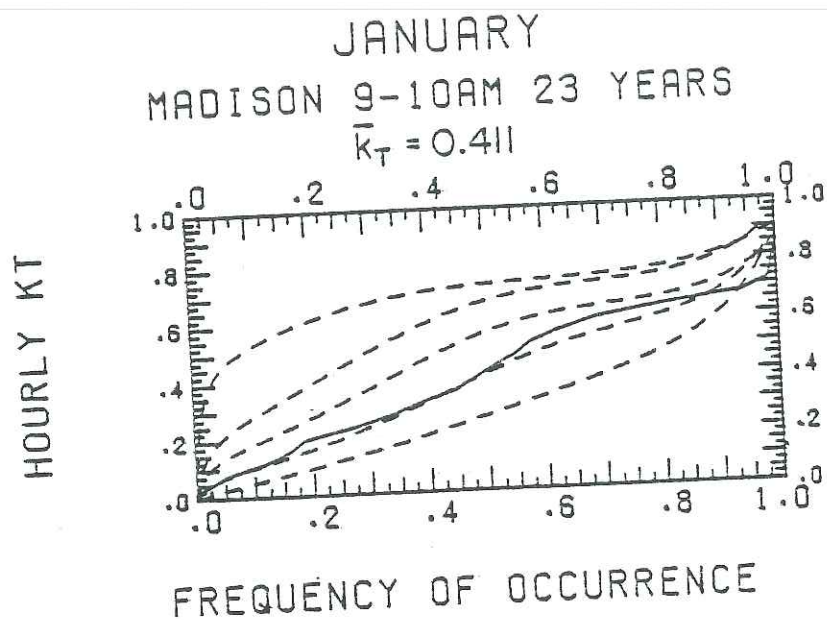
Figure 4.4-11a:  Comparison of 23 year $k_T$ and generalized $K_T$ distributions for Madison; January (from Theilacker)

APRIL

MADISON 9-10AM 23 YEARS

$\overline{k}_T = 0.507$

HOURLY KT

FREQUENCY OF OCCURRENCE

APRIL

MADISON 11-12AM 23 YEARS

$\overline{k}_T = 0.512$

HOURLY KT

FREQUENCY OF OCCURRENCE
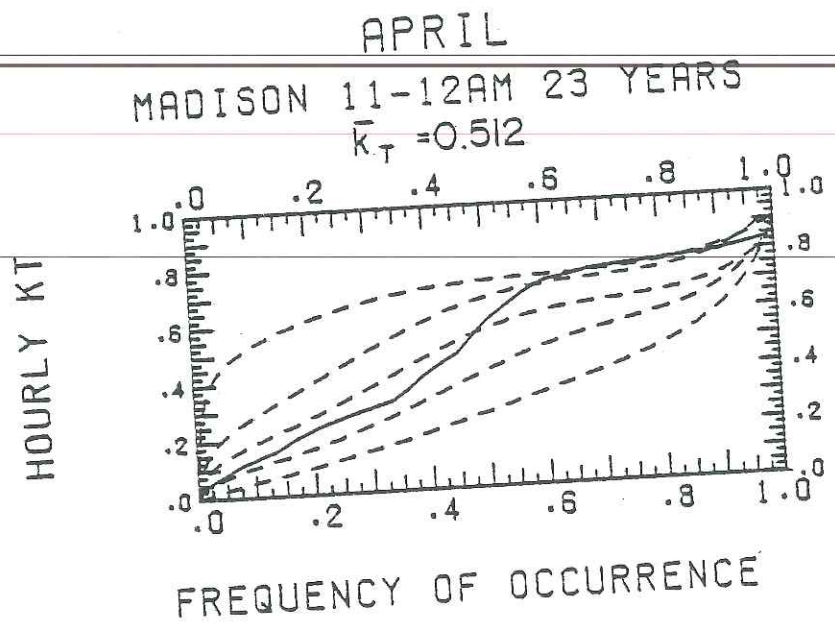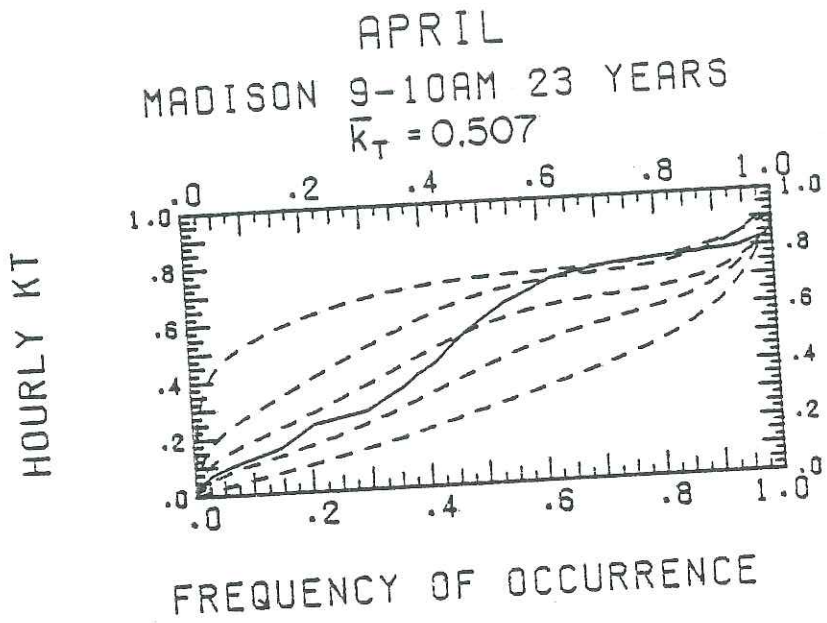
Figure 4.4-11b: Comparison of 23 year $k_T$ and generalized $K_T$ distributions for Madison; April (from Theilacker)

JUNE
MADISON 9-10AM 23 YEARS
$\overline{k}_T = 0.566$



HOURLY KT

FREQUENCY OF OCCURRENCE

JUNE
MADISON 11-12AM 23 YEARS
$\overline{k}_T = 0.584$



HOURLY KT

FREQUENCY OF OCCURRENCE
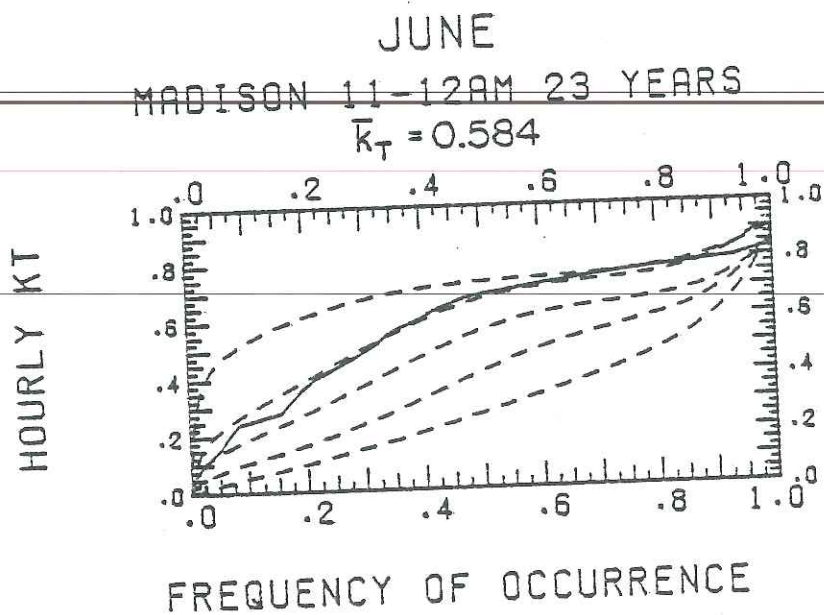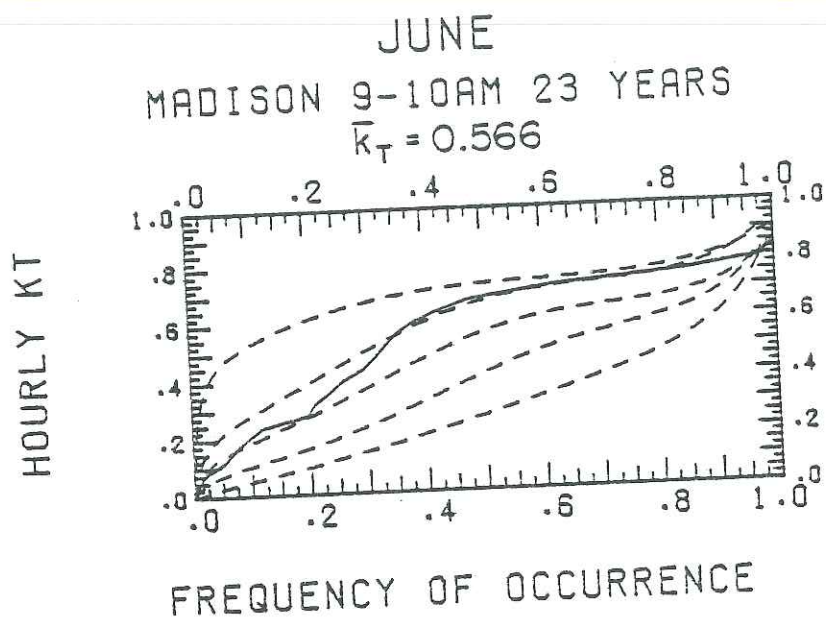
Figure 4.4-11c:   Comparison of 23 year $k_T$ and generalized $K_T$
distributions for Madison; June (from
Theilacker)

$$\overline{R}_h = (1 - \overline{I}_d/\overline{I}) \, \overline{R}_{b-h} + \overline{I}_d/\overline{I} \, \left(\frac{1 + \cos\beta}{2}\right) + \rho \left(\frac{1 - \cos\beta}{2}\right) \quad (4.4\text{-}20)$$

where:

$\overline{I}_d/\overline{I}$ = Long-term monthly-average hourly diffuse fraction

$\overline{R}_{b-h}$ = Long-term monthly-average ratio of hourly beam radiation on a tilted surface to that on a horizontal surface.

As was the case with the hourly diffuse fraction, the long-term monthly-average hourly diffuse fraction will be approximated by the corresponding daily diffuse fraction given by Equation 4.4-15. Since we are concerned with an hour, the atmospheric transmittance changes markedly and is not known with any certainty. Because of this, $\overline{R}_{b-h}$ can be approximated by $R_b$ as given in Equation 4.3-3.

A computer program, PHIGENHR, was developed to generate $\phi$-curves on an hourly basis in the same manner used on daily radiation relations. A listing of this program is presented in Appendix C. Using PHIGENHR, the $\phi$-curves of Figure 4.4-12 are obtained. Here, the correlating parameter

$$V_{bd} = R_b - \frac{1 + \cos\beta}{2} \quad (4.4\text{-}21)$$

is the hourly beam-diffuse view factor. The curves presented are specifically for a slope of 45°, but as Figure 4.4-10 indicates, using this median value for $\beta$ will have at most a difference of about 0.02 in $\phi$ for $\overline{k}_T = 0.5$.
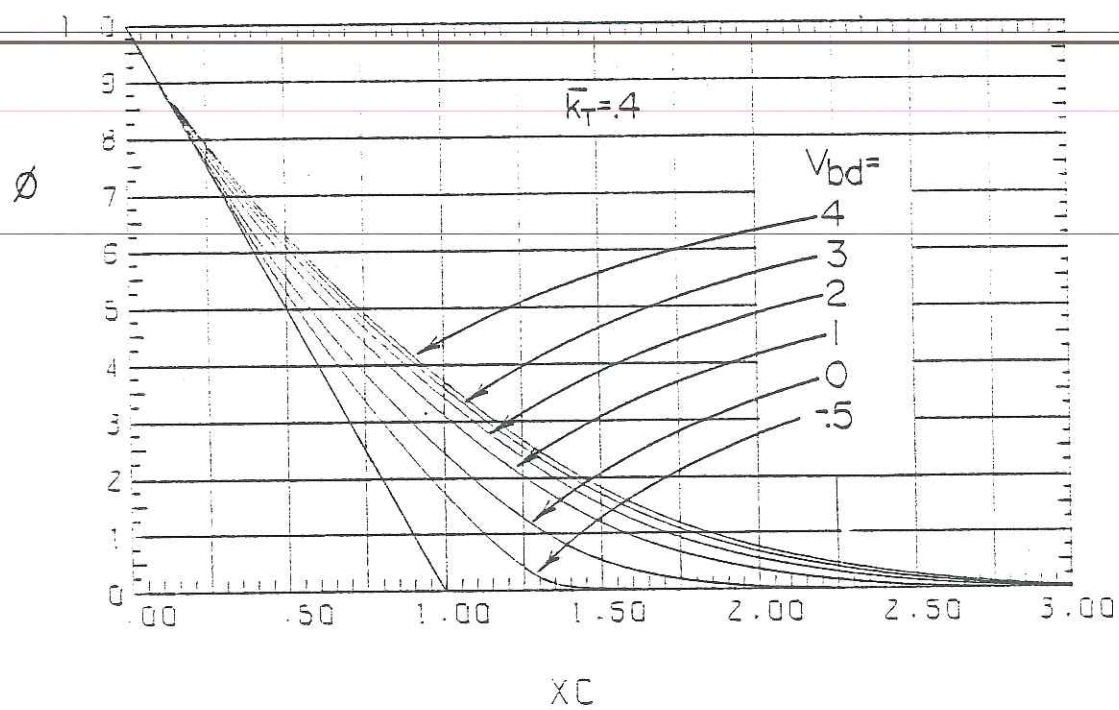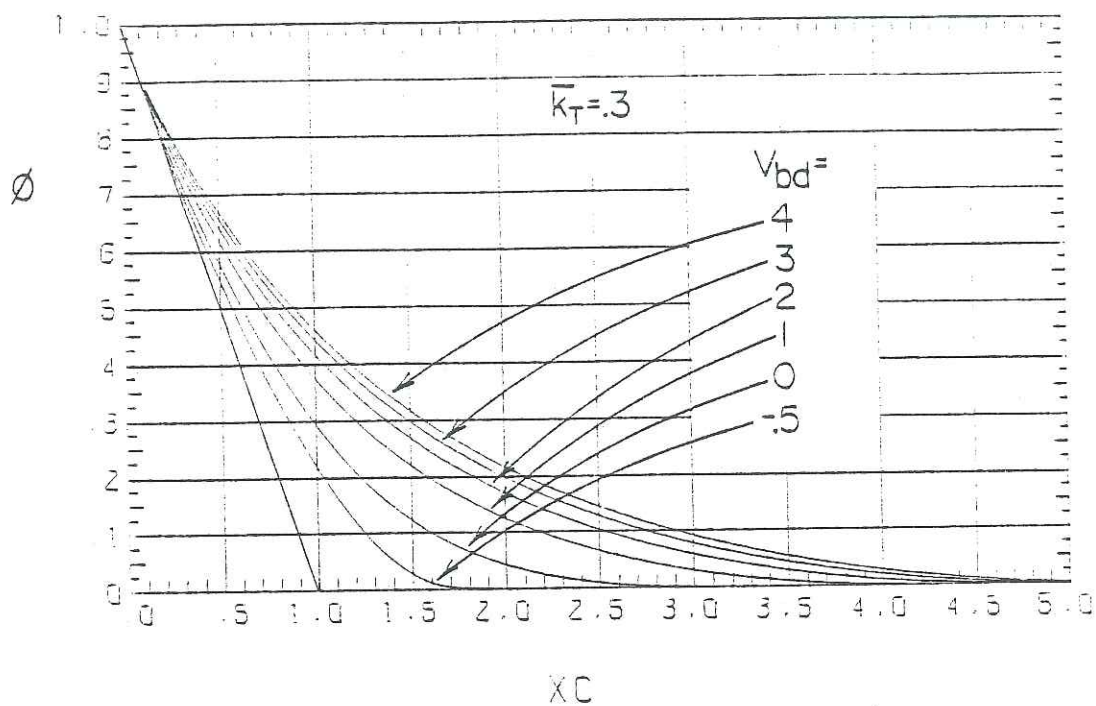
Figure 4.4-12:  Hourly generalized φ-curves
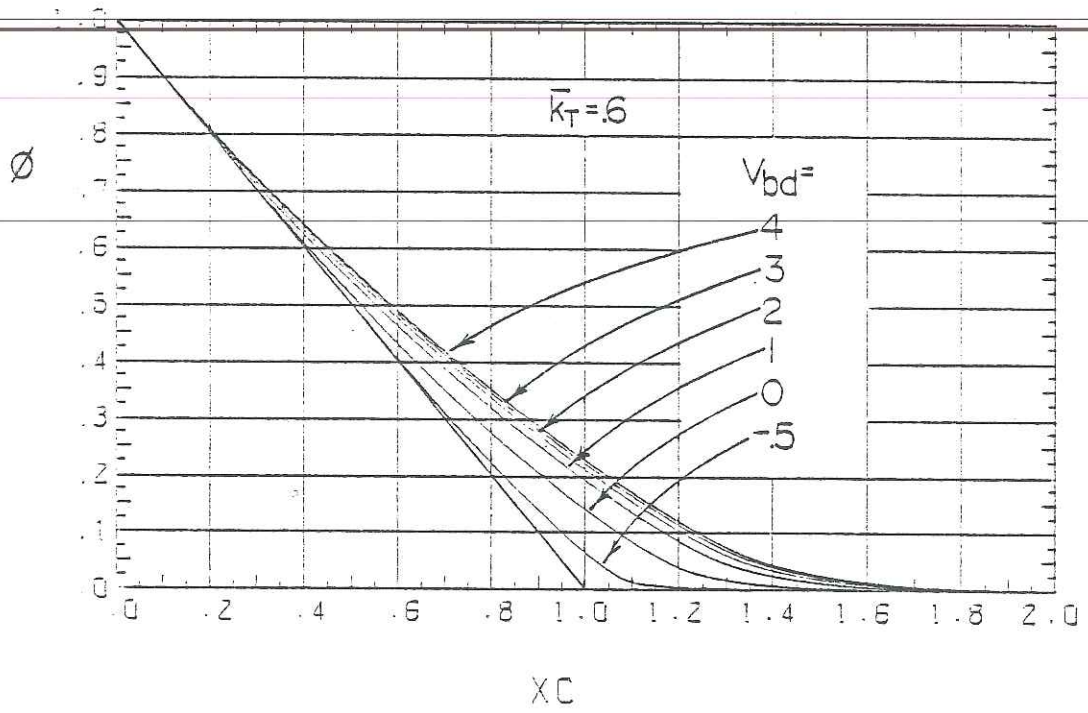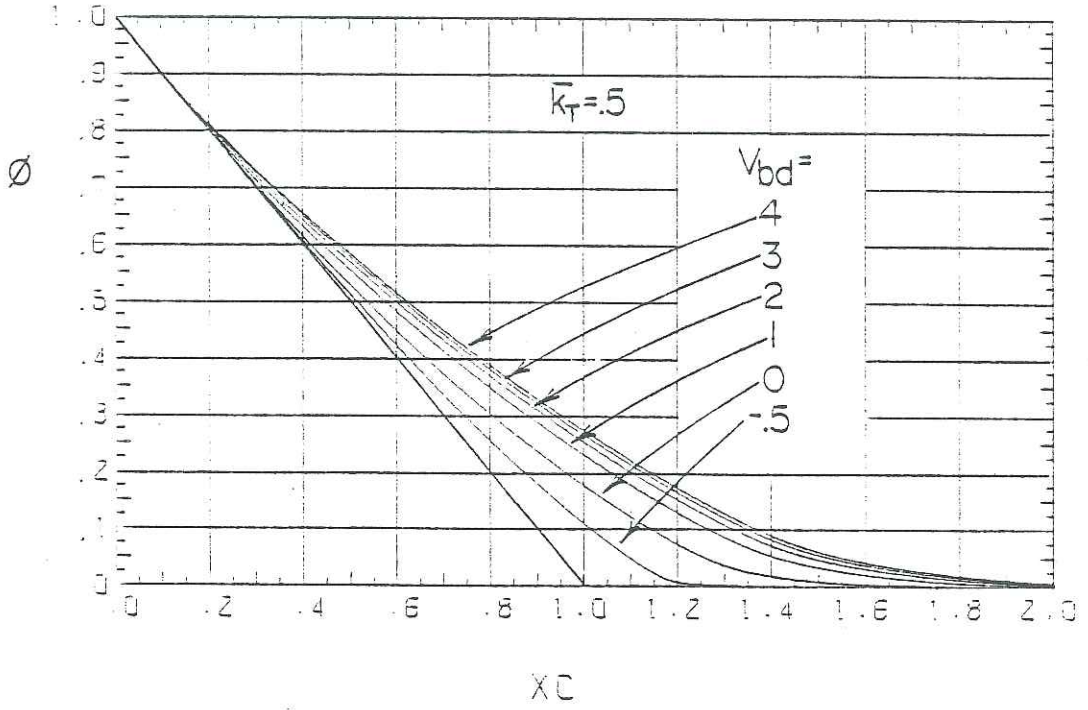
Figure 4.4-12: (continued)
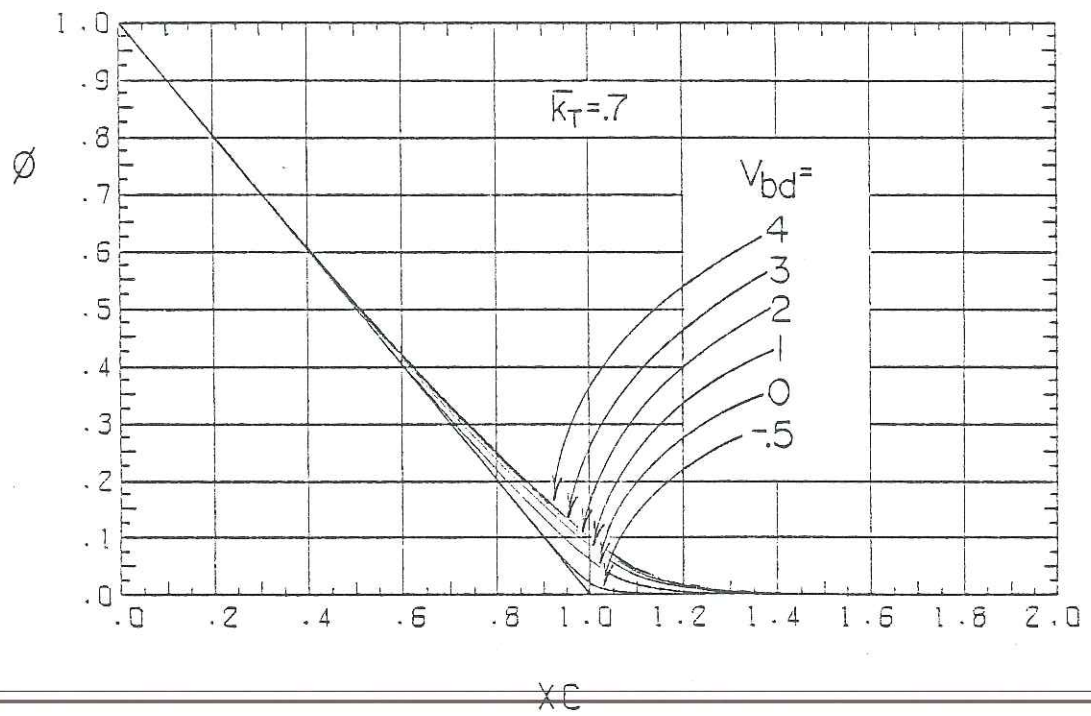
Figure 4.4-12: (continued)

Since daily diffuse fraction correlations and clearness index distributions were used, the only difference between the $\phi$-curves of Figure 4.4-12 and those of Figure 4.4-10 is that the current curves are to be used with $R_b$ and $\overline{k}_T$ rather than $\overline{R}_b$ and $\overline{K}_T$. The use of single hour radiation parameters offers one very distinct advantage: the curves of Figure 4.4-12 can be used for other than south facing surfaces, because $R_b$ is an hourly, rather than average daily, parameter. An example is presented in Section 4.6.

The difference in the hourly $\phi$-curves for tilted and horizontal surfaces shown in Section 4.3 can now be quantified. For a horizontal surface, $V_{bd}$ is zero for all hours of the day. For a tilted surface, $R_b$ (and thus $V_{bd}$) changes throughout the day. The magnitude of this effect can be seen by examination of Figures 4.3-1 and 4.4-12. In the winter, $V_{bd}$ will increase dramatically over the day, resulting in an "outward" spread in the $\phi$-curves. In the summer, $V_{bd}$ will increase slightly over the day. This would result in a slight "inward" spread of the curves if it were not for the second main reason for the spread of $\phi$-curves, the change in $\overline{k}_T$ over the day.

Long-term average hourly clearness indexes can be estimated from daily ones by:

$$\overline{k}_T = \overline{K}_T \frac{r_T}{r_o} \qquad (4.4-22)$$

where $r_o$ is the ratio of long-term average hourly extraterrestrial

insolation on a horizontal surface to its daily counterpart. The value of $r_o$ is determined from geometrical considerations to be (30),

$$r_o = \frac{\pi}{24} \frac{\cos\omega - \cos\omega_s}{\sin\omega_s - \omega_s\cos\omega_s} \qquad (4.4\text{-}23)$$

The ratio of $r_T$ and $r_o$ is shown in Figure 4.4-13 as a function of hour from solar noon for two different sunset hour angles. The curve with $\omega_s = 60°$ corresponds to a winter month and $\omega_s = 120°$ to a summer month. Inspection of Figure 4.4-13 reveals the second reason for the larger spread of the calculated $\phi$-curve sets for winter months than for summer months exhibited in Section 4.3. In winter, $r_T/r_o$ changes much more drastically than it would for the same hour spread in the summer. This means that the $\bar{k}_T$ s for winter months vary much more than for the summer months. As for daily derived $\phi$-curves, hourly derived curves are a strong function of $\bar{k}_T$, thus the wide spread $\phi$-curves for the winter and the lack of "inward" spread for summer.

The expected value of $\bar{k}_T$ from using Equation 4.4-22 on 23 year $\bar{K}_T$ s, is compared in Table 4.4-2 to observed values based on 23 years of data, 3 hours either side of solar noon, in Madison and Abluquerque. For all this data combined, the relation of Equation 4.4-22 underpredicted $\bar{k}_T$ by 1.6%. This is quite acceptable and well within the accuracy of the data.
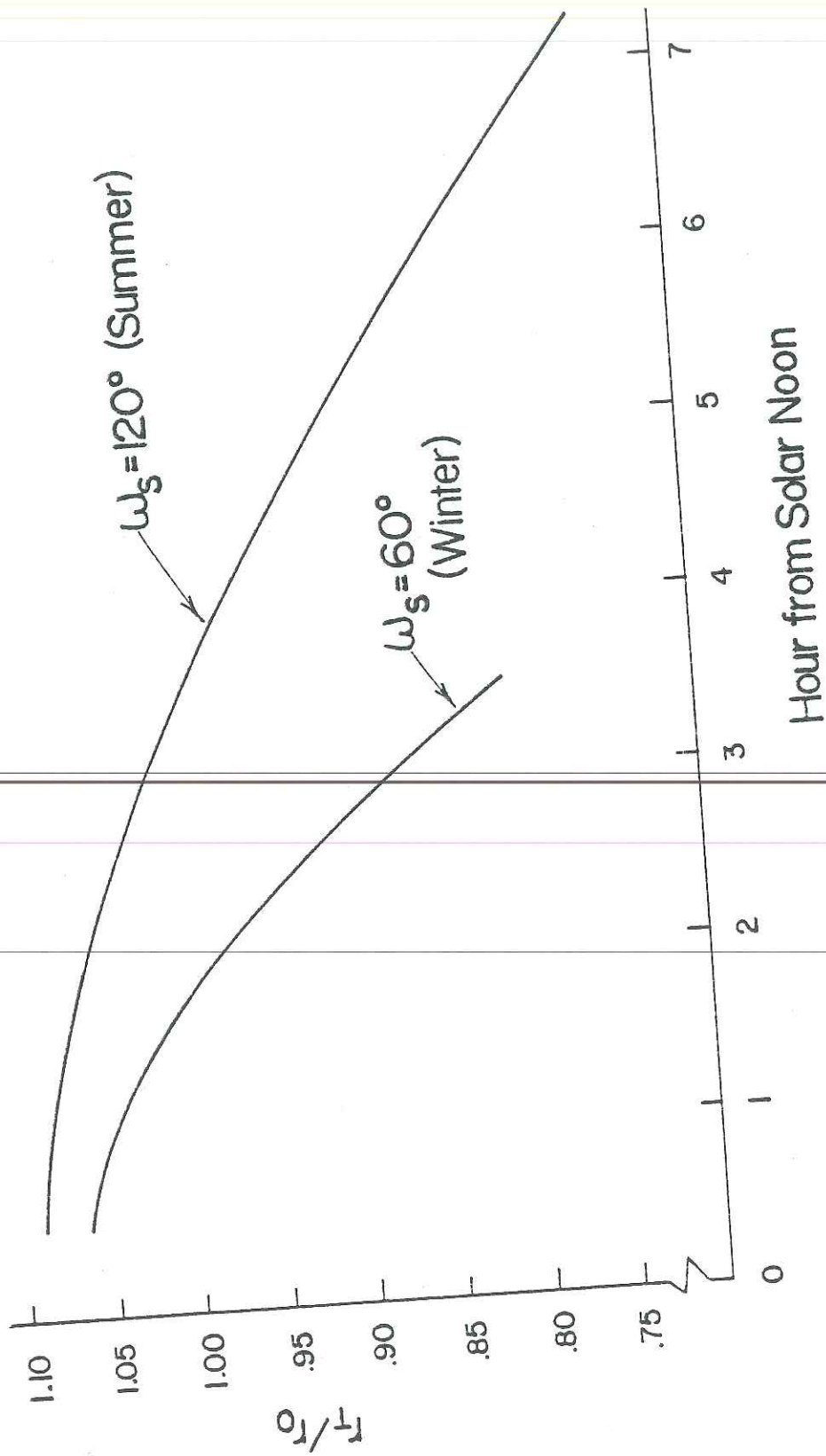
Figure 4.4-13: $r_T/r_o$ as a fraction of season and time of day

Table 4.4-2a:  Estimated and 23 Year Calculated Monthly-Average Hourly Clearness Indexes for Madison.

MADISON $\overline{k}_T$ s

| Month | $\overline{K}_T$ | Hour from Solar Noon | | | | | | | | |
|---|---|---|---|---|---|---|---|---|---|---|
| | | 1/2 | | | 1 1/2 | | | 2 1/2 | | |
| | | a.m. | est. | p.m. | a.m. | est. | p.m. | a.m. | est. | p.m. |
| Jan. | .438 | .478 | .468 | .477 | .454 | .451 | .464 | .411 | .417 | .425 |
| Feb. | .493 | .537 | .529 | .529 | .524 | .512 | .513 | .487 | .478 | .484 |
| March | .499 | .539 | .538 | .527 | .536 | .523 | .517 | .524 | .494 | .495 |
| April | .474 | .512 | .513 | .505 | .513 | .502 | .496 | .507 | .479 | .474 |
| May | .507 | .552 | .551 | .544 | .546 | .540 | .538 | .533 | .520 | .526 |
| June | .534 | .584 | .581 | .576 | .583 | .571 | .566 | .566 | .551 | .556 |
| July | .546 | .589 | .593 | .585 | .591 | .583 | .584 | .579 | .562 | .568 |
| Aug. | .549 | .594 | .595 | .583 | .595 | .583 | .585 | .582 | .559 | .566 |
| Sept. | .517 | .569 | .558 | .558 | .555 | .544 | .546 | .535 | .516 | .526 |
| Oct. | .496 | .534 | .533 | .534 | .529 | .517 | .520 | .501 | .485 | .497 |
| Nov. | .393 | .426 | .420 | .424 | .414 | .405 | .409 | .385 | .376 | .380 |
| Dec. | .376 | .415 | .401 | .413 | .395 | .386 | .393 | .353 | .356 | .353 |

Table 4.4-2b: Estimated and 23 Year Calculated Monthly-Average Hourly Clearness Indexes for Albuquerque.

ALBUQUERQUE $\overline{k}_T$ s

| Month | $\overline{K}_T$ | 1/2 | | | 1 1/2 | | | 2 1/2 | | |
|---|---|---|---|---|---|---|---|---|---|---|
| | | a.m. | est. | p.m. | a.m. | est. | p.m. | a.m. | est. | p.m. |
| Jan. | .635 | .683 | .680 | .676 | .676 | .657 | .658 | .634 | .612 | .621 |
| Feb. | .665 | .714 | .715 | .705 | .702 | .692 | .694 | .675 | .650 | .662 |
| March | .684 | .738 | .737 | .729 | .732 | .717 | .713 | .707 | .678 | .675 |
| April | .712 | .770 | .770 | .761 | .768 | .752 | .737 | .754 | .717 | .711 |
| May | .728 | .798 | .789 | .780 | .801 | .773 | .760 | .790 | .742 | .720 |
| June | .739 | .815 | .802 | .808 | .814 | .787 | .778 | .804 | .757 | .733 |
| July | .700 | .793 | .760 | .786 | .785 | .745 | .753 | .769 | .715 | .693 |
| Aug. | .703 | .785 | .761 | .777 | .780 | .744 | .755 | .758 | .712 | .699 |
| Sept. | .714 | .784 | .771 | .772 | .775 | .751 | .746 | .749 | .713 | .707 |
| Oct. | .706 | .757 | .759 | .751 | .744 | .737 | .734 | .722 | .693 | .702 |
| Nov. | .672 | .720 | .721 | .715 | .708 | .697 | .700 | .672 | .650 | .657 |
| Dec. | .632 | .676 | .677 | .671 | .663 | .653 | .658 | .630 | .607 | .620 |

Hour from Solar Noon

To incorporate the relation between $\overline{k}_T$ and $\overline{K}_T$ given by Equation 4.4-22, the computer program PHIGENHRS was developed. This program is listed in Appendix C. Using PHIGENHRS, sets of $\phi$-curves were generated for Madison using $\overline{K}_T$s from the 23 years of data previously analyzed. The results for January, April, and June are compared in Figure 4.4-14 to the calculated $\phi$-curves (shown dashed) from Section 4.3. In general, these generated curves represented the data much better than the single curve obtained from the Liu and Jordan scheme. The worst agreement is in April, because of the large disagreement between its $k_T$ and the generalized $K_T$ distribution (Figure 4.4-11).

Since Albuquerque's $k_T$ distributions more closely follow the generalized $K_T$ distributions (40), the use of PHIGENHRS would produce better agreement with the Albuquerque $\phi$-curves calculated from data.

### 4.4.3 Treatment of Diffuse Radiation

In the previous work, the following assumptions were made in regard to the treatment of diffuse radiation:

1. Daily diffuse fraction correlations can be used as hourly correlations.

2. The Liu and Jordan diffuse fraction correlations are correct.

3. The ground reflectance equals 0.2.

The validity and effects of these assumptions will be examined here. The long-term monthly-average daily diffuse fraction is defined
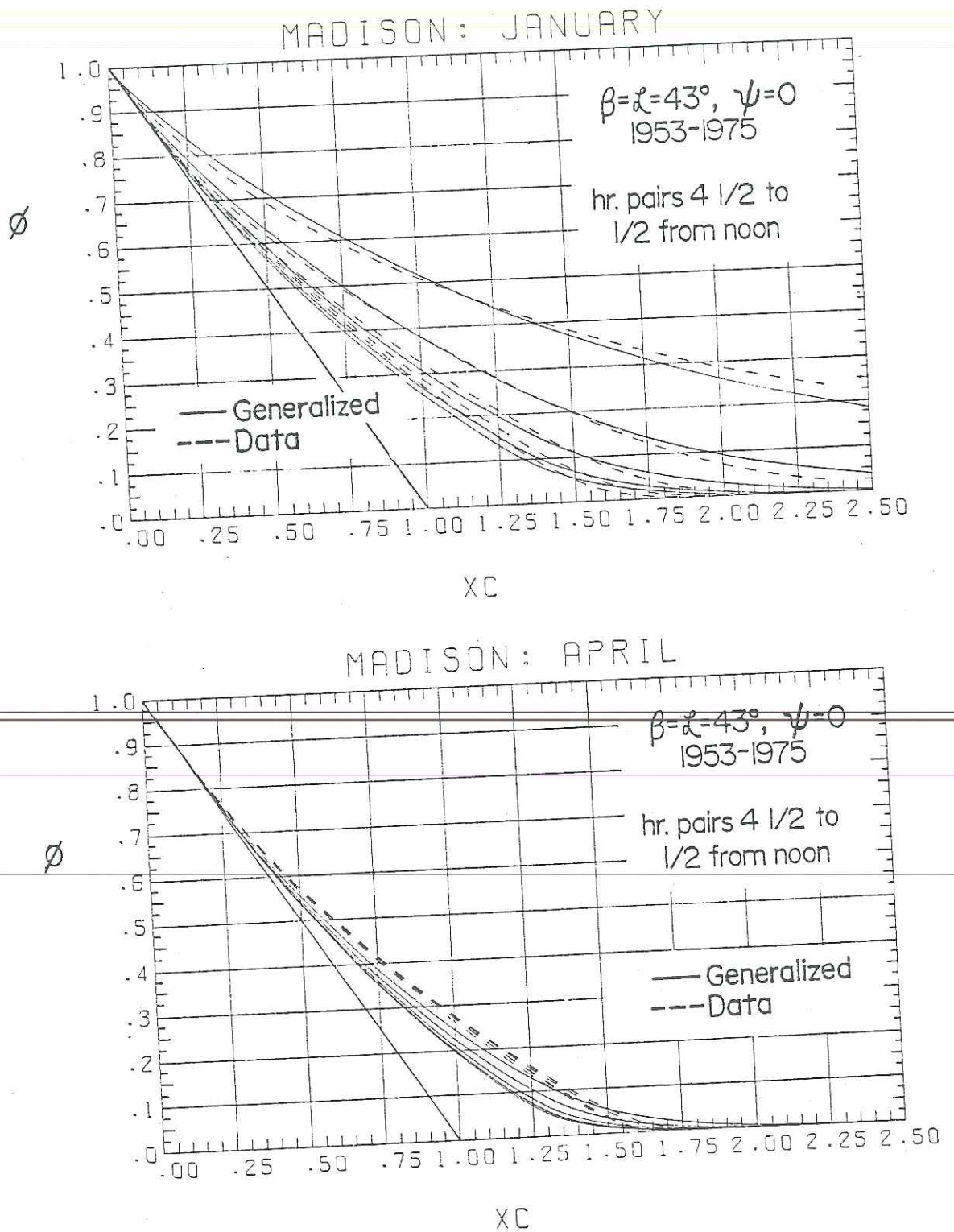
Figure 4.4-14:   Comparison of 23 year calculated and hourly
generalized φ-curves
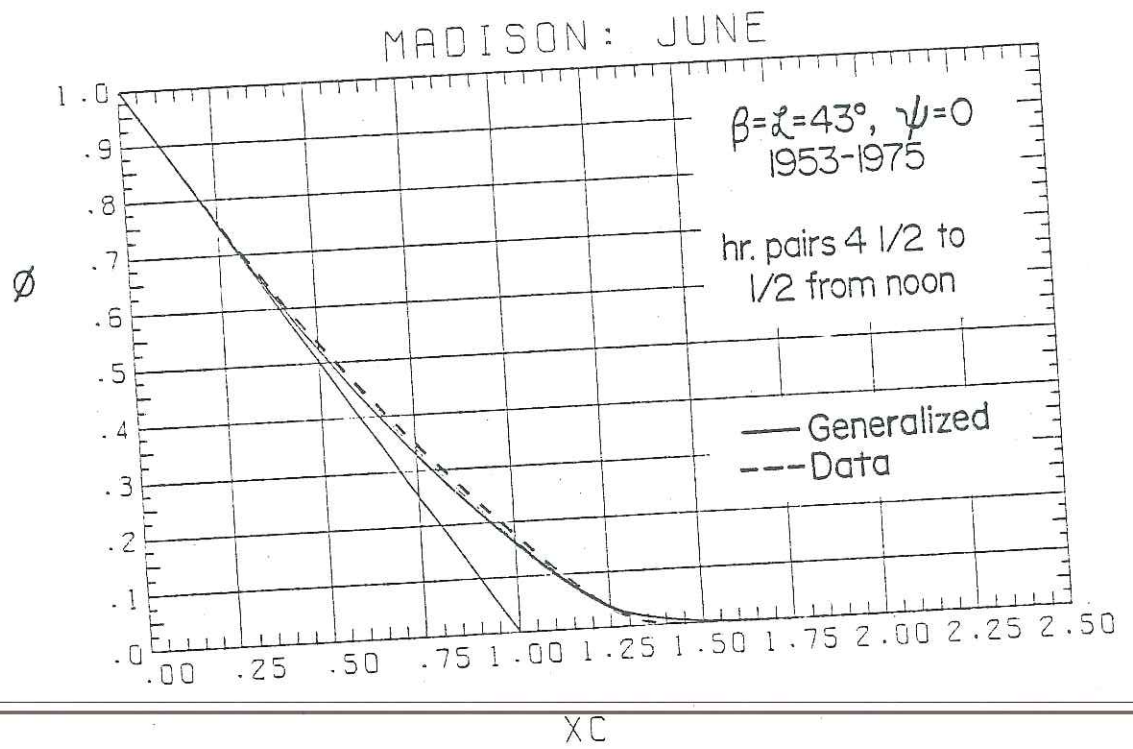
Figure 4.4-14: (continued)

as:

$$\frac{\overline{H}_d}{\overline{H}} = \frac{\sum\limits_{y=1}^{Y} \sum\limits_{d=1}^{D} \sum\limits_{h=1}^{24} I_d}{\sum\limits_{y=1}^{Y} \sum\limits_{d=1}^{D} \sum\limits_{h=1}^{24} I} \qquad (4.4-24)$$

As Figure 4.4-11 indicates (also see Theilacker (40)), all the hours for a particular month have about the same $k_T$ distribution (although they do have different $\overline{k}_T$ s). This means that a diffuse correlation for the hour from 9-10 would be the same as one for 11 to 12 etcetera. Because of the likeness in hours, Equation 4.4-24 is also the monthly-average hourly diffuse fraction, $\overline{I}_d/\overline{I}$.

The monthly-average daily diffuse fraction can be obtained from the daily diffuse fraction integration:

$$\frac{\overline{H}_d}{\overline{H}} = \int_0^1 \frac{H_d}{H} P\left(H_d/H\right) d\left(H_d/H\right) \qquad (4.4-25)$$

Similarly, the monthly-average hourly diffuse fraction is:

$$\frac{\overline{I}_d}{\overline{I}} = \int_0^1 \frac{I_d}{I} P\left(I_d/I\right) d\left(I_d/I\right) \qquad (4.4-26)$$

Since $\overline{I}_d/\overline{I} \simeq \overline{H}_d/\overline{H}$, the integrals of Equations 4.4-25 and 4.4-26 must be equal. Thus, the $I_d/I$ and $H_d/H$ correlations differ only by their probability distributions.

What the above means is that the assumption of using $H_d/H$ for $I_d/I$ is the same as assuming the hourly and daily clearness index distributions are the same. Since it has been shown that both of these assumptions are reasonable, the results obtained are internally consistent.

To test the effect of different diffuse fraction correlations, two of the more extreme correlation sets available were compared. Tuller's (41) daily and monthly average relations:

$$H_d/H = 1.20 - 1.20 \, \overline{K}_T \tag{4.4-27}$$

and

$$\overline{H}_d/\overline{H} = 0.84 - 0.62 \, \overline{K}_T \tag{4.4-28}$$

were used as the upper limit, and Liu and Jordan's (Equations 4.3-7 and 4.4-15) as the lower limit.

The results of using these two sets of diffuse fraction correlations are shown in Figure 4.4-15 for $\overline{k}_T = 0.5$ and various $V_{bd}$s. As $V_{bd}$ decreases, the difference between the two curves becomes indistinguishable as $V_{bd}$ approaches zero. This indicates that the results presented previously are fairly independent of the diffuse correlation used. The reader is cautioned, that while for the dimensionless $\phi$-curve representation the choice of diffuse fraction is of no great consequence, when calculating $I_T$ (or $\overline{I}_T$) the diffuse fraction can be of significance.
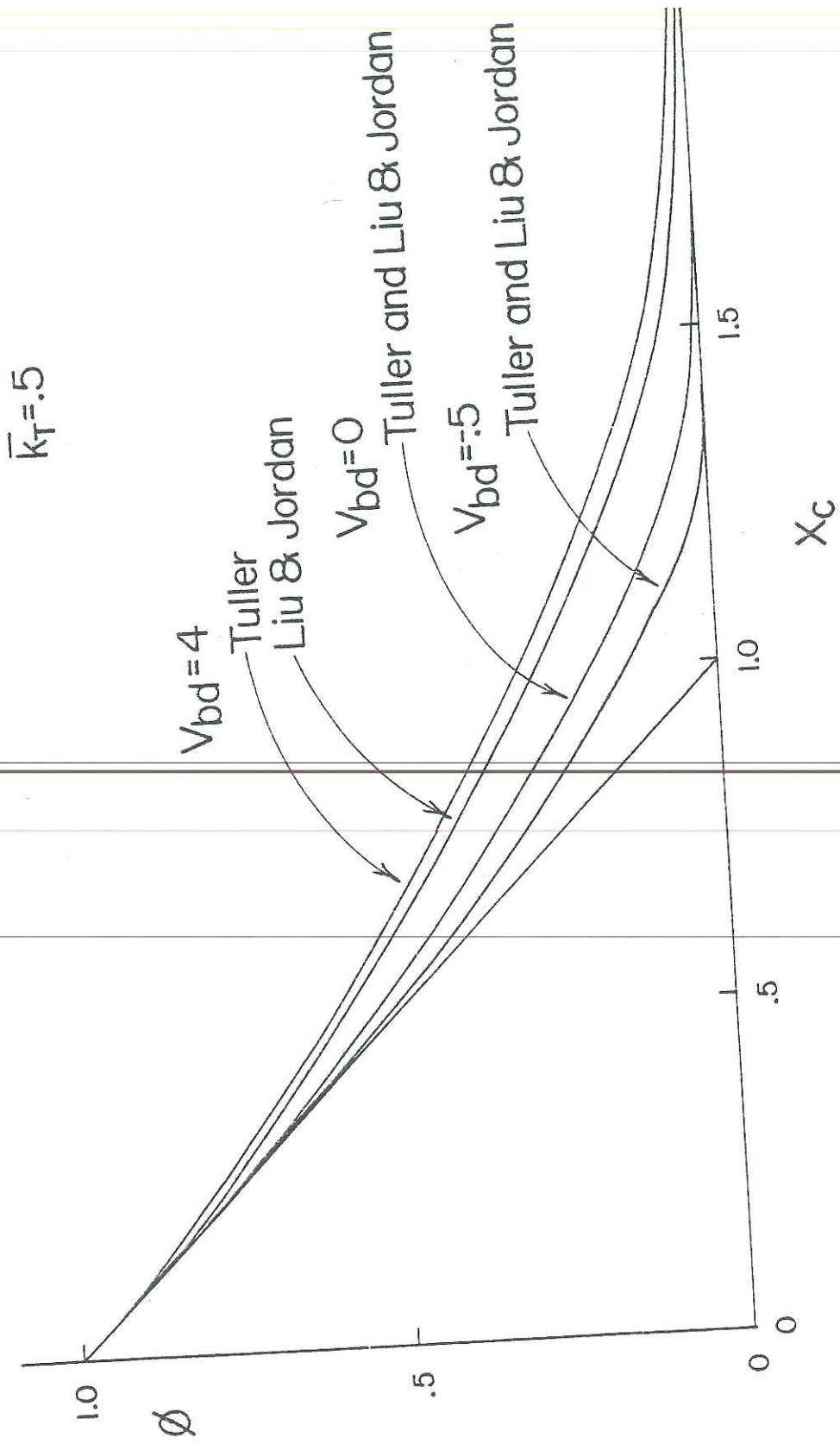
Figure 4.4-15: Effect of diffuse correlation on $\phi$

The use of a ground reflectance equal to 0.2 was tested by generating $\phi$-curves taking the ground reflectance equal to 0.7. The difference in resulting $\phi$-curves was indistinguishable for all the situations examined.

### 4.4.4 Conclusions

Based on the evidence presented in this section, the following conclusions can be drawn:

1. The generalized method of obtaining $\phi$ as presented by Liu and Jordan was examined. It was determined that a single curve based on daily radiation relations did not adequately describe the data for months very far from summer solstice.

2. The collector-sky view factor in conjunction with $R_b$ was found to be a better correlating parameter for $\phi$-curves than $R_b$ alone.

3. Hourly $\phi$-curves based on hourly radiation parameters are fairly accurate in predicting $\phi$ for all hours and months.

4. Hourly $\phi$-curves have a larger spread in the winter than the summer because of the seasonal effect on the change in $R_b$ and $\overline{k}_T$ over a day.

5. Hourly radiation relations allow the use of Figure 4.4-12 for other than south facing surfaces.

6. The frequency distribution of $k_T$ (and thus $I_T/\bar{I}_T$) is what determines the shape of $\phi$-curves.

7. The choice of diffuse fraction correlation and ground reflectance have little effect on the obtained $\phi$-curves.

After making the improvements mentioned above, $\phi$ can be predicted more accurately than previously possible. Unfortunately, the determination of all the $\phi$ s required to estimate a systems annual performance would be quite cumbersome. The next section poses an analytical expression for $\phi$ that is obtained from a derived $k_T$ distribution. The use of this expression will simplify the task of finding $\phi$ s.

## 4.5 Derivation of Hourly Utilizability from a Random Insolation Sequence

To use the generalized hourly utilizability of the previous section requires either the interpolative use of Figure 4.4-12, or the computer program that generated them. An analytical expression for $\phi$ would greatly reduce the effort of determining a systems performance.

Writing equation 4.4-16 in an hourly form:

$$\phi = \frac{\int_{I_c}^{I_{max}} (I R - I_c) P(I) \, dI}{\int_{I_{min}}^{I_{max}} I R P(I) \, dI} \qquad (4.5-1)$$

where:

P(I) = Long-term average probability of I occurring

$I_{max}$ = Maximum observed hourly insolation

$I_{min}$ = Minimum observed hourly insolation

$I_c$ = Critical insolation level.

Dividing top and bottom of Equation 4.5-1 by $I_o^2$:

$$\phi = \frac{\displaystyle\int_{k_c}^{k_{max}} (k_T R - k_c) \, P(k_T) \, dk_T}{\displaystyle\int_{k_{min}}^{k_{max}} k_T R \, P(k_T) \, dk_T} \qquad (4.5-2)$$

where $k_{min}$ and $k_{max}$ are the minimum and maximum observed hourly clearness indices. The critical clearness index can be obtained by setting the radiation on a tilted surface equal to $I_c$.

$$k_c = \frac{I_c}{I_o R} \qquad (4.5-3)$$

Since R is a function of $k_T$ through a diffuse fraction of the form,

$$I_d/I = a_1 + a_2 k_T + a_3 k_T^2 + a_4 k_T^3 \qquad (4.5-4)$$

Equation 4.5-3 can not be solved explicitly for $k_c$. An iterative solution for $k_c$ is presented in Appendix B.

Bendt et al. ( 3 ) have proposed a $k_T$ probability distribution by:

1. Assuming the occurrence of $k_T$ s is random (that is, the $k_T$ at noon today has no effect on $k_T$ at noon tomorrow).

2. Restricting $k_T$ between the minimum and maximum observed ($k_{min}$ and $k_{max}$).

3. Specifying $\bar{k}_T$.

The random $k_T$ occurrence assumption used in the development of the up-coming probability distribution is not quite true. As indicated earlier the spring weather fronts of Madison Aprils tend to produce less than random $k_T$ occurrences.

Using the above assumption and restrictions, Bendt et al. (3) derived a $P(k_T)$ distribution from purely statistical considerations. It is of the form:

$$P(k_T) = C \exp (\gamma k_T) \tag{4.5-5}$$

where C and $\gamma$ are constants. Since the cumulative probability must be unity, integration of the above relation from $k_{min}$ to $k_{max}$ yields:

$$C = \frac{\gamma}{\exp(\gamma k_{max}) - \exp(\gamma k_{min})} \tag{4.5-6}$$

Also, since $\bar{k}_T$ is the expected value of $k_T$,

$$\bar{k}_T = \int_{k_{min}}^{k_{max}} k_T \, P(k_T) \, dk_T \tag{4.5-7}$$

Integration of this relation yields:

$$\bar{k}_T = \frac{(k_{max} - 1/\gamma)\exp(\gamma k_{max}) - (k_{min} - 1/\gamma)\exp(\gamma k_{min})}{\exp(\gamma k_{max}) - \exp(\gamma k_{min})} \qquad (4.5\text{-}8)$$

The solution of this transcendental equation for $\gamma$ is shown in Figure 4.5-1 for $k_{min} = 0.05$ and various $k_{max}$s. An extended discussion of the solution for $\gamma$ is presented in Appendix A.

A cumulative frequency distribution can be obtained by integrating the probability distribution. Substituting Equation 4.5-6 back into Equation 4.5-5 and integrating,

$$f(k_T) = \frac{\exp(k_{min}) - \exp(k_T)}{\exp(k_{min}) - \exp(k_{max})} \qquad (4.5\text{-}9)$$

This will enable a direct comparison with the frequency distributions previously presented.

Bendt et al. (3) originally proposed the above probability function to be used for $K_T$. They recommended using $K_{min} = 0.05$ and the $K_{max}$s shown in Table 4.5-1. Using these recommended values, the $K_T$ frequency distributions are plotted in Figure 4.5-2 along with the Liu and Jordan generalized distributions from Figure 4.4-5. Both distributions have their areas equal to the particular $\bar{K}_T$. The analytical distribution does not have the inflected tail at $f \geq 0.9$.

Inspection of Figures 4.5-1 and 4.5-2 gives some insight to this exponential distribution. If $K_{max}$ (or $k_{max}$) were equal to $\bar{K}_T$ (or $\bar{k}_T$), $\gamma$ would be infinite, the $K_T$ (or $k_T$) distribution would
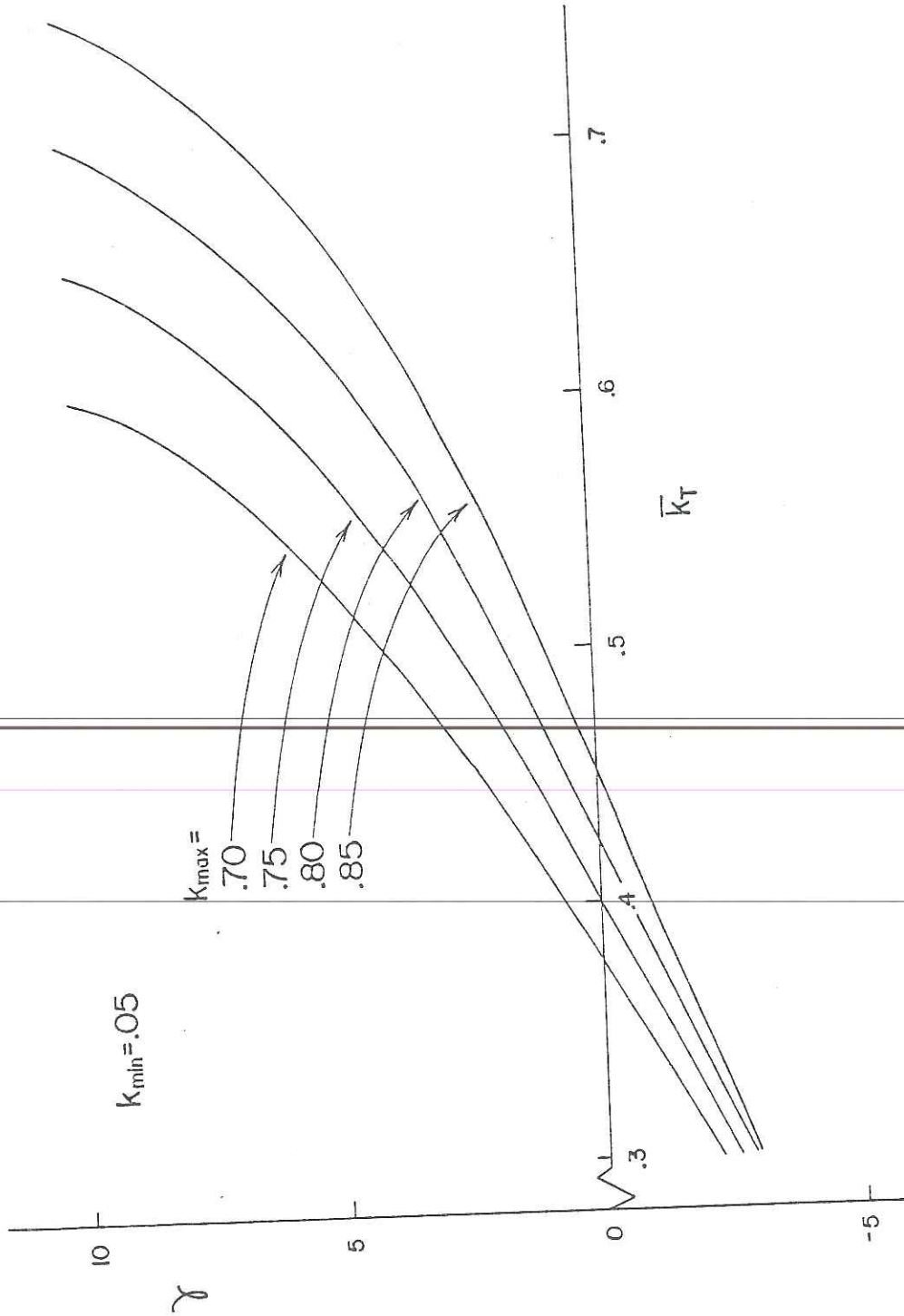
Figure 4.5-1: Solution for $\gamma$ as a function of $k_{max}$ and $\overline{k}_T$

Table 4.5-1:  Recommended Values of $K_{max}$ (from Bendt et al.)

| $\overline{K}_T$ | $K_{max}$ |
|---|---|
| .3 | .68 |
| .4 | .73 |
| .5 | .76 |
| .6 | .79 |
| .7 | .82 |
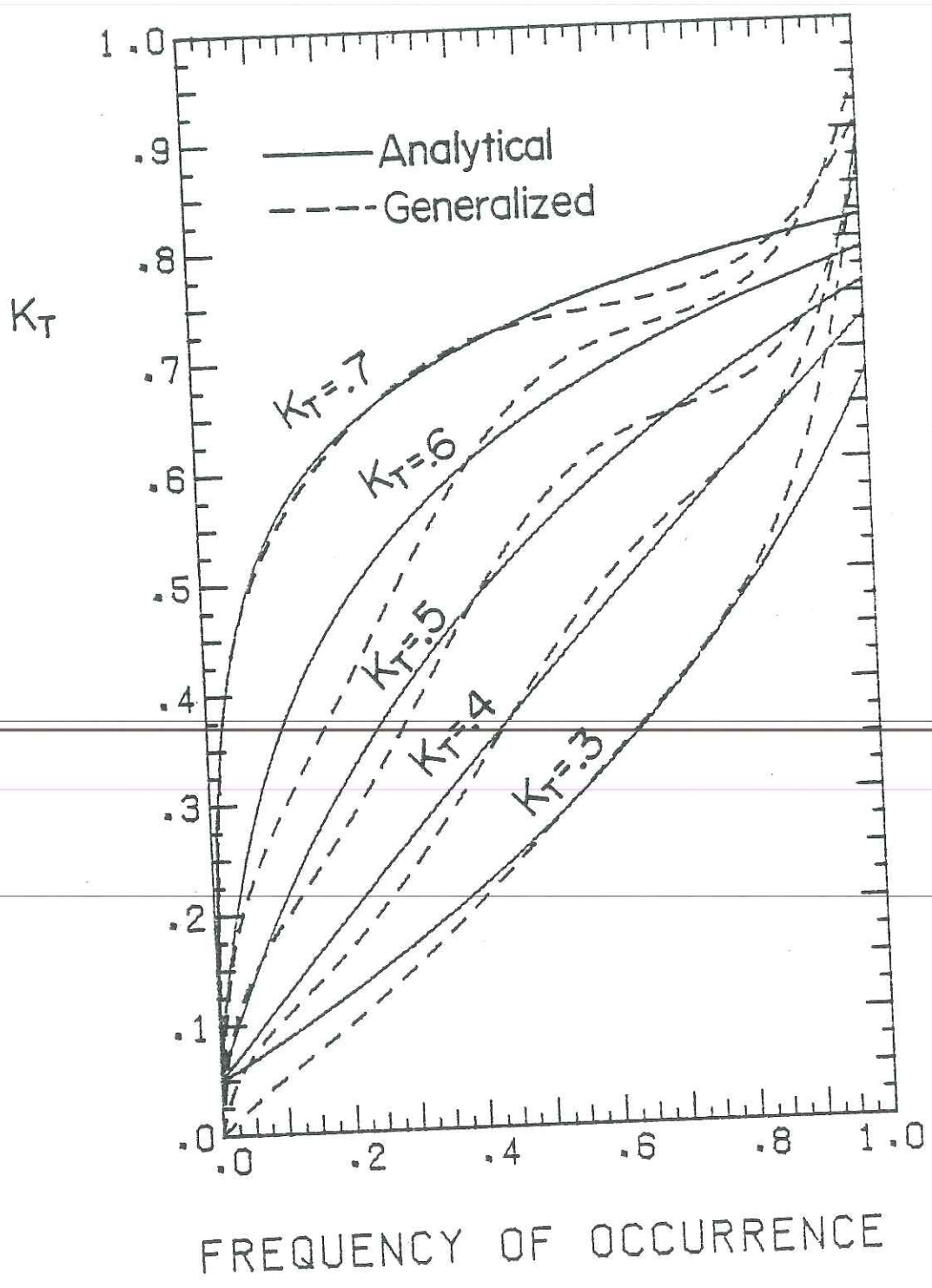
Figure 4.5-2: Comparison of analytical and generalized $K_T$ distributions

approach a horizontal line at $K_{max}$ (or $k_{max}$) and a $\phi$-curve based on this distribution would be the identical day limit. Although $\gamma=0$ is a valid solution (see Appendix A) to Equation 4.5-8, it must be approximated by a small number to avoid division by zero in the upcoming expression for $\phi$.

When using the $k_T$ probability distribution of Equation 3.5-2, the selection of $k_{min}$ and $k_{max}$ becomes difficult. A $k_{min}$ of 0.05 seems to agree with the data and otherwise be a reasonable assumption. If $k_{max}$ were selected from 23 consecutive years of data for Madison and Albuquerque, it would be between 0.9 and 1 for all $\bar{k}_T$'s. This is quite in excess of "clear sky" models (20, 29). Using these inflated $k_{max}$ s would result in $k_T$ distributions that greatly overpredict the frequency of higher $k_T$ s and underpredict lower $k_T$ s. Since $k_{max}$ has an effect on the whole $k_T$ distribution, it should be chosen to give the best overall agreement with all the available data. At this point, $k_{max}$ is still not known with real certainty.

A comparison of 23 year and analytical frequency distributions for some Madison hours is shown in Figure 4.5-3. The analytical distribution was obtained in all cases with $k_{min} = 0.05$ and $k_{max} = 0.80$. The analytical $k_T$ distribution agrees about as well as the generalized curves of Figure 4.4-11. For Albuquerque, the analytical distribution will agree slightly better than the generalized one, because Albuquerque data (40) more closely resembles an exponential
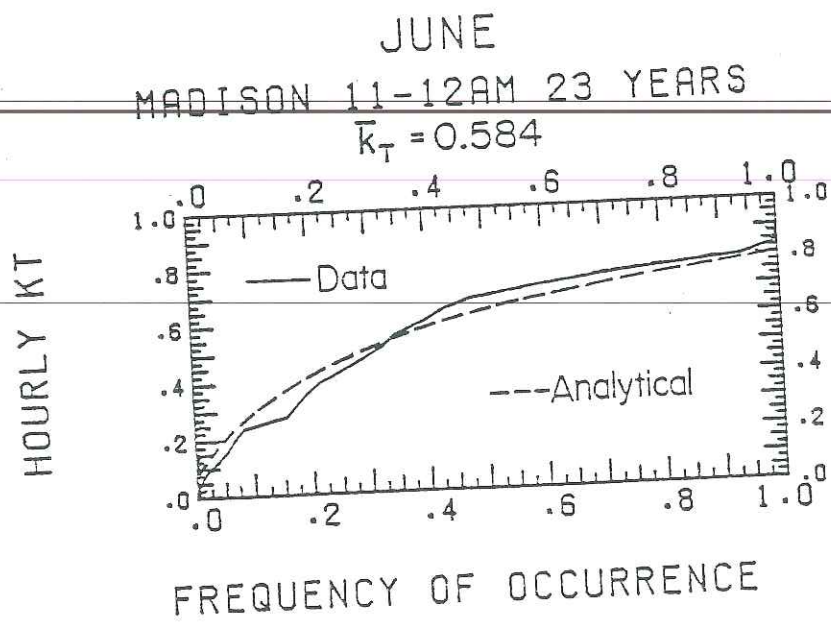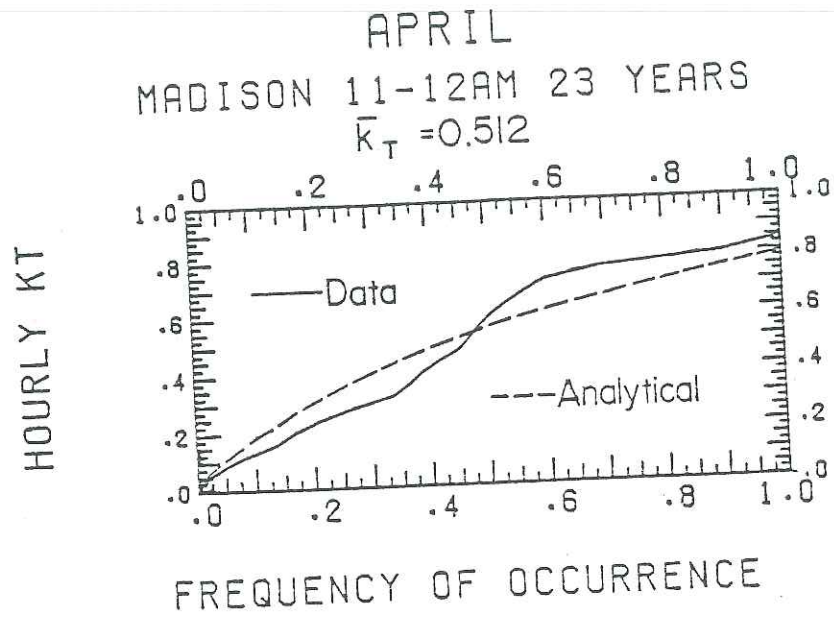
Figure 4.5-3: Comparison of 23 year and analytical $k_T$ distributions

distribution. It will be assumed that the analytical $k_T$ distribution adequately describes the data.

Substituting Equations 4.3-2, 4.4-21, 4.5-4, 4.5-5, and 4.5-6 into Equation 4.5-2 and performing the integration yields;

$$\phi = \frac{C\left[\left(A(k_{max})-I_c/\gamma I_o\right)\exp(\gamma k_{max})-\left(A(k_c)-A(k_c)-I_c/\gamma I_o\right)\exp(\gamma k_c)\right]}{C\left[A(k_{max})\exp(\gamma k_{max})-A(k_{min})\exp(\gamma k_{min})\right]} \quad (4.5-10)$$

where:

$$A(k_T) = (R_b+D)\varepsilon_1-V_{bd}(a_1\varepsilon_1+a_2\varepsilon_2+a_3\varepsilon_3+a_4\varepsilon_4)$$

with;

$$D = \rho\ \frac{1-\cos\beta}{2}$$

$$\varepsilon_1 = k_T/\gamma - 1/\gamma^2$$

$$\varepsilon_2 = k_T^2/\gamma - 2\ k_T/\gamma^2 + 2/\gamma^3$$

$$\varepsilon_3 = k_T^3/\gamma - 3\ k_T^2/\gamma^2 + 6\ k_T/\gamma^3 - 6/\gamma^4$$

$$\varepsilon_4 = k_T^4/\gamma - 4\ k_T^3/\gamma^2 + 12\ k_T^2/\gamma^3 - 24\ k_T/\gamma^4 + 24/\gamma^5$$

This expression for $\phi$ can be programmed on a hand held calculator. The values of $\gamma$ can be obtained from Figure 4.5-1 or as described in Appendix A. The critical clearness index must be determined by the iterative scheme presented in Appendix B. It has been found that $\phi$ changes in the 3rd decimal place for a change in $\gamma$ in the third decimal place. Thus the case of $\gamma=0$ can be well approximated by a small number.

To compare analytical $\phi$ s against previously obtained ones, a relation for $X_c$ is required. Since the denominator of Equation 4.5-10 is $\bar{I}_T$, the critical insolation ratio can be expressed as:

$$X_c = \frac{I_c}{C\left[A(k_{max})\exp(\gamma k_{max})-A(k_{min})\exp(\gamma k_{min})\right]} \qquad (4.5\text{-}11)$$

The computer program AYLPHY was developed to evaluate the above relations for $\phi$ and $X_c$, using the Liu and Jordan diffuse correlation in Equation 4.3-7. A listing of this program can be found in Appendix C. Using AYLPHI with a $k_{min}$ of 0.05 a $k_{max}$ of 0.80 and the relation for $\bar{k}_T$ given by Equation 4.4-22, the Madison $\phi$-curves for January, April, and June shown in Figure 4.5-4 were obtained. The dashed curves in this figure are the calculated $\phi$-curves from Section 4.3. The agreement here between the analytical and calculated $\phi$-curves is comparable to the generated generalized curves of Figure 4.4-14.

Using AYLPHI with a constant $k_{max}$ of 0.75 and $k_{min}$ of 0.05 resulted in poorer agreement with the Madison data than the $k_{max} = 0.80$ described above. Using a variable $k_{max}$;

$$k_{max} = b_1 + b_2 \bar{k}_T \qquad (4.5\text{-}12)$$

with $b_1 = 0.5875$ and $b_2 = 0.375$, the agreement between analytical and calculated $\phi$-curves was comparable to the $k_{max} = 0.8$ case. (For the estimated $\bar{k}_T$ s for Madison listed in Table 4.4-2, $k_{max}$ ranged from

MADISON: JANUARY

$\beta = \mathcal{L} = 43°, \ \psi = 0$
1953-1975

hr. pairs 4 1/2 to
1/2 from noon

—— Analytical
--- Data

XC

MADISON: APRIL

$\beta = \mathcal{L} = 43°, \ \psi = 0$
1953-1975

hr. pairs 4 1/2 to
1/2 from noon

—— Analytical
--- Data

XC
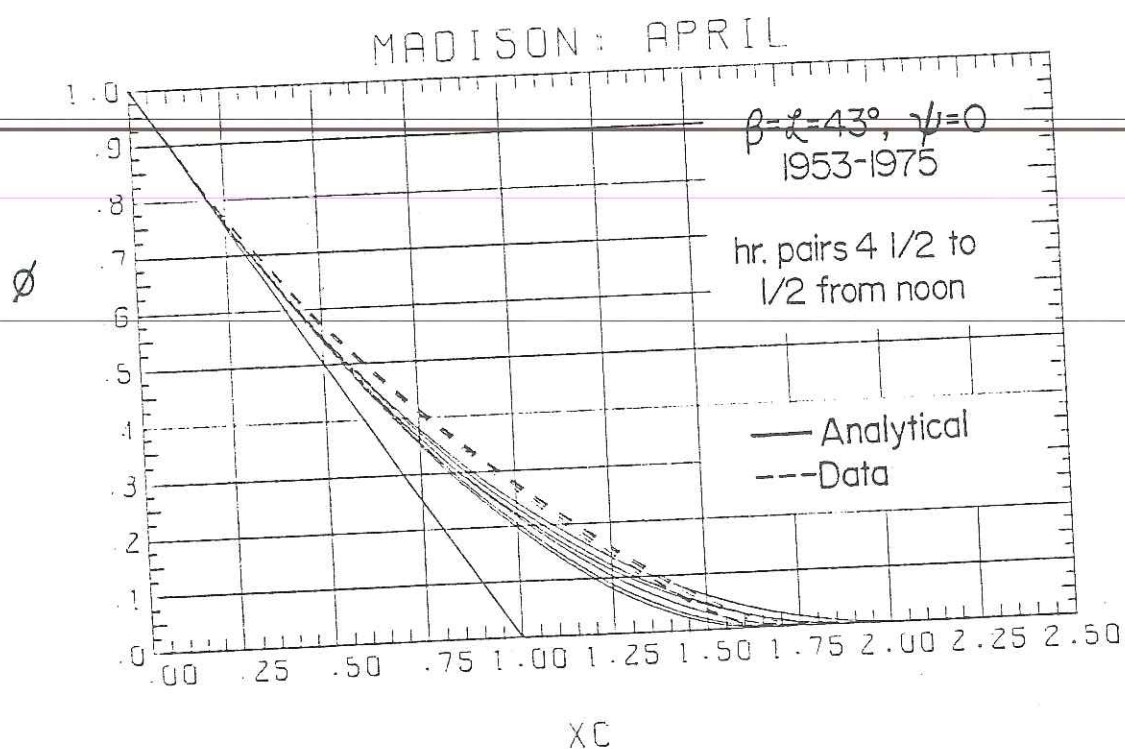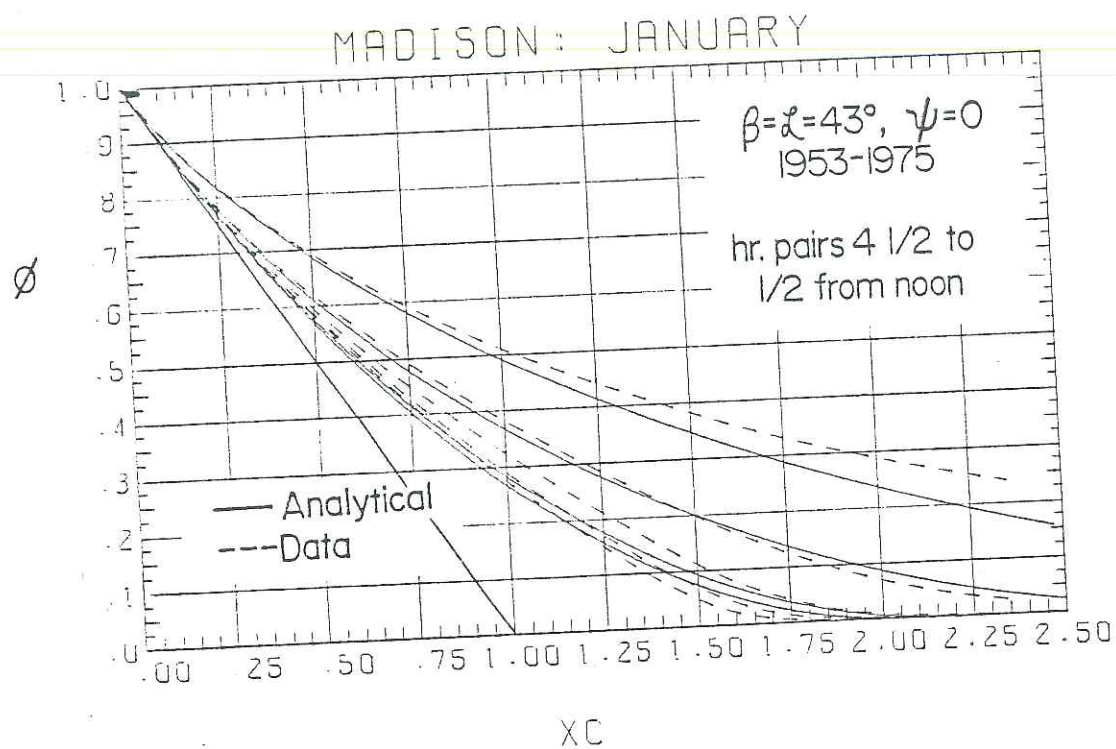
Figure 4.5-4:  Comparison of 23 year calculated and
analytical $\phi$-curves

MADISON: JUNE

$\beta = \mathcal{L} = 43°, \ \psi = 0$
1953-1975

hr. pairs 4 1/2 to
1/2 from noon

—— Analytical
--- Data
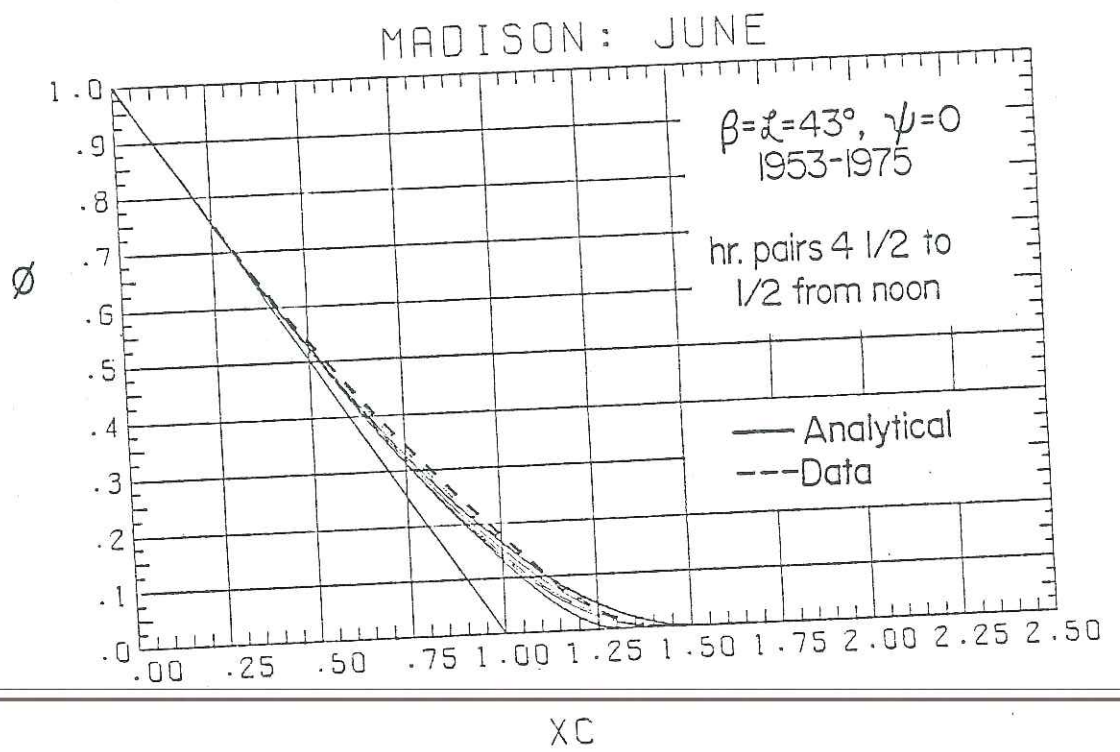
Figure 4.5-4:  (continued)

0.72 to 0.81.) Since a $k_{max}$ of 0.80 would probably not be sufficient for a location such as Albuquerque with $\overline{k}_T$ s significantly higher than Madison's, a relation like Equation 4.5-12 is recommended for general use. If a relation like this is used, the solution of Equation 4.5-8 for $\gamma$ can be plotted as a unique function of $\overline{k}_T$. A preliminary investigation indicated that $\gamma$ would be nearly linear with $\overline{k}_T$ for $b_1 = 0.5875$ and $b_2 = 0.375$.

The agreement between the derived analytical expression and extensive single location data is convenient. It allows the direct calculation of $\phi$ rather than interpolating Figure 4.4-12. The next section will compare the usage and results of the hourly generalized and analytical relations for $\phi$.

## 4.6 Comparing Hourly Utilizability Methods

### 4.6.1 Predicting Usable Energy

The previous sections indicated that the $\phi$-curves obtained for a single location were equally well approximated by generating them from a long-term-average daily clearness index distribution (used on an hourly basis) and calculating them from a random insolation sequence $k_T$ distribution. Recalling Equations 3.4-7 and 3.4-13 it becomes apparent that the product of $\phi$ and $\overline{I}_T$ is the quantity of real interest.

To facilitate a comparison on this basis, the long-term average yearly usable energy between hours i and j is defined as:

$$U_{ij} = \sum_{m=1}^{12} \sum_{h=i}^{j} \phi_{mh} \, \overline{I}_{T-mh} \, D_m \qquad\qquad (4.6-1)$$

Examination of Equation 3.4-7 reveals that $U_{ij}$ is the long-term average, yearly total energy per unit of effective area, between hours i and j, that could be used (or dumped if $\phi'_{mh}$ is used) by a collector with a perfect $(\tau\alpha)$.

A comparison of $U_{ij}$, based on the Madison $\phi$s of the previous sections, for the hours from 8 to 16, is shown in Figure 4.6-1 as a function of a critical level held constant over the year. The data curve was obtained by using the $\overline{I}_T$s from RADAVE and linearly interpolating between HRPHIXC calculated $\phi$-$X_c$ pairs. The hourly generated curve was obtained by estimating $\overline{I}_T$ using Equations 4.3-6, 4.4-20, and 4.4-22 and linearly interpolating between PHIGENHRS generated $\phi$-$X_c$ pairs. The analytical curve of Figure 4.6-1 was arrived at by evaluating the numerator of Equation 4.5-10 for various $I_c$s.

The comparison in Figure 4.6-1 shows that the hourly generated and analytical methods both underpredict the $U_{8-16}$ calculated from Madison data for all critical levels. If the entire range of $I_c$ (0 to 1000 $W/m^2$) is considered, the generated prediction of $U_{8-16}$ is the more accurate prediction method. If only values of $I_c$ above a reasonable flat-plate collector $I_{min}$ (200 $W/m^2$) are considered, the analytical prediction is the more accurate one. Thus, the analytical method predicts dumped energy better for this location and selection of $k_{min}$ and $k_{max}$.
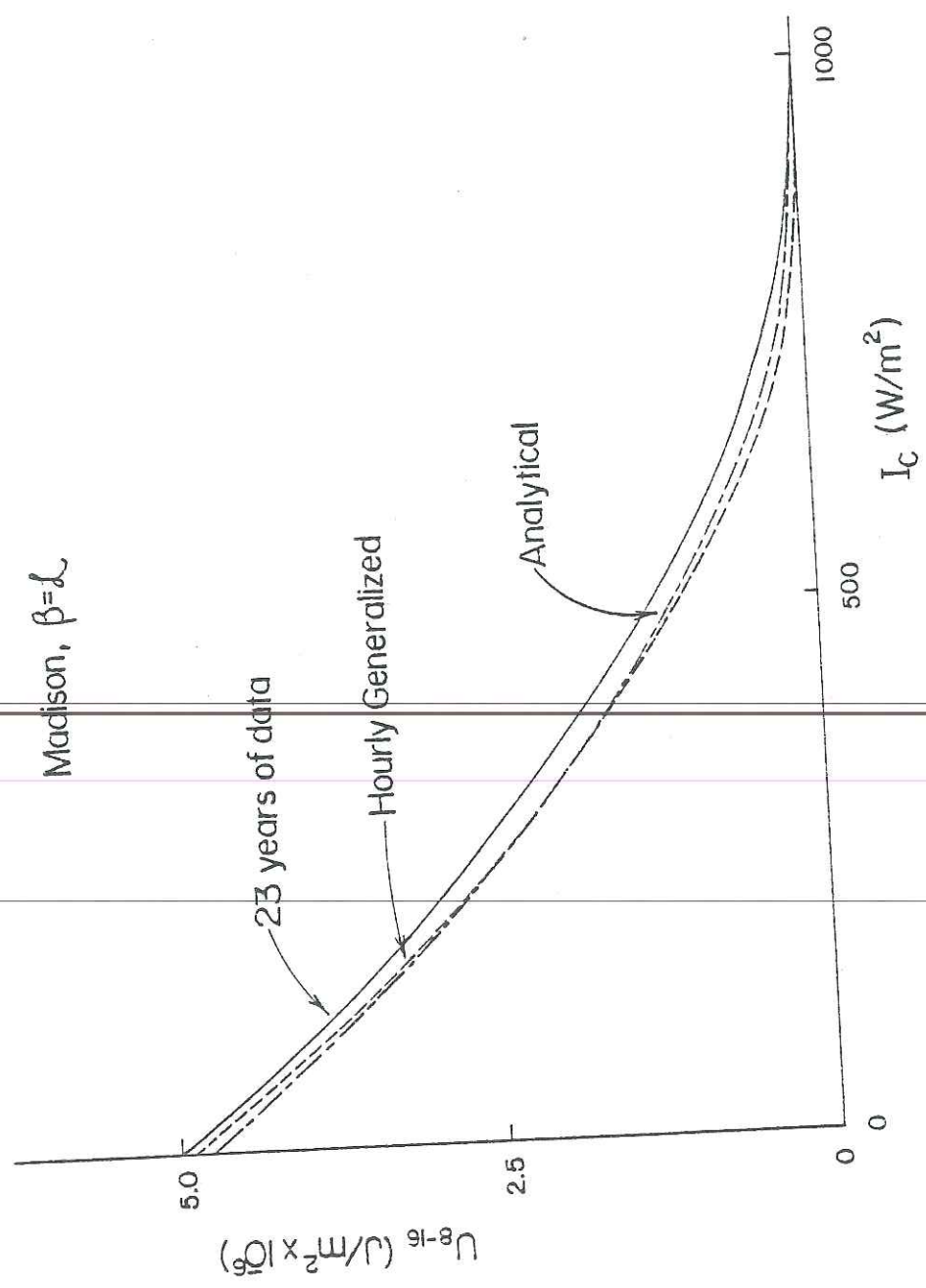
Figure 4.6-1: Comparison of 23 year, hourly generalized, and analytical predictions of usable energy.

### 4.6.2  Example for a No Storage System

It is desired to estimate the performance of a no storage system to be built in Madison, Wisconsin (Latitude = 43°).  The total year's load is 2 TJ/yr with a minimum useful temperature of 80°C. This load is distributed over 52 weeks, 5 days per week, 8 hours per day.  The flat-plate collector array has the following characteristics.

$$A = 600 \text{ m}^2$$

$$\beta = 43° \text{ (Fixed)}$$

$$F_R(\tau\alpha) = 0.797$$

$$F_R U_L = 2.59 \text{ W/°C-m}^2$$

For an initial estimate of system performance, the load heat exchanger will be assumed infinite, and no heat losses from pipes will be considered.

To predict the performance of this system using generalized hourly utilizability, the procedure outlined below should be carried out for the 4 hour pairs about noon (2 x 4 = 8 hours per day) for all 12 months of the year.

For June, the Madison 23 year average daytime temperature was found from Equation 3.4-4 to be $\overline{T}_a = 22°C$, and the monthly-average daily clearness index is found from Table 4.4-2, $\overline{K}_T = 0.53.$*

---

*In general, $\overline{T}_a$ s and $\overline{K}_T$ s can be obtained from reference 2.

From Equation 3.4-2,

$$I_{min} = \frac{2.59 \ (80-22)}{0.797}$$

$$I_{min} = 189 \ W/m^2$$

Using Equation 3.4-9,

$$I_{max} = 189 + \frac{2 \times 10^{12} \ J}{Yr} \left| \frac{yr}{52 \ wk} \right| \frac{wk}{5 \ day} \left| \frac{day}{8 \ hr} \right| \frac{W\text{-}hr}{3600 \ J} \left| \frac{1}{600 \ m^2} \right| 0.797$$

$$I_{max} = 748 \ W/m^2$$

Considering the hour pair centered 1/2 hour from noon, the hourly radiation relations are obtained as follows.  From Equation 4.3-3,

$$\overline{R}_{bh} = 0.976$$

Using this in Equation 4.4-21,

$$V_{bd} = 0.976 - \frac{1 + \cos(43)}{2}$$

$$V_{bd} = 0.110$$

By first employing Equation 4.4-4,

$$r_T = 0.116$$

and then Equation 4.4-23,

$$r_o = 0.107$$

$\overline{k_T}$ can be determined from Equation 4.4-22.

$$\overline{k_T} = 0.53 \frac{0.116}{0.107}$$

$$\overline{k_T} = 0.576$$

The extraterrestrial radiation for this hour can be obtained through Equation 4.3-7 as:

$$I_o = 1225 \text{ W/m}^2$$

To determine $\overline{I_T}$, $\overline{R_h}$ must first be calculated. From Equation 4.4-15,

$$\overline{I_d}/\overline{I} = 1.37 - 4.027(0.576) + 5.531(0.576)^2 - 3.108(0.576)^3$$

$$\overline{I_d}/\overline{I} = 0.312$$

incorporating this into Equation 4.4-20,

$$\overline{R_h} = (1-0.312)0.976 + 0.312 \frac{1 + \cos(43)}{2} + 0.2 \frac{1 - \cos(43)}{2}$$

$$\overline{R_h} = 0.968$$

enlisting the hourly equivalent of Equation 4.4-13,

$$\overline{I_T} = 1225 \frac{W}{m^2} \left| 0.576 \right| 0.968$$

$$\overline{I_T} = 683 \text{ W/m}^2$$

Critical ratios can now be obtained for the minimum and maximum insolation levels.

$$X_{c-min} = \frac{189}{683}$$

$$X_{c-min} = 0.277$$

And

$$X_{c-max} = \frac{748}{683}$$

$$X_{c-max} = 1.095$$

From Figure 4.4-12 with $\bar{k}_T = 0.576$ and $V_{bd} = 0.110$,

$$\phi = 0.67$$

and

$$\phi' = 0.10$$

The energy supplied to the load, for the hours from 11 to 13 in June would be,

$$\bar{Q}_{sup\ 6-11\ \&\ 12} = \frac{5}{7}\left|\frac{600\ m^2}{1}\right|\frac{.797}{1}\left|\frac{30}{1}\right|\frac{2\ hrs}{1}\left|\frac{683\ W}{m^2}\right|\frac{3600\ J}{W-hr}\left|(.67-.10)\right.$$

$$\bar{Q}_{sup\ 6-11\ \&\ 12} = 2.87 \times 10^{10}\ J$$

Completing this analysis for the entire year,

$$\bar{Q}_{sup} = 0.933\ TJ$$

To predict the performance of the same system using analytical utilizability, the following procedure should be used, for each of the 4 hour pairs, and all 12 months of the year.

The previously calculated required variables to determine the supplied energy for the 11-12/12-13 hour pairs in June are:

$$\overline{K}_T = 0.53$$

$$\overline{T}_a = 22°C$$

$$I_{min} = 189 \ W/m^2$$

$$I_{max} = 748 \ W/m^2$$

$$\overline{R}_{bh} = 0.976$$

$$V_{bd} = 0.110$$

$$r_T = 0.116$$

$$r_o = 0.107$$

$$\overline{k}_T = 0.576$$

$$\rho = 0.2$$

$$I_o = 1225 \ W/m^2$$

Assuming a $k_{min}$ of 0.05 and $k_{max} = 0.80$, the exponential con-
stant of equation 4.5-8 can be obtained from Figure 4.5-1 (or by
the iterative method presented in Appendix A),

$$\gamma = 3.604$$

Using the iterative method presented in Appendix B, the critical
clearness indexes are,

$$k_{c-min} = 0.174$$

$$k_{c-max} = 0.621$$

From the denominator of Equation 4.5-10,

$$\overline{I}_T = 684 \text{ W/m}^2$$

Using Equation 4.5-10,

$$\phi = 0.727$$

$$\phi' = 0.088$$

The energy supplied to the load, for the hours from 11 to 13 in June would be

$$\overline{Q}_{\text{sup 6-11 \& 12}} = \frac{5|600|.797|30|2|684|3600|(.727-.088)}{7|\ |\ |\ |\ |\ |\ |\ |}$$

$$\overline{Q}_{\text{sup 6-11 \& 12}} = 3.22 \times 10^{10} \text{ J}$$

Completing this analysis for the entire year,

$$\overline{Q}_{\text{sup}} = 0.932 \text{ TJ}$$

Performing a 23 year simulation for the above system, the average annual energy supplied to the load was 0.912 TJ. Thus, both methods predicted the simulated annual performance to within 2%. This agreement is well within the accuracy of the data. The generalized and analytical method differed from each other by 10% at most for any one hour pair. A comparison of collected and dumped energy for the above situation using a 23 year simulation, Liu and Jordan $\phi$s, and the two new $\phi$ methods is presented in Table 4.6-1.

Table 4.6-1:  Comparison of annual collected and dumped energy.

|  | $\overline{Q}_u$ (TJ) | $\overline{Q}_{dump}$ (TJ) |
|---|---|---|
| Simulation (23 years) | 1.51 | 0.604 |
| Liu and Jordan | 1.37 | 0.473 |
| Generalized Hourly | 1.38 | 0.451 |
| Analytical | 1.40 | 0.465 |

## 4.7 Conclusions

The extended generalized monthly-average hourly utilizability accounts for hourly variations and has a better correlating parameter than the old generalized method. The discrepancy between this new generalized method and $\phi$ s calculated from extensive data is mainly due to the difference between the actual $k_T$ and generalized $K_T$ distributions. Using this method is rather cumbersome because it requires the double interpolation (once on $\overline{k}_T$ and once on $V_{bd}$) of Figure 4.4-12.

The analytically derived expression for $\phi$ can agree with those calculated from extensive data as well as (and possibly better than) the new generalized method. As with the generalized method, the analytical $\phi$-curves agree with data based ones only as well as the agreement in their $k_T$ distributions. At this point, the ambiguities involved in the determination of $k_{min}$ and $k_{max}$ inhibits the general use of the derived expression.

Both the extended generalized and analytically derived methods do a reasonable job in predicting usable energy. The analytical method does a better job of predicting unusable energy.

# 5. CONCLUSIONS AND RECOMMENDATIONS

## 5.1 Conclusions

The IPH load distribution has little effect on closed load loop system performance for reasonable storage sizes. An existing design method (25) does a reasonable job in predicting the simulated performance of these systems. For all systems without storage, utilizability concepts can be used directly with the hourly version being more versatile than the daily one.

Using the Liu and Jordan generalized long-term average daily clearness index for a hourly one, generalized hourly utilizability can be developed on a true hourly basis. A combination of the hourly tilted surface beam radiation ratio and the collector-sky view factor does a reasonable job in correlating hourly utilizability. This new generalized method is applicable to non-south facing surfaces. Due to the graphical nature of the results, using this generalized method gets a bit tedious.

If the random occurrence of hourly insolation assumption is made, the Bendt et al. clearness index probability distribution can be used to derive an analytical expression for hourly utilizability. This expression is also applicable to surfaces facing other than south. The ambiguities involved in the determination of constants restricts the extent to which this expression can currently be applied.

Both the methods of predicting hourly utilizability agree with values obtained from data only as well as their clearness index distributions agreed. Locations such as Abluquerque that have clearness distributions more like the two generalized ones studied here, will have less of a difference between the data calculated and predicted hourly utilizabilities. The converse is also true of course.

## 5.2 Recommendations

### 5.2.1 Verifications

The simulated and design method predicted system performance should be compared to the measured performance of various demonstration projects (37) to verify the results presented in Chapter 3.

To determine the generality of the hourly utilizability methods, comparisons of $\phi$-curves and usable energy against data should be performed for a number of diverse locations.

### 5.2.2 Improvements and Extensions

Although an existing design method works reasonably well for closed load loop IPH systems and utilizability can be used directly for systems without storage, a significant gap still exists between the two where load profiles do make a difference.

A preliminary investigation indicates that, multiplying $\bar{\phi}$ based on $T_{min}$, by a parameter that relates what fraction of the total load occurs during times of solar energy collection, gives an indication

of an actual attainable $\overline{\phi}$ (i.e., indicates the tank temperature and resulting $I_{min}$ fluxuations that actually determine the attained $\overline{\phi}$ for the operating system).

To facilitate the use of the new generalized $\phi$-curves, a curve fit should be done using $V_{bd}$ as a correlating parameter. One other possible correlating aid would be the hourly tilted surface beam radiation ratio plus the ground reflectance term in the relation for R. This is likely because it is the constant term in the integration of $I \cdot R$.

To generalize the analytical expression for $\phi$, $k_{min}$ and $k_{max}$ should be determined by optimizing the agreement between the random insolation and many data $k_T$ distributions. Next, a curve fit for $\gamma$ based on these $k_{min}$ s and $k_{max}$ s would be very beneficial.

Since the $k_T$ distribution is the main factor in utilizability, a thorough examination of other possible statistical distributions is in order. Possibly one with the assumption that the value of $k_T$ today at noon is affected by at most two days prior would help approximate the data better. On the other hand, the Liu and Jordan generalized distributions may be the best approximation. If these distributions were curve fit as a single probability function rather than a set of frequency functions, an analytical expression could be derived eliminating the need to curve fit the generalized $\phi$-curves.

For concentrating collectors, the optical cut off must be accounted for. This can be done by the methods suggested by

Collares-Pereira and Rabl (14).

Since $\overline{\phi}$ is just the difference of a summation across the day from $\phi$, $\overline{\phi}$ s for non-south facing surfaces can be obtained from $\phi$ s for non-south facing surfaces. This will be of benefit to many types of solar energy systems.

Hourly utilizability could be used in conjunction with load patterns to determine the optimum collector slope and azimuth.

Finally, with the aid of a method to determine shading (26) hourly utilizability can be used for many passive solar applications.

It should now be apparent that hourly utilizability is useful for many more applications than just no storage IPH systems.

## APPENDIX A

The solution for $\gamma$ in,

$$\overline{k}_T = \frac{\left(k_{max} - 1/\gamma\right) \exp\left(\gamma k_{max}\right) - \left(k_{min} - 1/\gamma\right) \exp\left(\gamma k_{min}\right)}{\exp\left(\gamma k_{max}\right) - \exp\left(\gamma k_{min}\right)} \quad (A-1)$$

will be obtained by a numerical approach using a combination of the bisection and Newton's methods.

To find the solution(s) of Equation A-1, a function $F(\gamma)$ is defined such that $F(\gamma)$ goes to zero when $\gamma$ satisfies the Equation A-1.

$$F = \frac{\left(k_{max} - 1/\gamma\right) e^{\gamma k_{max}} - \left(k_{min} - 1/\gamma\right) e^{\gamma k_{min}}}{e^{\gamma k_{max}} - e^{\gamma k_{min}}} - \overline{k}_T \quad (A-2)$$

At first glance, $\gamma = 0$ seems to be an undefined solution but, with a little algebraic manipulation,

$$F = \frac{\gamma\left(\overline{k}_T - k_{min}\right) + 1}{\gamma\left(\overline{k}_T - k_{max}\right) + 1} - e^{\left(\gamma k_{max} - k_{min}\right)} \quad (A-3)$$

From this form, it is apparent that $\gamma = 0$ is always a solution to Equation A-1.

Newtons method employs the iterative scheme,

$$\gamma_{n+1} = \gamma_n + \frac{F\left(\gamma_n\right)}{F'\left(\gamma_n\right)} \quad (A-4)$$

where $F'$ is the derivative of $F$ with respect to $\gamma$.

$$F' = \frac{\left[\gamma\left(\overline{k}_T - k_{max}\right) + 1\right]\left(\overline{k}_T - k_{min}\right) - \left[\gamma\left(\overline{k}_T - k_{min}\right) + 1\right]\left(\overline{k}_T - k_{max}\right)}{\left[\gamma\left(\overline{k}_T - k_{max}\right) + 1\right]^2}$$

$$- \left(k_{max} - k_{min}\right) e^{\gamma\left(k_{max} - k_{min}\right)}$$

(A-5)

A computer subroutine, SUBGAMA, was developed to use Equation A-4 with the bisection method. This subprogram is listed with AYLPHI in Appendix C. Using SUBGAMA uncovers the fact that there are usually 3 attainable solutions to Equation A-1 for $\gamma$ (zero being one of them).

From experience, the smallest non-zero solution gives $\phi$-curves that are smooth and continuous while the other does not. This is the solution that is plotted in Figure 4.5-1. Fortunately, for the indicated solutions of $\gamma=0$, all three solutions collapsed to the single one.

# APPENDIX B

## CRITICAL CLEARNESS INDEX

The solution of

$$k_c = \frac{I_c}{I_o R} \tag{B-1}$$

will be obtained by a numerical approach known as Newton's method. The solution of Equation B-1 for $k_c$ is also the solution of

$$F = \frac{I_c}{I_o R} - k_c \tag{B-2}$$

for zero.

Introducing Equations 4.3-2 and 4.5-4,

$$F = \frac{I_c}{I_o \left[ R_b - V_{bd}\left(a_1 + a_2 k_c + a_3 k_c^2 + a_4 k_c^3\right) + D \right]} - k_c \tag{B-3}$$

Newtons method is to estimate the root of Equation B-2 from a previous guess by

$$k_{c-(n+1)} = k_{c-n} - \frac{F(k_{c-n})}{F'(k_{c-n})} \tag{B-4}$$

where $F'$ is the derivation of $F$ with respect to $k_c$.

$$F' = \frac{I_c}{I_o} \left\{ \frac{-V_{bd}\left(a_2 + 2 a_3 k_c + 3 a_4 k_c^2\right)}{\left[ R_b + D - V_{bd}\left(a_1 + a_2 k_c + a_3 k_c^2 + a_4 k_c^3\right)\right]^2} \right\} - 1 \tag{B-5}$$

Equations B-3 through B-5 are programmed in subroutine
SUBKTC which is a subroutine to program AYLPHI listed in Appendix
C.

APPENDIX C

COMPUTER PROGRAM LISTINGS

This appendix contains listings of computer programs used in this study. They are:

PHIBAR-F      A TRNSYS deck for closed load loop systems

ZIP           A TRNSYS deck for no storage systems

PREPHI        A TRNSYS deck for calculating $I_T$ s and $\overline{T}_a$ s

RADAVE        Calculates $\overline{I}_T$ s using $I_T$ s from PREPHI

HRPHIXC       Calculates $\phi - X_c$ pairs using PREPHI and RADAVE output

PHIGEN        Generates $\phi$ s and $X_c$ s using the Liu and Jordan generalized $K_T$ distribution and daily radiation parameters

PHIGENHR      Same as PHIGEN only it uses hourly radiation parameters

PHIGENHRS     Same as PHIGENHR only it calculates $\overline{k}_T$ s from $\overline{K}_T$ s

AYLPHI        Calculates $\phi$ s and $X_c$ s using a random insolation sequence $k_T$ probability distribution

```
*******************************************************************
*                                                                 *
*                          PHIBAR-F                               *
*                                                                 *
*                   PHIBAR-FCHART  SYSTEM                          *
*              ALL  ENERGY  ABOVE  TMIN  IS  EQUAL                 *
*                                                                 *
*  *******************************************************************
*
SIMULATION   0   8760   0.50
TOLERANCES   -0.01   -0.01
LIMITS  25   15   20
*
*
CONSTANTS    FPRM = 0.95, CP=4.19,   ALPHA=0.95, UL=10.0, TOW=0.90,SLP=40
CONSTANTS    TMIN = 80, AREA = 750, VOL = 56.25, LOAD = 3.5E+9
CONSTANTS    FLOW = AREA * 60,   UTANK=0
CONSTANTS    TSTART = TMIN - 10, THIST = TMIN + 90
CONSTANTS    TAUX = TMIN + 50, MMAX = VOL * 1000. * 2.
CONSTANTS    HRPDAY = 12, DAYPWK = 7
CONSTANTS    HRLD = LOAD / 52.0 / DAYPWK / HRPDAY
CONSTANTS    KONST = HRLD / CP
UNIT 14  TYPE 14  LOAD CONTROL; DAILY
     PARAMETERS 12
       0,0   6,0   6,1   18,1   18,0   24,0
UNIT 7 TYPE 14  LOAD CONTROL; WEEKLY
     PARAMETERS 4
       0,1   168,1
UNIT 13 TYPE 15  LOAD BOLEAN 'AND'
     PARAMETERS 3
       0   0   11
     INPUTS 2
       14,1   7,1
         0     1
UNIT 9 TYPE 9   CARD READER
     PARAMETERS 7
       2   1   1   3.6   0   0   1
     (T20,F4.0,T29,F5.1)
UNIT 16 TYPE 16   RADIATION PROCESSOR
     PARAMETERS 6
       2   1   34.6   4871   0   -1
     INPUTS 6
       9,1   9,19   9,20   0,0   0,0   0,0
         0     0      0    0.2   SLP    0
UNIT 2 TYPE 2   COLLECTION CONTROL
     PARAMETERS 3
       3   3   0
     INPUTS 3
       1,1   4,1   2,1
       TMIN   TMIN   0
```

```
UNIT 3 TYPE 3   PUMP; COLLECTOR TO STORE
   PARAMETERS 1
    FLOW
    INPUTS 3
    4,1  4,2  2,1
     TMIN   0    0
UNIT 1 TYPE 1  FIXED FLAT PLATE COLLECTOR
   PARAMETERS 7
    1  AREA  FPRM  CP  ALPHA  UL  TOW
    INPUTS 4
    3,1  3,2  9,2  16,6
    TMIN  0   TMIN   0
UNIT 4 TYPE 4 STORAGE TANK
   PARAMETERS 5
    VOL  9.72  CP  1000  UTANK
    INPUTS  5
    1,1  1,2  10,1  10,2  9,2
     TMIN   0     TMIN    0   0
   DERIVATIVES 1
    TMIN
UNIT 8 TYPE 15  'PUMP'; TANK TO LOAD - TEMP. CTRL. FLOW RATE
   PARAMETERS 25
    -1   0  -12  -1  TMIN  4  -21  -31  9  -22  -32  10
     -1  KONST  1  -11  1  -31  -32  3  2  -1  MMAX  11  -4
    INPUTS 2
    13,1  4,3
        0   TMIN
UNIT 10 TYPE 5  HEAT EX.; LOAD
   PARAMETERS 4
    4  1  CP  CP
    INPUTS  4
    4,3  8,1  0,0  0,0
     TMIN  0   TMIN  MMAX
UNIT 17 TYPE 15  'PUMP'; AUXILIARY
   PARAMETERS 24
    -1  HRLD  -11  -1  TMIN  4  -1  CP  1  -12  1  4  -1  TAUX
     -1  TMIN  4  2  -1  CP  2  -13  1  -4
    INPUTS 3
    4,3  8,1  13,1
    TMIN  0   0
UNIT 6 TYPE 6   AUXILIARY HEATER
   PARAMETERS 3
    HRLD  TAUX  CP
    INPUTS 3
    0,0  17,1  0,0
    TMIN  0   1
UNIT 29 TYPE 28   ENERGY BALANCE SIM SUM
   PARAMETERS 32
    -1   0  8760  0   1  -11  -12  -4  -4  -13  -4  -14  -4
     -15  -3  -21  -1  HRLD  -17  1  -3  -23  -33  -31  4  -33  2  -4
```

```
          -16   -2   2   -4
      INPUTS 7
       4,7  1,3   4,5   4,6   6,3    4,9   13,1
      LABELS 8
       QU  DE  QENV  QTANK  QAUX  QLOAD  SFRAC  TTAVE
      CHECK .50  1,-2,-3,-4
UNIT 28 TYPE 28    RADIATION SIM SUM
      PARAMETERS  8
       -1   0   8760   0   -11   -4   -12   -4
      INPUTS 2
       16,4  16,6
      LABELS 2
       HHOR  HINC
UNIT 27 TYPE 27   TANK TEMP. HISTOGRAM
      PARAMETERS 8
       1   -1   -1   0   8760   TSTART   THIST   20
      INPUTS 1
       4,9
       TTAVE
END
```

```
**********************************************************************
*                                                                    *
*                              ZIP                                   *
*                                                                    *
*                    PHIBAR-FCHART  SYSTEM                           *
*              ALL  ENERGY  ABOVE  TMIN  IS  'EQUAL'                  *
*                         NO  STORAGE                                *
*                                                                    *
**********************************************************************
*
*
SIMULATION  1  8760  1.0
TOLERANCES  -0.01  -0.01
LIMITS  25  15  20
*
*   ALBUQUERQUE (SET UP FOR TMY DATA)
*
CONSTANTS   FPRM = 0.95, CP=4.19, ALPHA=0.95, UL=10.0, TOW=0.90
CONSTANTS   TMIN = 80, AREA = 2000, LOAD = 3.5E+9
CONSTANTS   FLOW = AREA * 60, LAT = 35.05, SLP = LAT
CONSTANTS   TAUX = TMIN + 50, MMAX = FLOW * 2.
CONSTANTS   HRPDAY = 12, DAYPWK = 5
CONSTANTS   HRLD = LOAD / 52.0 / DAYPWK / HRPDAY
CONSTANTS   KONST = HRLD / CP
*
*
UNIT 11 TYPE 14   MONTHLY AVEAGE DAYTIME TEMP'S
    PARAMETERS 48
    0,3.32   744,3.32   744,5.01   1416,5.01   1416,8.80   2160,8.80
    2160,14.9   2880,14.9   2880,20.9   3624,20.9   3624,24.7
    4344,24.7   4344,27.6   5088,27.6   5088,25.6   5832,25.6
    5832,21.6   6552,21.6   6552,16.3   7296,16.3   7296,7.97
    8016,7.97   8016,3.56   8760,3.56
UNIT 14  TYPE 14  LOAD CONTROL; DAILY
    PARAMETERS 12
    0,0   6,0   6,1   18,1   18,0   24,0
UNIT 7 TYPE 14  LOAD CONTROL; WEEKLY
    PARAMETERS 10
    0,0   0,1   120,1   120,0   168,0
UNIT 13 TYPE 15   LOAD BOLEAN 'AND'
    PARAMETERS 3
    0   0   11
    INPUTS 2
    14,1  7,1
       0    1
UNIT 9 TYPE 9  CARD READER
    PARAMETERS 4
    2   1   0   1
(T25,F4.0,T30,F4.1)
UNIT 16 TYPE 16  RADIATION PROCESSOR
```

```
      PARAMETERS 6
       1  1  LAT   4871   0  -1
      INPUTS 6
       9,1  9,19  9,20  0,0  0,0  0,0
        0    0     0    0.2  SLP   0
UNIT 2 TYPE 2  COLLECTION CONTROL; TEMPERATURE LEVEL
     PARAMETERS 3
      3  3  0
      INPUTS 3
       1,1  0,0  2,1
       TMIN  TMIN   0
UNIT 3 TYPE 3  PUMP; COLLECTOR TO H.X.
     PARAMETERS 1
      FLOW
      INPUTS 3
       0,0  0,0  2,1
       TMIN TMIN   0
UNIT 1 TYPE 1  FIXED FLAT PLATE COLLECTOR
     PARAMETERS 7
       1  AREA  FPRM  CP  ALPHA  UL  TOW
      INPUTS 4
       3,1  3,2  9,2  16,6
       TMIN  0   TMIN   0
UNIT 10 TYPE 5  HEAT EX.; LOAD
     PARAMETERS 4
       4  1  CP  CP
      INPUTS 4
       1,1  1,2  0,0  0,0
       TMIN  0   TMIN  MMAX
UNIT 17 TYPE 15  "PUMP"; AUXILIARY & QDUMP
     PARAMETERS 25
       -1  HRLD  -11  4  8  -12  1  -1  TAUX
       -1  TMIN  4  2  -1  CP  2  -4  -11  -1
       HRLD  -12  1  4  8  -4
      INPUTS 2
       10,5  13,1
        0    0
UNIT 6 TYPE 6    AUXILIARY HEATER
     PARAMETERS 3
      HRLD  TAUX  CP
      INPUTS 3
       0,0  17,1  0,0
       TMIN  0   1
UNIT 29 TYPE 28  ENERGY BALANCE SIM SUM
     PARAMETERS 30
       -1  1  8760  0  -11  -4  -12  -4  -1  HRLD  -13  1  -3
       -21  -31  -12  4  -31  2  -4  -16  -4  -11  -16  4
       -4  -14  -4  -15  -4
      INPUTS 6
       1,3  6,3  13,1  9,1  16,6  17,2
```

```
    LABELS 8
     QU QAUX QLOAD SFRAC QDUMP QSUP HHOR HINC
    CHECK 0.05  3,-1,-2,+5
UNIT 31 TYPE 15     SIM, SUM, PREMANIPULATOR
    PARAMETERS 78
     -11  -1  TMIN -12  4  -1  UL  1  -13  2  -3  -21 -31
      9  -3 -22 -32 -14  1  -4 -13 -15  1 -16  1  -4
     -11 -31  4  8  -3 -23 -33 -14  1 -24 -34 -15  1
      -3 -11 -31  -1 HRLD  -1 AREA  2  3  4  8 -14  1
     -25 -35 -15  1  -3  4  -4  -1 HRLD -14  1 -32  1
      -4 -33 -15  1  -4 -34 -35  4 -24 -11 -15  1 -26
    INPUTS 6
     16,6  11,1  1,5  13,1  1,6  2,1
       0     0     0     0     0     0
UNIT 28 TYPE 28   SIM SUM;  PHIBAR AND LOAD PARAMETERS
    PARAMETERS  47
     -1  1  8760  0    -11 -12  2  -4 -13 -2  2  -4 -14
     -15  2  -4 -16  -1 AREA  2 -11 -12  2  2 -15  2
      -4 -17  -4 -18 -17  2  -4 -18 -19  2  -4 -20 -1
     HRLD -17  1  2  -1 AREA  1  -4
    INPUTS 10
     31,4  2,1  31,1  31,5  16,6  1,3  13,1  31,3  31,2  31,6
    LABELS 8
       FRTALF  IMIN  PHIMAX  PHIACT  LDHRS  LSSS  SSSS  ROW1
UNIT 32 TYPE 28   SIM SUM; LOAD PARAMETERS
    PARAMETERS 39
     -1  1  8760  0  -11  -1 AREA  1 -12  -1 HRLD  1  2
     -4 -11  -1 AREA  1 -14  2  -4 -16 -13  2  -4
    -17  -1 AREA  1 -12  -1 HRLD  1  2  -4 -16 -15
      2  -4
    INPUTS 7
     31,8  13,1  31,5  31,9  16,6  31,14  31,16
    LABELS 5
     ROW2  ROW3  ROW4  INC/LD  LDFEE
END
```

```
****************************************************************
*                                                            *  *
*                         PREPHI                             *  *
*                                                            *  *
*    THIS PROGRAM PUTS SIMULATION TIME, MONTH, HOUR, INCIDENT *  *
*     RADIATION, AND AMBIENT TEMPERATURE INTO A FILE ON A    *  *
*      HOURLY BASIS.  IT ALSO CALCULATES AVERAGE AMBIENT     *  *
*             TEMPERATURES AND DEGREE HOURS.                 *  *
*                                                            *  *
*  ****************************************************************
*
*
*   MADISON, 23 YEARS OF SOLMET DATA.
*
SIMULATION  1  201480  1.0
TOLERANCES  -0.01  -0.01
*
CONSTANT  LAT = 43.13, SLOPE = 0.0, FILE = 10
*
*
UNIT 9 TYPE 9  CARD READER
    PARAMETERS 7
    4  1  1  3.6  0  0  1
(T25,F4.0,T11,F2.0,T17,F2.0,T35,F6.1)
UNIT 16 TYPE 16  RADIATION PROCESSOR
    PARAMETERS 6
    1  1  LAT  4871  0  -1
    INPUTS 6
    9,1  9,19  9,20  0,0  0,0  0,0
     0    0    0    0.2   SLOPE   0
UNIT 25 TYPE 25  PRINTER
    PARAMETERS 4
    1  1  201480  FILE
    INPUTS 4
    9,2  9,3  16,6  9,4
     MO   HR  HINC  TAMB
UNIT 15 TYPE 15
PAR 14
-11 -1 0.1 9 -3 -12 1 -4 -1 18.
-12 4 8 -4
INPUTS 2
9,1 9,4
0.0 0.0
UNIT 28 TYPE 28 SIM SUM
PAR 16
-1 1 201480 0 -11 -4 -12 -2 2 -4 -14 -13 2 -4 -15 -4
INPUTS 5
9,1 9,4 15,1 15,2 15,3
LABELS 4
HHOR TAMB DTAMB DEGHRS
END
```

```
CCCCCCCCCCCCCCCCCCCCCCCCCCCCCCCCCCCCCCCCCCCCCCCCCCCCCCCCC
C                                                       C
C                    RADAVE                             C
C                                                       C
C     THIS PROGRAM AVERAGES HOURLY INSOLATION VALUES    C
C     (FROM TRNSYS (DS*0.PREPHI)) AND WRITES THEM INTO  C
C     IFILE IN A FORM CONVIENT FOR DS*0.PLOTHRINS.      C
C                                                       C
CCCCCCCCCCCCCCCCCCCCCCCCCCCCCCCCCCCCCCCCCCCCCCCCCCCCCCCCC
C
      DIMENSION X(12,24),H(12,24)
      DO 3 I=1,12
      DO 1 J = 1,24
      X(I,J) = 0.
      H(I,J) = 0.
  1   CONTINUE
  3 CONTINUE
      READ(-,-) IFILE,NYEARS
  5 READ(-,100,END=20) XMO,HR,HTILT
      HR = HR + 0.1
      XMO = XMO + 0.1
      MO = IFIX(XMO)
      IHR = IFIX(HR)
      IF (IHR.EQ.0) IHR = 24
      H(MO,IHR) = H(MO,IHR) + HTILT
      X(MO,IHR) = X(MO,IHR) + 1.
      GO TO 5
 20 DO 30 I = 1,12
      DO 25 J=1,24
      IF (X(I,J).GT.0.0) H(I,J) = H(I,J) / X(I,J)
 25   CONTINUE
 30 CONTINUE
      WRITE (-,500) NYEARS
      DO 40 I=1,12
      WRITE (6,550) I,(H(I,J),J=6,19)
      IF (IFILE.GT.0) WRITE (IFILE,600) (H(I,J),J=6,12)
      IF (IFILE.GT.0) WRITE (IFILE,600) H(I,19),H(I,18),
     '   H(I,17),H(I,16),H(I,15),H(I,14),H(I,13)
 40 CONTINUE
      IF (IFILE.GT.0) WRITE(-,650) IFILE
100 FORMAT (T11,E11.3,E11.3,E11.3)
500 FORMAT ('1',5X,'MO',25X,I2,' YEAR(S) AVERAGE INSOLATION FOR HOURS
     '5-6 TO 18-19')
550 FORMAT ('0',5X,I2,14F7.0)
600 FORMAT (1X,7(1X,F6.0))
650 FORMAT ('0',//,33X,'THESE VALUES WERE PUT IN FILE ',I2)
900 STOP
      END
```

```
CCCCCCCCCCCCCCCCCCCCCCCCCCCCCCCCCCCCCCCCCCCCCCCCCC
C                                                 C
C                  HRPHIXC                        C
C                                                 C
C     THIS PROGRAM CALCULATES HOURLY PHIS AND XCS  C
C      USING TILTED SURFACE RADIATION DATA FROM    C
C               PREPHI AND RADAVE                  C
C                                                 C
CCCCCCCCCCCCCCCCCCCCCCCCCCCCCCCCCCCCCCCCCCCCCCCCCC
C
      REAL SUM(12,24,50), IC(12,24,50), IAVE(12,24), IT(12,24)
      REAL KTB(12), RBBAR(12), RBAR(12), XC(12,24,50)
      READ  (-,-)   IFILET, IFILEI, NFILE, NYEARS
      READ  (-,-) (KTB(I),RBBAR(I),RBAR(I),I=1,12)
      DO 10 I=1,12
        READ (IFILEI,-) (IAVE(I,J),J=6,12)
        READ (IFILEI,-) IAVE(I,19),IAVE(I,18),IAVE(I,17),
     /          IAVE(I,16),IAVE(I,15),IAVE(I,14),IAVE(I,13)
   10 CONTINUE
      READ (-,-) X1, X2
      DX = (X2 - X1) / 50.
      DO 20 I=1,12
      DO 20 J=6,19
      DO 20 K=1,50
        SUM(I,J,K)=0.
        XC(I,J,K)=0.
        KM1=K-1
        IC(I,J,K) = KM1 * DX * IAVE(I,J)
        IF (IAVE(I,J).GT.0.01) XC(I,J,K) = IC(I,J,K) / IAVE(I,J)
   20 CONTINUE
   60 READ (IFILET,500,END=100)  XMO, HR, HINC
      XMO = XMO + 0.1
      HR = HR + 0.1
      IHR = IFIX(HR)
      MO = IFIX(XMO)
      IT(MO,IHR) = IT(MO,IHR) + HINC
      DO 70 K=1,50
        DIF = HINC - IC(MO,IHR,K)
        IF (DIF.LT.0.0) DIF = 0.0
        SUM(MO,IHR,K) = SUM(MO,IHR,K) + DIF
   70 CONTINUE
      GO TO 60
  100 DO 110 I=1,12
      DO 110 J=6,19
      DO 110 K=1,50
        IF (IT(I,J).LT.0.1) GO TO 110
        SUM(I,J,K) = SUM(I,J,K) / IT(I,J)
  110 CONTINUE
      WRITE (-,600) NYEARS
      PRINT 610
```

```
      DO 200 I=1,12
      WRITE (-,620) I,(IAVE(I,J),J=6,19)
200 CONTINUE
      DO 210 I=1,12
      PRINT 630
      WRITE (-,640) I,KTB(I),RBBAR(I),RBAR(I)
      IF (NFILE.GT.0) WRITE(NFILE,-) I,KTB(I),RBBAR(I),RBAR(I)
      DO 210 J=6,19
      JJ=J-1
      WRITE (-,650) JJ,J
      WRITE (-,660) (XC(I,J,K),SUM(I,J,K),K=1,50)
      IF (NFILE.GT.0) WRITE(NFILE,-) (XC(I,J,K),SUM(I,J,K),K=1,50)
210 CONTINUE
500 FORMAT (T11,3(E11.3))
600 FORMAT ('1',///,37X,'CALCULATED PHIS BASED ON ',I2,
     *    ' YEARS OF DATA')
610 FORMAT ('0',/////,6X,'MO',29X,'AVERAGE INSOLATION FOR HOURS 5-6 TO
     *18-19')
620 FORMAT ('0',5X,I2,14F7.0)
630 FORMAT ('1',//,43X,'MO',7X,'KTBAR',7X,'RBBAR',6X,'RBARLJ')
640 FORMAT ('0',42X,I2,3(5X,F7.3))
650 FORMAT ('0',///,35X,'CRITICAL RATIOS AND PHI''S FOR THE HOUR FROM
     *',I2,' TO ',I2)
660 FORMAT (1X,5(//,1X,10(F6.3,F6.3)))
      STOP
      END
```

```
          F=AIC/ABIN
          IF (KTFLAG.LT.6) AKT=XKT(IC,KT)
          IF (KTFLAG.LT.6) GO TO 40
          IF (XKTB.GT.0.70.OR.XKTB.LT.0.30) GO TO 37
          DO 35 I=1,5
   35     AKTS(I)=XKT(IC,I)
          CALL LAGRNG (5,XKTB,XKTBAR,AKTS,AKT)
          GO TO 40
   37     IF (XKTB.GT.0.7) GO TO 39
          AKT=XKT(IC,1)*XKTB/0.3
          GO TO 40
   39     DELTA=(0.9-XKT(IC,5))*(XKTB-0.7)/0.2
          IF (DELTA.LT.0.0) DELTA=0.0
          AKT=XKT(IC,5)+DELTA
   40     MODE=2
          RDAY=RBARLJ(MODE,MO,ALAT,SLOPE,AZMTH,AKT,RHO,RBBAR)
          XC(IC) = (RDAY*AKT)/(RBAR*XKTB)
          AREA(IC) = AREAK + (XC(IC)-XCOLD)*((1.-F) + 0.5*DP)
          AREAK = AREA(IC)
          XCOLD = XC(IC)
   50     CONTINUE
          TOTAL = AREA(NBINSH)
          DO 60  I=1,NBINSH
           PHI(I) = (TOTAL-AREA(I))/TOTAL
   60     CONTINUE
          WRITE (-,20)
   20     FORMAT (1H1,///,21X,'MO',6X,'LATITUDE',8X,'SLOPE',11X,'RHO')
          WRITE(-,30) MO,ALAT,SLOPE,RHO
   30     FORMAT (21X,I2,8X,F5.2,9X,F5.2,10X,F4.2)
          WRITE(-,678) XKTB
  678     FORMAT(//38X,'KTBAR =',F5.3)
          WRITE(-,6)
    6     FORMAT ('0',28X,'RBBAR',6X,'RBAR',6X,'RDAY')
          WRITE(-,7) RBBAR,RBAR,RDAY
    7     FORMAT (28X,F6.3,4X,F6.3,4X,F6.3)
          WRITE(-,8)
    8     FORMAT ('0',/,31X,'XC''S',5X,'AND',5X,'PHI''S')
          WRITE(-,9) (XC(IC),PHI(IC),IC=1,NBINSH,IPRT)
    9     FORMAT ('0',5(3X,F6.3,1X,F6.3))
          WRITE (-,15) TOTAL
   15     FORMAT ('0',30X,'TOTAL AREA = ',F5.3)
          WRITE(-,450)
  450     FORMAT ('0',/,32X,'BINS',8X,'FILE')
          WRITE(-,500)  NBINSH,IFILE
  500     FORMAT(' ',32X,I3,10X,I2)
          IF (IFILE.NE.0) WRITE(IFILE,-) RBAR,RBBAR,RDAY,
        '   (XC(IC),PHI(IC),IC=1,NBINSH)
   31     CONTINUE
          GO TO 1
   99     STOP
```

```
      FUNCTION RBARLJ(MODE,MN,ALAT,SLOPE,AZMTH,XKT,RHO,RD)
CCCCCCCCCCCCCCCCCCCCCCCCCCCCCCCCCCCCCCCCCCCCCCCCCC
C                                                    C
C     THIS SUBPROGRAM CALCULATES RADIATION RATIOS    C
C     MODE1: LONG-TERM AVERAGE DAILY                 C
C     MODE2: DAILY                                   C
C                                                    C
CCCCCCCCCCCCCCCCCCCCCCCCCCCCCCCCCCCCCCCCCCCCCCCCC
C
      DIMENSION DAY(12)
      DATA DAY/17.,47.,75.,105.,135.,162.,198.,228.,258.,288.,
     1  318.,344.,/
C.  THIS FUNCTION SUBPROGRAM WILL CALCULATE THE RATIO OF DAILY
C.  EXTRATERRESTRIAL RADIATION INCIDENT ON A TILTED SURFACE (FOR
C.  ANY AZMTH ANGLE) TO THAT ON A HORIZONTAL SURFACE
      DATA PI/3.14159/
      RBARLJ=1.0
      RD=1.0
      IF ( ABS(SLOPE) .LT. 0.001 ) RETURN
      RDCONV=2.*PI/360.
      DECL=23.45*SIN((284.+DAY(MN))/365.*2.0*PI)
      FKT=1.390-4.027*XKT+5.531*XKT*XKT-3.108*XKT**3
      IF (MODE.EQ.2) FKT=1.0045 + ((2.6313 * XKT - 3.5227)
     '   * XKT + 0.04349) * XKT
      COSS=COS(SLOPE*RDCONV)
      SINS=SIN(SLOPE*RDCONV)
      TANS=SINS/COSS
      IF ( ABS(AZMTH) .LT. 0.001 ) AZMTH = 0.001
      COSAZM=COS(AZMTH*RDCONV)
      SINAZM=SIN(AZMTH*RDCONV)
      TANAZM=SINAZM/COSAZM
      SINLAT=SIN(ALAT*RDCONV)
      COSLAT=COS(ALAT*RDCONV)
      TANLAT=SINLAT/COSLAT
      SINDEC=SIN(DECL*RDCONV)
      COSDEC=COS(DECL*RDCONV)
      TANDEC=SINDEC/COSDEC
      WS=ACOS(-TANDEC*TANLAT)
C.  WS IS THE SUNSET HOUR ANGLE FOR A HORIZONTAL SURFACE
C.
      AC=COSLAT/SINAZM/TANS+SINLAT/TANAZM
      BC=TANDEC*(COSLAT/TANAZM-SINLAT/SINAZM/TANS)
      SQ = AC*AC-BC*BC+1.
      WSR = -WS
      WSS =  WS
      IF ( SQ .LT. 0.0 ) GO TO 45
      ARG = (AC*BC+SQRT(SQ))/(AC*AC+1.)
      IF ( ARG .GT. 1.0 ) ARG = 1.0
      IF ( ARG .LT. -1. ) ARG = -1.0
      WSR = ACOS(ARG)
```

```
      WSR=AMIN1(WS,WSR)
      WSR1=WSR
      ARG = (AC*BC-SQRT(SQ))/(AC*AC+1.)
      IF ( ARG .GT.  1.0 ) ARG =  1.0
      IF ( ARG .LT. -1.0 ) ARG = -1.0
      WSS = ACOS(ARG)
      WSS=AMIN1(WS,WSS)
      WSS1=WSS
C.  WSR AND WSR ARE THE ABSOLUTE VALUES OF THE SUNRISE AND SUNSET
C.  HOUR ANGLES (IN RADIANS) FOR THE TILTED SURFACE
      IF (AZMTH.LT.0.) GO TO 44
C.  AZMTH IS GREATER THAN ZERO   IMPLIES SURFACES FACES WEST
      WSS=AMAX1(WSR1,WSS1)
      WSR=-AMIN1(WSR1,WSS1)
      GO TO 45
C.  FOR A SURFACE FACING DIRECTLY TOWARDS THE EQUATOR, WSS=WSR
 44   CONTINUE
C.  AZMTH IS LESS THAN ZERO      IMPLIES SURFACE FACES EAST
      WSR=-AMAX1(WSR1,WSS1)
      WSS=AMIN1(WSR1,WSS1)
 45    CONTINUE
      RD=COSS*SINDEC*SINLAT*(WSS-WSR)
     1  -SINDEC*COSLAT*SINS*COSAZM*(WSS-WSR)
     2 +COSDEC*COSLAT*COSS*(SIN(WSS)-SIN(WSR))
     3 +COSDEC*SINLAT*SINS*COSAZM*(SIN(WSS)-SIN(WSR))
     4  -COSDEC*SINS*SINAZM*(COS(WSS)-COS(WSR))
      RD=RD/2./(COSLAT*COSDEC*SIN(WS)+WS*SINLAT*SINDEC)
      RBARLJ=(1.-FKT)*RD+FKT*(1.+COSS)/2+RHO*(1-COSS)/2.
      RETURN
      END
```

```
      SUBROUTINE LAGRNG(NPTS,XBETWN,X,F,ANSWER)
CCCCCCCCCCCCCCCCCCCCCCCCCCCCCCCCCCCCCCCCCCCCCCCCCCCCCCC
C                                                      C
C      THIS SUBROUTINE PERFORMS LAGRANGE INTERPOLATION,  C
C                                                      C
CCCCCCCCCCCCCCCCCCCCCCCCCCCCCCCCCCCCCCCCCCCCCCCCCCCCCCC
C
      DIMENSION COEFL(10),X(10),F(10)
      DO 10 I=1,NPTS
   10    COEFL(I)=1,0
      DO 20 I=1,NPTS
         DO 30 J=1,NPTS
            IF ( J ,EQ, I ) GO TO 30
            COEFL(I)=COEFL(I)*(XBETWN-X(J))/(X(I)-X(J))
   30    CONTINUE
   20 CONTINUE
      ANSWER=0,0
      DO 40 I=1,NPTS
   40    ANSWER=ANSWER+COEFL(I)*F(I)
      RETURN
      END
```

```
CCCCCCCCCCCCCCCCCCCCCCCCCCCCCCCCCCCCCCCCCCCCCCCCCCCC
C                                                   C
C                    PHIGENHR                       C
C       THIS PROGRAM GENERATES PHIS USING HOURLY    C
C       RADIATION PARAMETERS AND THE LIU AND JORDAN C
C       KT DISTRIBUTIONS.                           C
C                                                   C
CCCCCCCCCCCCCCCCCCCCCCCCCCCCCCCCCCCCCCCCCCCCCCCCCCCC
          DIMENSION COEF(5,5),AKTS(5)
          DIMENSION XKT(100,5),PHI(100),XKTBAR(7),XC(100),AREA(100)
          COMMON /DT/ SLOPE,RHO
          DATA COEF/1.5222,5.38682,-19.0553,25.37202,-12.10546,
         1   0.3071,8.84065,-28.45748,37.01945,-16.58585,
         2   0.11382,5.66517,-17.42259,23.99726,-11.19355,
         3   0.07104,3.7203,-10.42775,15.03488,-7.34399,
         4   0.0192,1.9276,-2.89291,4.73631,-2.69085/
          DATA XKTBAR/0.30,0.40,0.50,0.60,0.70,0.0,0.0/
          READ(-,-) NBINSH,IPRT,IFILE
          READ(-,-) RHO
          DP=1.0/NBINSH
          DO 10 KT=1,5
          P=0.0
          C1=COEF(1,KT)
          C2=COEF(2,KT)
          C3=COEF(3,KT)
          C4=COEF(4,KT)
          C5=COEF(5,KT)
          DO 10 J=1,NBINSH
          P=P+DP
          XKT(J,KT)=P/(C1+C2*P+C3*P*P+C4*P**3+C5*P**4)
   10     CONTINUE
C.
C.    THIS FIT OF THE LIU AND JORDAN DISTRIBUTION CURVES IS FROM
C.    R. COLE,"LONG-TERM AVERAGE PERFORMANCE PREDICTIONS FOR CPC'S",
C.    PROCEEDINGS OF THE AMERICAN SECTION OF I.S.E.S.,ORLANDO
C.    FLORIDA, (1977), P36-6
C.
          READ (-,-) KTFLAG, KT1
        1 READ (-,-,END=99) MO,IHR,ALAT,SLOPE,AZMTH
          IF (KTFLAG.GT.5) READ(-,-,END=99) XKTBAR(6)
          DO 31 KT=KT1,KTFLAG
          XKTB=XKTBAR(KT)
          IF ( IFILE .NE. 0 ) WRITE(IFILE,-) XKTB
          MODE=1
          RBARH=RBARHR(MODE,MO,IHR,ALAT,SLOPE,AZMTH,XKTB,RHO,RB)
          AREAK=0.0
          XCOLD=0.0
          ABIN=FLOAT(NBINSH)
          DO 50 IC=1,NBINSH
          AIC=FLOAT(IC)
```

```
        F=AIC/ABIN
        IF (KTFLAG.LT.6) AKT=XKT(IC,KT)
        IF (KTFLAG.LT.6) GO TO 40
        IF (XKTB.GT.0.70.OR.XKTB.LT.0.30) GO TO 37
        DO 35 I=1,5
   35   AKTS(I)=XKT(IC,I)
        CALL LAGRNG (5,XKTB,XKTBAR,AKTS,AKT)
        GO TO 40
   37   IF (XKTB.GT.0.7) GO TO 39
        AKT=XKT(IC,1)*XKTB/0.3
        GO TO 40
   39   DELTA=(0.9-XKT(IC,5))*(XKTB-0.7)/0.2
        IF (DELTA.LT.0.0) DELTA=0.0
        AKT=XKT(IC,5)+DELTA
   40   MODE=2
        RHR=RBARHR(MODE,MO,IHR,ALAT,SLOPE,AZMTH,AKT,RHO,RB)
        XC(IC) = (RHR*AKT)/(RBARH*XKTB)
        AREA(IC) = AREAK + (XC(IC)-XCOLD)*((1.-F) + 0.5*DP)
        AREAK = AREA(IC)
        XCOLD = XC(IC)
   50   CONTINUE
        TOTAL = AREA(NBINSH)
        DO 60  I=1,NBINSH
         PHI(I) = (TOTAL-AREA(I))/TOTAL
   60   CONTINUE
        WRITE (-,20)
   20   FORMAT (1H1,///,21X,'MO',6X,'LATITUDE',8X,'SLOPE',11X,'RHO')
        WRITE(-,30) MO,ALAT,SLOPE,RHO
   30   FORMAT (21X,I2,8X,F5.2,9X,F5.2,10X,F4.2)
        WRITE(-,678) XKTB
  678   FORMAT(//38X,'KTBAR =',F5.3)
        WRITE(-,6)
    6   FORMAT ('0',29X,'HR',7X,'RBARH',6X,'RB')
        WRITE(-,7) IHR,RBARH,RB
    7   FORMAT (30X,I1,7X,F6.3,4X,F6.3)
        WRITE(-,8)
    8   FORMAT ('0',//,31X,'XC''S',5X,'AND',5X,'PHI''S')
        WRITE(-,9) (XC(IC),PHI(IC),IC=1,NBINSH,IPRT)
    9   FORMAT ('0',5(3X,F6.3,1X,F6.3))
        WRITE (-,15) TOTAL
   15   FORMAT ('0',30X,'TOTAL AREA = ',F5.3)
        WRITE(-,450)
  450 FORMAT ('0',//,32X,'BINS',8X,'FILE')
        WRITE(-,500)  NBINSH,IFILE
  500   FORMAT(' ',32X,I3,10X,I2)
        IF (IFILE.NE.0) WRITE(IFILE,-) RBARH,RB,RHR,
     '    (XC(IC),PHI(IC),IC=1,NBINSH)
   31   CONTINUE
        GO TO 1
   99   STOP
```

```
      FUNCTION RBARHR(MODE,MO,IHR,ALAT,SLOPE,AZMTH,XKT,RHO,RB)
CCCCCCCCCCCCCCCCCCCCCCCCCCCCCCCCCCCCCCCCCCCCCCCCCCCCCCC
C                                                        C
C     THIS SUBPROGRAM CALCULATES RADIATION RATIOS        C
C     MODE1: LONG-TERM AVERAGE HOURLY                    C
C     MODE2: HOURLY                                      C
C                                                        C
CCCCCCCCCCCCCCCCCCCCCCCCCCCCCCCCCCCCCCCCCCCCCCCCCCCCCCC
C
      DIMENSION DAY(12),OMEGA(9)
      DATA DAY/17.,47.,75.,105.,135.,162.,198.,228.,258.,288.,
     1    318.,344./
      DATA OMEGA/7.5,22.5,37.5,52.5,67.5,82.5,97.5,112.5,127.5/
      DATA PI/3.14159/
      RDCONV=2.*PI/360.
      RBARHR=1.0
      RB=1.0
      IF ( ABS(SLOPE) .LT. 0.001 ) RETURN
      GO TO (10,20), MODE
   10 FKT = 1.390-4.027*XKT+5.531*XKT*XKT-3.108*XKT**3
      GO TO 50
   20 FKT = 1.0045+((2.6313*XKT-3.5227)*XKT+0.04349)*XKT
   50 DEC = 23.45*SIN((360.*(284.+DAY(MO))/365.)*RDCONV)
      COSDEC = COS(DEC*RDCONV)
      SINDEC = SIN(DEC*RDCONV)
      SINLAT = SIN(ALAT*RDCONV)
      COSLAT = COS(ALAT*RDCONV)
      SINSLP = SIN(SLOPE*RDCONV)
      COSSLP = COS(SLOPE*RDCONV)
      SINAZM = SIN(AZMTH*RDCONV)
      COSAZM = COS(AZMTH*RDCONV)
      SINOMG = SIN(OMEGA(IHR)*RDCONV)
      COSOMG = COS(OMEGA(IHR)*RDCONV)
      COST = SINDEC*SINLAT*COSSLP - SINDEC*COSLAT*SINSLP*COSAZM
     '    + COSDEC*COSLAT*COSSLP*COSOMG
     '    + COSDEC*SINLAT*SINSLP*COSAZM*COSOMG
     '    + COSDEC*SINSLP*SINAZM*SINOMG
      COSZ = SINDEC*SINLAT + COSDEC*COSLAT*COSOMG
      RB = COST/COSZ
      RBARHR=(1.-FKT)*RB+FKT*(1.+COSSLP)/2+RHO*(1-COSSLP)/2.
      RETURN
      END
```

149

```
CCCCCCCCCCCCCCCCCCCCCCCCCCCCCCCCCCCCCCCCCCCCCCCCCC
C                                                C
C                  PHIGENHRS                     C
C                                                C
C     THIS PROGRAM GENERATES PHIS USING HOURLY   C
C     RADIATION PARAMETERS AND THE LIU AND JORDAN C
C     KT DISTRIBUTIONS.                          C
C     HOURLY KTS ARE CALCULATED FROM DAILY ONES. C
C                                                C
CCCCCCCCCCCCCCCCCCCCCCCCCCCCCCCCCCCCCCCCCCCCCCCCCC
C
      REAL K0,K1,K2,K3,K4,K5
      DIMENSION COEF(5,5),AKTS(5),DAY(12)
      DIMENSION XKT(100,5),PHI(100),XKTBAR(7),XC(100),AREA(100)
      COMMON /DT/ SLOPE,RHO
      DATA COEF/1.5222,5.38682,-19.0553,25.37202,-12.10546,
     1    0.3071,8.84065,-28.45748,37.01945,-16.58585,
     2    0.11382,5.66517,-17.42259,23.99726,-11.19355,
     3    0.07104,3.7203,-10.42775,15.03488,-7.34399,
     4    0.0192,1.9276,-2.89291,4.73631,-2.69085/
      DATA XKTBAR/0.30,0.40,0.50,0.60,0.70,0.0,0.0/
      DATA DAY/17.,47.,75.,105.,135.,162.,148.,228.,258.,
     '  288.,318.,344./
      PI = 3.14159
      RDCONV = PI/180.
      NBINS = 100
      K0 = PI/24.
      K1 = 0.409
      K2 = 0.5016
      K3 = 0.6609
      K4 = 0.4767
      K5 = 1.0472
      DP=1.0/NBINS
      DO 10 KT=1,5
        P=0.0
        C1=COEF(1,KT)
        C2=COEF(2,KT)
        C3=COEF(3,KT)
        C4=COEF(4,KT)
        C5=COEF(5,KT)
        DO 10 J=1,NBINS
        P=P+DP
        XKT(J,KT)=P/(C1+C2*P+C3*P*P+C4*P**3+C5*P**4)
   10 CONTINUE
C
C     THIS FIT OF THE LIU AND JORDAN DISTRIBUTION CURVES IS FROM
C     R. COLE,"LONG-TERM AVERAGE PERFORMANCE PREDICTIONS FOR CPC'S",
C     PROCEEDINGS OF THE AMERICAN SECTION OF I.S.E.S.,ORLANDO
C     FLORIDA, (1977), P36-6
C
```

```
      READ(-,-) IPRT,IFILE
      READ (-,-,END=99) ALAT,SLOPE,AZMTH
1  READ (-,-,END=99) MO,BIGKTB,RHO
   WRITE (-,20)
   WRITE(-,30) ALAT,SLOPE,AZMTH
   WRITE (-,76)
   WRITE (-,77) MO,BIGKTB,RHO
   SINLAT = SIN(ALAT*RDCONV)
   COSLAT = COS(ALAT*RDCONV)
   TANLAT = SINLAT/COSLAT
   COSSLP = COS(SLOPE*RDCONV)
    IF ( IFILE .NE. 0 ) WRITE(IFILE,-) MO,BIGKTB
   DEC = 23.45*SIN((284.+DAY(MO))*.9863*RDCONV)*RDCONV
   SINDEC = SIN(DEC)
   COSDEC = COS(DEC)
   TANDEC = SINDEC/COSDEC
   OMEGAS = ACOS(-TANLAT*TANDEC)
   SINOS = SIN(OMEGAS)
   COSOS = COS(OMEGAS)
   A = K1+K2*SIN(OMEGAS-K5)
   B = K3-K4*SIN(OMEGAS-K5)
   DO 31 IHR = 1,7
    Q = FLOAT(IHR)
    Q = Q-1.
    OMEGA = 7.5 + Q*15.
    OMEGA = OMEGA*RDCONV
    IF (OMEGA.GT.OMEGAS) GO TO 31
    COSOMG = COS(OMEGA)
    RD = K0*(COSOMG-COSOS)/(SINOS-OMEGAS*COSOS)
    RT = RD*(A+B*COSOMG)
    IF (RT.LT.0.0001.OR.RD.LT.0.0001) GO TO 31
    SMLKTB = BIGKTB*RT/RD
    MODE=1
    RBARH=RBARHR(MODE,MO,IHR,ALAT,SLOPE,AZMTH,SMLKTB,RHO,RB)
    IF (RB.LT.0.0001) GO TO 31
    VBD = RB-(1+COSSLP)/2.
    AREAK=0.0
    XCOLD=0.0
    ABIN=FLOAT(NBINS)
    DO 50 IC=1,NBINS
     AIC=FLOAT(IC)
     F=AIC/ABIN
     IF (SMLKTB.GT.0.70.OR.SMLKTB.LT.0.30) GO TO 37
     DO 35 I=1,5
35    AKTS(I)=XKT(IC,I)
     CALL LAGRNG (5,SMLKTB,XKTBAR,AKTS,HRKT)
     GO TO 40
37    IF (SMLKTB.GT.0.7) GO TO 39
     HRKT=XKT(IC,1)*SMLKTB/0.3
     GO TO 40
```

```
  39    DELTA=(0.9-XKT(IC,5))*(SMLKTB-0.7)/0.2
        IF (DELTA.LT.0.0) DELTA=0.0
        HRKT=XKT(IC,5)+DELTA
  40    MODE=2
        RHR=RBARHR(MODE,MO,IHR,ALAT,SLOPE,AZMTH,HRKT,RHO,RB)
        XC(IC) = (RHR*HRKT)/(RBARH*SMLKTB)
        AREA(IC) = AREAK + (XC(IC)-XCOLD)*((1.-F) + 0.5*DP)
        AREAK = AREA(IC)
        XCOLD = XC(IC)
  50    CONTINUE
        TOTAL = AREA(NBINS)
        DO 60  I=1,NBINS
         PHI(I) = (TOTAL-AREA(I))/TOTAL
  60    CONTINUE
        WRITE(-,6)
        WRITE(-,7) IHR,RBARH,RB,VBD
        WRITE(-,678) SMLKTB
        WRITE(-,8)
        WRITE(-,9) (XC(IC),PHI(IC),IC=1,NBINS,IPRT)
        WRITE (-,15) TOTAL
        WRITE(-,450)
        WRITE(-,500)  NBINS,IFILE
        IF (IFILE.NE.0) WRITE(IFILE,-) RBARH,RB,VBD,
      '     (XC(IC),PHI(IC),IC=1,NBINS)
  20    FORMAT (1H1,////,21X,'LATITUDE',8X,'SLOPE',8X,'AZIMUTH')
  30    FORMAT (23X,F5.2,9X,F5.2,9X,F5.2)
  76    FORMAT ('0',23X,'MO',8X,'KTBAR',10X,'RHO')
  77    FORMAT (24X,I2,9X,F4.3,10X,F3.2)
  678    FORMAT(//38X,'HRKTBAR =',F5.3)
  6      FORMAT ('0'//,29X,'HR',7X,'RBARHR',6X,'RB',8X,'VBD')
  7      FORMAT (30X,I1,7X,F6.3,4X,F6.3,4X,F6.3)
  8      FORMAT ('0',//,31X,'XC''S',5X,'AND',5X,'PHI''S')
  9      FORMAT ('0',5(3X,F6.3,1X,F6.3))
  15    FORMAT ('0',30X,'TOTAL AREA = ',F5.3)
  450   FORMAT ('0',//,32X,'BINS',8X,'FILE')
  500   FORMAT(' ',32X,I3,10X,I2)
  31    CONTINUE
        GO TO 1
  99    STOP
        END
```

```
CCCCCCCCCCCCCCCCCCCCCCCCCCCCCCCCCCCCCCCCCCCCCCCCCC
C                                                 C
C                                                 C
C                    AYLPHI                        C
C                                                 C
C                                                 C
C     THIS PROGRAM CALCULATES PHIS AND USABLE      C
C     ENERGY.  THE BASIS OF THIS ANALYTICAL        C
C     EXPRESSION IS BENDT ET.AL.'S RANDOM          C
C     INSOLATION SEQUENCE PROBABILITY              C
C     DISTRIBUTION.                                C
C                                                 C
CCCCCCCCCCCCCCCCCCCCCCCCCCCCCCCCCCCCCCCCCCCCCCCCCC
C
      DIMENSION DAY(12)
      REAL LAT,KMIN,KMAX,KC,IO,IPLUS,IC,IBTILT,IMAX,LOW,LOSUM
      REAL KMIN2,KMIN3,KMIN4,KMAX2,KMAX3,KMAX4,KC2,KC3,KC4
      REAL K0,K1,K2,K3,K4,K5
      DATA DAY/17.,47.,75.,105.,135.,162.,198.,228.,258.,288.,318.,344./
      DATA PI/3.14159/
      RDCONV = PI/180.
      A1 = 1.0045
      A2 = 0.04349
      A3 = -3.5227
      A4 = 2.6313
      K0 = PI/24.
      K1 = 0.409
      K2 = 0.5016
      K3 = 0.6609
      K4 = 0.4767
      K5 = 1.0472
      SC = 1353.
      ROW = 0.2
      READ (-,-) LAT,SLP,AZMTH
      READ (-,-) IFILE
      SINLAT = SIN(LAT*RDCONV)
      COSLAT = COS(LAT*RDCONV)
      TANLAT = SINLAT/COSLAT
      SINSLP = SIN(SLP*RDCONV)
      COSSLP = COS(SLP*RDCONV)
      SINAZM = SIN(AZMTH*RDCONV)
      COSAZM = COS(AZMTH*RDCONV)
      B = (1.+COSSLP)/2.
      D = ROW*(1.-COSSLP)/2.
   10 READ (-,-,END=900) MO,BIGKTB
      IMAX = 1353.
      DI = 100.
      WRITE(-,600) LAT,SLP,AZMTH
      WRITE (-,605) MO,BIGKTB
      DEC = 23.45*SIN((360.*(284.+DAY(MO))/365.)*RDCONV)
      COSDEC = COS(DEC*RDCONV)
      SINDEC = SIN(DEC*RDCONV)
```

```
      TANDEC = SINDEC/COSDEC
      OMEGAS = ACOS(-TANLAT*TANDEC)
      SINOS = SIN(OMEGAS)
      COSOS = COS(OMEGAS)
      C1 = K1+K2*SIN(OMEGAS-K5)
      C2 = K3-K4*SIN(OMEGAS-K5)
      DO 550 IHR = 1,9
       OMEGA = (7.5+(IHR-1.)*15.)*RDCONV
       IF (OMEGA.GT.OMEGAS) GO TO 550
       COSOMG = COS(OMEGA)
       SINOMG = SIN(OMEGA)
       RO = KO*(COSOMG-COSOS)/(SINOS-OMEGAS*COSOS)
       RT = RO*(C1+C2*COSOMG)
       IF (RT.LT.0.0001.OR.RO.LT.0.0001) GO TO 550
       SMLKTB = BIGKTB*RT/RO
       KMIN = 0.05
       KMAX = 0.80
       CALL GAMA(SMLKTB,KMIN,KMAX,GAM)
       EXPO = EXP(GAM*(KMAX-KMIN))
       CHECK = (1.+(GAM*KMAX-1.)*EXPO-GAM*KMIN)/(GAM*(EXPO-1.))
       IF (ABS(CHECK-SMLKTB).GT.0.0005) GO TO 570
       G2 = GAM*GAM
       G3 = G2*GAM
       G4 = G3*GAM
       G5 = G4*GAM
       KMAX2 = KMAX*KMAX
       KMAX3 = KMAX2*KMAX
       KMAX4 = KMAX3*KMAX
       EP1MAX = (KMAX/GAM-1./G2)
       EP2MAX = (KMAX2/GAM-2.*KMAX/G2+2./G3)
       EP3MAX = (KMAX3/GAM-3.*KMAX2/G2+6.*KMAX/G3-6./G4)
       EP4MAX = (KMAX4/GAM-4.*KMAX3/G2+12.*KMAX2/G3-24.*KMAX/G4+24./G5)
       KMIN2 = KMIN*KMIN
       KMIN3 = KMIN2*KMIN
       KMIN4 = KMIN3*KMIN
       EP1MIN = (KMIN/GAM-1./G2)
       EP2MIN = (KMIN2/GAM-2.*KMIN/G2+2./G3)
       EP3MIN = (KMIN3/GAM-3.*KMIN2/G2+6.*KMIN/G3-6./G4)
       EP4MIN = (KMIN4/GAM-4.*KMIN3/G2+12.*KMIN2/G3-24.*KMIN/G4+24./G5)
       C = GAM/(EXP(GAM*KMAX)-EXP(GAM*KMIN))
       DFUBAR = A1+((A4*SMLKTB+A3)*SMLKTB+A2)*SMLKTB
       COST = SINDEC*SINLAT*COSSLP - SINDEC*COSLAT*SINSLP*COSAZM
     '   + COSDEC*COSLAT*COSSLP*COSOMG
     '   + COSDEC*SINLAT*SINSLP*COSAZM*COSOMG
     '   + COSDEC*SINSLP*SINAZM*SINOMG
       COSZ = SINDEC*SINLAT + COSDEC*COSLAT*COSOMG
       IO = SC*COSZ*(1.0+0.033*COS(RDCONV*DAY(MO)*360./365.))
       RB = COST/COSZ
       IF (RB.LT.0.0) GO TO 550
       RKTBAR = (1.-DFUBAR)*RB + DFUBAR*B + D
```

```
      VBD = RB-(1.+COSSLP)/2.
      AMAX = (EP1MAX*(RB+D)+(B-RB)*(A1*EP1MAX+A2*EP2MAX+A3*EP3MAX+A4
     ,       *EP4MAX))
      AMIN = (EP1MIN*(RB+D)+(B-RB)*(A1*EP1MIN+A2*EP2MIN+A3*EP3MIN+A4
     ,       *EP4MIN))
      HISUM = C*EXP(GAM*KMAX)*AMAX*IO
      LOSUM = C*EXP(GAM*KMIN)*AMIN*IO
      IBTILT = HISUM-LOSUM
      IBTILT = AMAX1(IBTILT,0.)
      WRITE(-,610) SMLKTB,KMIN,KMAX,GAM
      WRITE (-,620) VBD
      WRITE(-,630)
      M = IFIX(IMAX/DI) + 1
      DO 500 J=1,M
        FJ = FLOAT(J)
        IC = (FJ-1.)*DI
        CALL KTC(IC,IO,RB,COSSLP,ROW,KC,RKC)
        THEKC = KC
        IF (KC.LT.KMIN) KC = KMIN
        IF (KC.GT.KMAX) GO TO 100
        HIGH = HISUM-C*EXP(GAM*KMAX)*IC/GAM
        IPLUS = 0.
        KC2 = KC*KC
        KC3 = KC2*KC
        KC4 = KC3*KC
        EP1KC = (KC/GAM-1./G2)
        EP2KC = (KC2/GAM-2.*KC/G2+2./G3)
        EP3KC = (KC3/GAM-3.*KC2/G2+6.*KC/G3-6./G4)
        EP4KC = (KC4/GAM-4.*KC3/G2+12.*KC2/G3-24.*KC/G4+24./G5)
        AKC = IO*(EP1KC*(RB+D)+(B-RB)*(A1*EP1KC+A2*EP2KC+A3*EP3KC+A4
     ,       *EP4KC))
        LOW = C*EXP(GAM*KC)*(AKC-IC/GAM)
        IPLUS = HIGH-LOW
        IPLUS = AMAX1(IPLUS,0.)
100     PHI = 0.
        IF (IBTILT.GT.0.) PHI = IPLUS/IBTILT
        XC = 0.
        IF (IBTILT.GT.0.) XC = IC/IBTILT
        WRITE(-,640) IHR,IO,RB,RKTBAR,IC,THEKC,IBTILT,
     ,  IPLUS,XC,PHI
        IF (IFILE.GT.0) WRITE(IFILE,-) IHR,IC,IPLUS,PHI
        IF (PHI.LT.0.0001) GO TO 550
500   CONTINUE
550   CONTINUE
      GO TO 10
570   WRITE(-,650) CHECK,SMLKTB,GAM
      GO TO 10
600   FORMAT('1',////,25X,'LATITUDE = ',F5.2,5X,
     -      ' SLOPE = ',F5.2,,5X,' AZIMUTH = ',F5.2)
605   FORMAT('0',30X,'MONTH ',I2,5X,' BIGKTBAR = ',F5.3)
```

```
610 FORMAT('0',//,25X,'SMLKTB = ',F4.3,'  KMIN = ',F4.3,'  KMAX = ',
   -  F4.3,'  GAMA = ',F9.5)
620 FORMAT('0',45X,'VBD = ',F6.3)
630 FORMAT('0',4X,'HOUR',6X,'IO',8X,'RB',6X,'RKTBAR',6X,'IC',
   -   8X,'KC',6X,'IBTILT',4X,'IPLUS',6X,'XC',8X,'PHI')
640 FORMAT('0',5X,I2,4X,F7.2,3X,F7.3,3X,F7.3,4X,F6.1,4X,
   -  F5.3,4X,F7.2,3X,F7.2,2X,F6.3,6X,F5.3)
650 FORMAT('0',15X,'AN ERROR IN SUBROTINE GAMA RESULTS IN A VALUE OF '
   -  ,F6.4,' WHEN A VALUE OF ',F6.4,' WAS SPECIFIED.  GAMA = ',F7.4)
900 STOP
    END
```

```
      SUBROUTINE GAMA(KTBAR,KMIN,KMAX,GAM)
CCCCCCCCCCCCCCCCCCCCCCCCCCCCCCCCCCCCCCCCCCCCCCCCCCCCCCCCCCC
C                                                         C
C   THIS SUBROUTINE USES NEWTONS METHOD TO FIND GAMA,     C
C   THE CONSTANT THAT SATISFIES BENDT & RABL'S EQUATION   C
C   IN KTBAR, KTMIN, AND KTMAX FROM THIER STATISTICAL     C
C   FREQUENCY DISTRIBUTION PAPER.                         C
C                                                         C
CCCCCCCCCCCCCCCCCCCCCCCCCCCCCCCCCCCCCCCCCCCCCCCCCCCCCCCCCCC
C
      REAL KTBAR,KMIN,KMAX
      GAM = -3.0
      DG = 0.01
      J = (10.-GAM)/DG
      F = (GAM*(KTBAR-KMIN)+1.)/(GAM*(KTBAR-KMAX)+1.)
     '    -EXP(GAM*(KMAX-KMIN))
      DO 10 I=1,J
        GAMO = GAM+DG
        IF (ABS(GAMO).LT.0.00001) GAMO = 0.0
        FO = (GAMO*(KTBAR-KMIN)+1.)/(GAMO*(KTBAR-KMAX)+1.)
     '    -EXP(GAMO*(KMAX-KMIN))
        IF (GAM.LT.0.0.AND.ABS(GAMO).LT.0.0001) GO TO 5
        IF (F.LT.0.0.AND.FO.GT.0.0) GO TO 20
        IF (F.GT.0.0.AND.FO.LT.0.0) GO TO 20
    5   GAM = GAMO
        F = FO
   10 CONTINUE
   20 GAM = GAMO
      IF (GAM.GT.9.0.AND.KTBAR.LT.0.5) GAM = 0.000001
      MAXITR = 50
      FMAX = 0.0000001
      DELMAX = 0.0000001
      DO 100 N = 1,MAXITR
        NITER = N
        F = (GAM*(KTBAR-KMIN)+1.)/(GAM*(KTBAR-KMAX)+1.)
     '      -EXP(GAM*(KMAX-KMIN))
        IF (ABS(F).LT.FMAX) GO TO 300
        FPRIM = ((GAM*(KTBAR-KMAX)+1.)*(KTBAR-KMIN)
     '    -(GAM*(KTBAR-KMIN)+1.)*(KTBAR-KMAX))/
     '    (GAM*(KTBAR-KMAX)+1.)**2. - (KMAX-KMIN)*EXP
     '    (GAM*(KMAX-KMIN))
        CORREC = F/FPRIM
        GAM = GAM-CORREC
        IF (ABS(CORREC).LT.DELMAX) GO TO 300
  100 CONTINUE
      WRITE (-,200) MAXITR
  200 FORMAT ('0',20X,'NEWTONS METHOD DIDN''T CONVERGE ON GAMA IN '
     '    ,I3,' ITERATIONS.')
  300 RETURN
      END
```

```
      SUBROUTINE KTC(IC,IO,RB,COSSLP,ROW,KC,RKC)
CCCCCCCCCCCCCCCCCCCCCCCCCCCCCCCCCCCCCCCCCCCCCCCCCCCCCCCCC
C                                                       C
C   THIS SUBROUTINE USES NEWTONS METHOD TO FIND A CRITICAL   C
C   CLEARNESS INDEX FOR A GIVEN CRITICAL RATIO AND LOCATION. C
C                                                       C
CCCCCCCCCCCCCCCCCCCCCCCCCCCCCCCCCCCCCCCCCCCCCCCCCCCCCCCCC
C
      REAL IC,IO,KC
      FMAX = 0.00001
      DELMAX = 0.00001
      MAXITR = 50
      A1 = 1.0045
      A2 = 0.04349
      A3 = -3.5227
      A4 = 2.6313
      B = (1.0+COSSLP)/2.0
      D = ROW*(1.0-COSSLP)/2.0
      KC = 0.2
      DO 100 N=1,MAXITR
      DIFUSE = A1+((A4*KC+A3)*KC+A2)*KC
      CONST = A2+(3.0*A4*KC+2.0*A3)*KC
      CON = ((B-RB)*DIFUSE+RB+D)**2.0
      RKC = (1.0-DIFUSE)*RB + DIFUSE*B + D
      F = IC/(IO*RKC) - KC
      IF (ABS(F).LT.FMAX) GO TO 500
      FPRIM = (IC/IO)*(RB-B)*CONST/CON-1.0
      CORREC = F/FPRIM
      IF (ABS(CORREC).LT.DELMAX) GO TO 500
      KC = KC-CORREC
100   CONTINUE
      WRITE (-,200) MAXITR
200   FORMAT ('0',20X,'NEWTONS METHOD DID NOT CONVERGE ON KTC IN '
     '    ,I3,' ITERATIONS.')
500   RETURN
      END
```

BIBLIOGRAPHY

1.  Beckman, W.A.  "Duct and Pipe Losses in Solar Energy Systems."
    Solar Energy 21 (1978): 531-532.

2.  Beckman, W.A., Klein, S.A., and Duffie, J.A.  Solar Heating
    Design.  New York: Wiley-Interscience, 1977.

3.  Bendt, P., Rabl, A., and Collares-Pereira, M.  "The Frequency
    Distribution of Daily Insolation Values."  Solar Energy Research
    Institute (submitted to Solar Energy: 1980).

4.  Bennington, G., Curto, P., Miller, G., Rebibo, K., and Spewak,
    P.  "Solar Energy - A Comparative Analysis to the Year 2020."
    MITRE Corp., MTR-7579.  McLean, Virginia: 1978.

5.  Boes, E.C., et al.  "Availability of Direct, Total, and Diffuse
    Solar Radiation to Fixed and Tracking Collectors in the U.S.A."
    Sandia Laboratories, SAND77-0885.  Albuquerque: 1977.

6.  Boes, E.C., et al.  "Distribution of Direct and Total Solar
    Radiation Availabilities for the U.S.A."  Sandia Laboratories,
    SAND76-0411.  Albuquerque: 1976.

7.  Brown, K.C.  "Applications and System Studies for Solar Indus-
    trial Process Heat."  Solar Energy Research Institute, TR-351-
    481.  Golden, Colorado:  1980.

8.  Brown, K.C., Hooker, D.W., Rabl, A., Stadjuhar, S.A., and West,
    R.E.  "End-Use Matching for Solar Industrial Process Heat."
    Solar Energy Research Institute, TR-34-091.  Golden, Colorado:
    1980.

9.  Bruno, R.  "A Correlation Procedure for Separating Direct and
    Diffuse Insolation on a Horizontal Surface."  Solar Energy 20
    (1978): 97-100.

10. Bugler, J.W.  "The Determination of Hourly Insolation on an In-
    clined Plane Using a Diffuse Irradiance Model Based on Hourly
    Measured Global Horizontal Insolation."  Solar Energy 19
    (1977): 477-492.

11. Castamajor, A.B., and Wood, R.L.  "Potential Industrial Process
    Heat Applications for Solar Energy at Temperatures < 170°C:
    Field Study."  Presented at the American Section of the Inter-
    national Solar Energy Society Annual Meeting.  Denver: August
    1978.

12. Cole, R. "Long-Term Average Performance Predictions for Compound Parabolic Concentrators Solar Collectors." Proceedings of the American Section of the International Solar Energy Society, Orlando, FL: 1977.

13. Collares-Pereira, M., and Rabl, A. "The Average Distribution of Solar Radiation-Correlations Between Diffuse and Hemispherical and Between Daily and Hourly Insolation Values." Solar Energy 22 (1976): 155-164.

14. Collares-Pereira, M., and Rabl, A. "Derivation of a Method for Predicting Long Term Average Energy Delivery of Solar Collectors." Solar Energy 23 (1979): 223-234.

15. de Winter, F. "Heat Exchanger Penalities in Double-Loop Solar Water Heating Systems." Solar Energy 17 (1975): 335-337.

16. Duffie, J.A., and Beckman, W.A. Solar Engineering of Thermal Processes. New York: Wiley-Interscience, 1980.

17. Fraser, M.D. "Analysis of the Economic Potential of Solar Thermal Energy to Provide Industrial Process Heat." Energy Research and Development Administration/Intertechnology No. 00028-1. Warrenton, Virginia: Intertechnology Corp., 1977.

18. Hall, E. "Survey of the Applications of Solar Thermal Energy Systems to Industrial Process Heat." Energy Research and Development Administration TID-27348/1. Columbus, Ohio: Battelle Columbus Labs, 1977.

19. Hall, I.J., Prairie, R.R., Anderson, H.E., and Boes, E.C. "Generation of a Typical Meteorological Year for 26 SOLMET Stations." Sandia Laboratories, SAND78-1601. Albuquerque: 1978.

20. Hottel, H.C. "A Simple Model for Estimating the Transmittance of Direct Solar Radiation Through Clear Atmospheres." Solar Energy 18 (1976): 129-134.

21. "Industrial Process Heat - Creative Opportunities in Solar Design." Solar Age 4 (1979): 19-21.

22. Klein, S.A. "Calculation of Flat-Plate Collector Utilizability." Solar Energy 21 (1978): 393-402.

23. Klein, S.A. "Calculation of Monthly Average Insolation on Tilted Surfaces." Solar Energy 19 (1977): 325-329.

24. Klein, S.A. "A Design Procedure for Solar Heating Systems." Ph.D. Thesis in Chemical Engineering. University of Wisconsin-Madison. Madison, Wisconsin: 1976.

25. Klein, S.A., and Beckman, W.A. "A General Design Method for Closed-Loop Solar Energy Systems." Solar Energy 22 (1979): 269-282.

26. Klein, S.A., et al. "TRNSYS - A Transient Simulation Program." University of Wisconsin-Madison, Engineering Experiment Station Report 38-10. Madison, Wisconsin: 1979.

27. Levonowich, P.F. "Determination of the Feasibility of Using Solar Energy in a Good Processing Plant." Master's Thesis in Chemical Engineering. University of Wisconsin-Madison. Madison, Wisconsin: 1978.

28. Liu, B.Y.H., and Jordan, R.C. "Daily Insolation on Surfaces Tilted Toward the Equator." ASHRAE Journal 3 (1961): 53-59.

29. Liu, B.Y.H., and Jordan, R.C. "The Interrelationship and Characteristic Distribution of Direct, Diffuse and Total Solar Radiation." Solar Energy 4 (1960): 1-19.

30. Liu, B.Y.H., and Jordan, R.C. "The Long-Term Average Performance of Flat-Plate Solar-Energy Collector." Solar Energy 7 (1963): 53-74.

31. Lund, D.B., et al. "Utilization of Solar Energy in Cheese Processing Operations." University of Wisconsin-Madison. Madison, Wisconsin: 1978.

32. Mitchell, J.C., et al. "FCHART4.0 - A Design Program for Solar Energy Systems." University of Wisconsin-Madison, Engineering Experiment Station Report 49-4. Madison, Wisconsin: 1980.

33. Morse, R.N. "Solar Industrial Process Heating for Can Warming." Commonwealth Scientific and Industrial Research Organization, 0-643-01955-3. East Melbourne, Australia: 1978.

34. Orgill, J.F., and Hollands, K.G.T. "Correlation Equation for Hourly Diffuse Radiation on a Horizontal Surface." Solar Energy 19 (1977): 357-359.

35. Peters, R.R. "A Method for Determining the Configuration of the Optimum Solar Total Energy System." Sandia Labs., SAND79-0422. Albuquerque: 1979.

36. Ruth, D.W., and Chant, R.E.  "The Relationship of Diffuse Radiation to Total Radiation in Canada."  Solar Energy 18 (1976): 153-154.

37. Solar Industrial Process Heat Symposium Proceedings.  Energy Research and Development Administration, CONF-770966.  College Park, Maryland: 1977.

38. SOLMET.  "Hourly Solar Radiation Surface Meteorological Observations."  TD-9724 (1979).

39. SOLMET Typical Meteorological Year, Tape Deck 9734.  National Oceanic and Atmospheric Administration, Environmental Data Service, National Climatic Center.  Asheville, North Carolina.

40. Theilacker, J.C.  "An Investigation of Monthly-Average Utilizability for Flat-Plate Solar Collectors."  Masters Thesis in Mechanical Engineering.  University of Wisconsin-Madison.  Madison, Wisconsin: 1980.

41. Tuller, S.E.  "The Relationship Between Diffuse, Total, and Extraterrestrial Solar Radiation."  Solar Energy 18 (1976): 259-264.

42. Whillier, A.  "Solar Energy Collection and Its Utilization for House Heating."  Ph.D. Thesis in Mechanical Engineering.  M.I.T. Cambridge, Massachusetts: 1953.